2010

Cytochrome C Oxidase from Rhodobacter Sphaeroides: Oligomeric Structure in the Phospholipid Bilayer and the Structural and Functional Effects of a C-Terminal Truncation in Subunit III

Teresa L. Cvetkov
Wright State University

CYTOCHROME *C* OXIDASE FROM *RHODOBACTER SPHAEROIDES*: OLIGOMERIC STRUCTURE IN THE PHOSPHOLIPID BILAYER AND THE STRUCTURAL AND FUNCTIONAL EFFECTS OF A C-TERMINAL TRUNCATION IN SUBUNIT III

A dissertation submitted in partial fulfillment of the
requirements for the degree of
Doctor of Philosophy

by

TERESA L. CVETKOV
B.S., Calvin College, 2003

2010
Wright State University

WRIGHT STATE UNIVERSITY

SCHOOL OF GRADUATE STUDIES

June 10, 2010

I HEREBY RECOMMEND THAT THE DISSERTATION PREPARED UNDER MY SUPERVISION BY Teresa L. Cvetkov ENTITLED Cytochrome *c* Oxidase from *Rhodobacter sphaeroides*: Oligomeric Structure in the Phospholipid Bilayer and the Structural and Functional Effects of a C-Terminal Truncation in Subunit III BE ACCEPTED IN PARTIAL FULFILLMENT OF THE REQUIREMENTS FOR THE DEGREE OF Doctor of Philosophy.

Lawrence J. Prochaska, Ph.D.
Dissertation Director

Gerald M. Alter, Ph.D.
Director, Biomedical Sciences
Ph.D. Program

John A. Bantle, Ph.D.
Vice President for Research and
Graduate Studies and Interim Dean,
School of Graduate Studies

Committee on Final Examination

Lawrence J. Prochaska, Ph.D.

Gerald M. Alter, Ph.D.

Mark D. Mamrack, Ph.D.

Robert W. Putnam, Ph.D.

Nicholas V. Reo, Ph.D.

ABSTRACT

Cvetkov, T.L. Ph.D., Biomedical Sciences Ph.D. Program, Wright State University, 2010. Cytochrome *c* Oxidase from *Rhodobacter sphaeroides*: Oligomeric Structure in the Phospholipid Bilayer and the Structural and Functional Effects of a C-Terminal Truncation in Subunit III.

Cytochrome *c* oxidase (COX) of the mitochondrial electron transport chain catalyzes the reduction of oxygen to water while concomitantly translocating protons across the inner mitochondrial membrane. This two part dissertation is a structural and functional investigation of COX using the bacterial model system from *Rhodobacter sphaeroides* (*R.sph.*).

First, the oligomeric structure of *R.sph.* COX within the lipid bilayer was investigated using discontinuous sucrose gradient ultracentrifugation. Utilizing this technique, liposomes containing *R.sph*. COX (pCOV) were separated from liposomes lacking enzyme (COV). The net buffering capacity and degree of light scattering per COX molecule were reduced in pCOVs, making them well suited for low buffer spectroscopic studies. Also, pCOVs maintained high oxygen reduction and proton pumping activities relative to COVs, indicating minimal damage induced by the centrifugation process. Quantitative lipid and protein concentrations were used to estimate the number of COX molecules per vesicle in the pCOVs. There was only one *R.sph*. COX molecule per vesicle, indicating that within the lipid bilayer, *R.sph*. COX exists in the monomeric state in contrast to the bovine enzyme which is dimeric. As a monomer, therefore, *R.sph.* COX is capable of maximal electron transfer and proton pumping efficiency.

Second, the structural and functional effects of a c-terminal subunit III truncation were characterized in *R.sph.* in order to gain insight into the critical role played by this subunit in proper COX functioning. The mutation was modeled after a human mitochondrial disease mutation which genetically truncates subunit III after the third of its seven helices (Δ114 COX). In *R.sph.* cells, Δ114 COX had lower expression levels and impeded rates of COX assembly. Altered levels of native *in vivo* processing of subunits II and IV were observed in Δ114 COX and in COX which had subunit III genetically removed (I-II COX). The truncated subunit III was incorporated into the COX complex with at least 70% stoichiometry and was subject to proteolytic processing at a specific cleavage site. Prior to enzymatic turnover induced inactivation, the proton pumping and oxygen reduction activities of Δ114 COX were half that of wildtype and equivalent to I-II COX at physiological pH. Δ114 and I-II COX had similar catalytic lifetimes in detergent micelle, but when supplemented with phospholipids from soybean, the catalytic lifetime of Δ114 COX was increased compared to I-II COX. Taken together, these results indicate that the c-terminal bundle of subunit III plays a role in the assembly of COX in *R.sph.* and in the native processing of subunits II and IV. They also highlight the role of the structural lipids within the v-shaped cleft of subunit III as being important for providing protection against turnover induced inactivation.

TABLE OF CONTENTS

Page

TABLE OF CONTENTS (Continued)

Page

TABLE OF CONTENTS (Continued)

Page

LIST OF FIGURES

Figure Page

LIST OF FIGURES (Continued)

Figure Page

LIST OF TABLES

ACKNOWLEDGEMENTS

I would like to acknowledge my dissertation director, Larry Prochaska, for providing a supportive training environment. Your mentorship has been an important component in my development as a scientist. I also thank you for your friendship and encouragement throughout the years.

The members of my dissertation committee were an inspiration and encouragement to me, and I am grateful for the time they spent reading my work and providing constructive and supportive feedback.

I have had the privilege of working with a number of great people during my time in the Prochaska laboratory. Many thanks to all, and special thanks to Rachel, Alagu and Khadijeh who were present and supportive during the writing process. Your humor and friendship helped me immeasurably.

I would also like to thank my parents for encouraging an interest in learning and a drive for excellence, and I thank my entire family and my friends for the love and support they have provided.

Graduate school is notorious for its many stressors and difficulties. Learning to believe in myself and to face the uncertainty and obstacles with increasing confidence and resilience has been an invaluable life experience. I extend my deepest and enduring gratitude to those who have patiently and persistently helped me in that process.

I. Introduction

The Mitochondrial Electron Transport Chain

The Mitochondrion

The processes of life utilize a myriad of biochemical reactions and interactions in order to maintain a state distinct from environmental equilibrium. These processes require a constant input of energy in a form readily useable by the enzymes which catalyze the constitutive reactions of life. The high energy phosphate bonds of adenosine tri-phosphate (ATP) have been harnessed as an anciently conserved mechanism for providing this requisite energy. As such, central to the sustenance of life is the ability of a cell to convert food energy into ATP, which in turn provides energy for the vast majority of that cell's reactions and processes. The cellular organelle responsible for this vital energy conversion process is the mitochondrion.

The mitochondrion is the remnant of an ancient α-proteobacterium which entered into a symbiotic relationship with a proto-eukaryotic host cell some two billion years ago (Gray et al., 1999; Wallace, 2005; Wallace and Fan, 2010). The proto-mitochondrion provided energy via its oxidative reactions to the host cell, which became the environment for the increasingly specialized organelle. Much of the genome original to the α-protobacterium was co-opted by the host cell, which eventually became dependent on the mitochondrion for its energy needs (Wallace, 2007). The signatures of this ancient rendezvous are evident in the structure and genetics of the mitochondrion.

The mitochondrion retains a small, double-stranded circular chromosome approximately 16 kb in size, for which the entire sequence is now known and confirms the evolutionary relatedness of mitochondria and α-proteobacteria (Andrews et al., 1999; Gray et al., 1999; Tuppen et al., 2010). The genome contains 37 genes, 13 encoding for polypeptides which form many of the core subunits of the complexes in the mitochondrial electron transport chain (Tuppen et al., 2010). There are multiple copies of the genome per mitochondrion, and up to thousands of copies per cell (Holt et al., 2007). The mitochondrion replicates its DNA and undergoes division within the cell largely independent of the cell cycle (Owusu-Ansah et al., 2008; Tuppen et al., 2010). Mitochondrial function requires the concerted expression of both mitochondrial and nuclear-encoded proteins, the details of which are still being elucidated and are becoming an increasing interest area in biomedical research (Wallace and Fan, 2010).

The mitochondrion is a double membranous structure, which is often ellipsoid in shape and around one micron in length (Figure 1A)(Frey and Mannella, 2000). The outer membrane bounds the organelle as a semi-permeable membrane studded with porin proteins, allowing for the exchange of substrates and molecules used in the various mitochondrial functions (Bay and Court, 2002; Neupert and Herrmann, 2007). The highly impermeable inner membrane, depicted in Figure 1A as an extensively baffled structure, is actually composed of two distinct regions (Figure 1B), an inner membrane boundary (light blue) and the cristae membrane (yellow) which is joined to the inner membrane boundary by small, tubular openings called cristae junctions (Zick et al., 2009). These two regions of the inner membrane are enriched in different types of proteins. The inner membrane boundary is enriched primarily with proteins involved in protein translocation

Figure 1

Structural compartmentalization of the mitochondrion. A) Schematic structure of the mitochondrion, indicating key structural components. The mitochondrion is a double membrane organelle, consisting of an outer and inner membrane. The outer membrane bounds the organelle. The inner membrane contains the aqueous matrix. The aqueous inner membrane space is enclosed between the two membranes. B) Three-dimensional electron tomographic reconstruction of the mitochondrion. The inner membrane is composed of two regions, the inner membrane boundary and the cristae membrane, which is joined to the inner membrane boundary by cristae junctions. Adapted from (Frey and Mannella, 2000).

A)

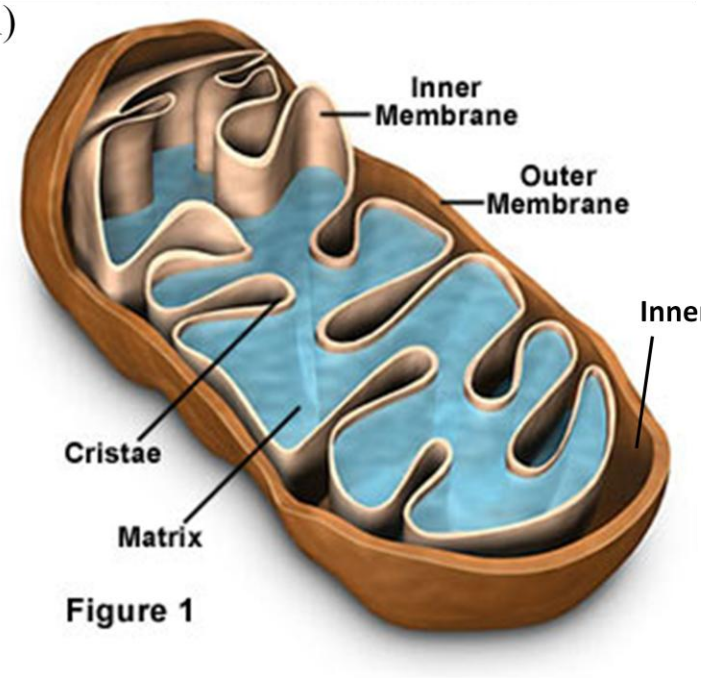
Inner Membrane
Outer Membrane
Inner membrane space
Cristae
Matrix

Figure 1

B)

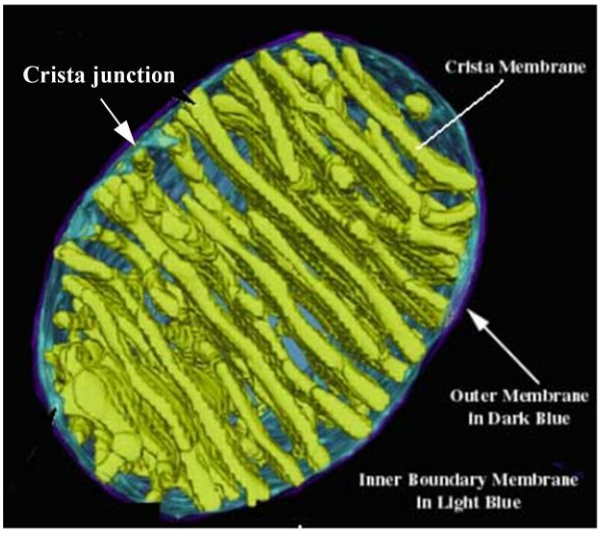
Crista junction
Crista Membrane
Outer Membrane In Dark Blue
Inner Boundary Membrane In Light Blue

and mitochondrial fusion. The cristae membrane houses the machinery of oxidative phosphorylation as well as proteins for protein translation, metabolite exchange and mitochondrial morphology (Vogel et al., 2006; Wurm and Jakobs, 2006; Zick et al., 2009). The inner membrane encloses the matrix, leaving an inner membrane space between the inner and outer membranes. The morphology of the cristae membrane can be highly variable in a manner that is likely reciprocally linked to the respiratory state of the mitochondrion, however the exact relationships between mitochondrial function and the structure of the cristae membrane are still under investigation (Mannella, 2006; Zick et al., 2009).

Historically, the major thrust of mitochondrial research has focused on its role in metabolism, although the organelle now has proven involvement in a diverse array of functions (Zick et al., 2009; Tuppen et al., 2010). A critical mitochondrial process is oxidative phosphorylation, wherein an electrochemical gradient is created by the electron transport chain across the inner membrane and is harnessed to synthesize ATP (Saraste, 1999). Other mitochondrial functions central to metabolism include the Krebs cycle, β-oxidation of fatty acids and the metabolism of various amino acids (Tuppen et al., 2010). The chemiosmotic potential of mitochondria has implications for additional mitochondrial functions, including calcium signaling and apoptosis (Tsujimoto and Shimizu, 2007; Walsh et al., 2009). The mitochondrion is also the site for heme biosynthesis and iron-sulfur cluster biogenesis (Zick et al., 2009; Tuppen et al., 2010).

The Mitochondrial Electron Transport Chain and Chemiosmotic Theory

Nearly fifty years ago, Peter Mitchell proposed an innovative hypothesis that has forever changed the way scientists view metabolism. In his 1961 *Nature* paper, he writes, "In the exact sciences, cause and effect are no more than events linked in sequence…The underlying thesis of the hypothesis put forward here is that…not only can metabolism be the cause of transport, but transport can be the cause of metabolism" (Mitchell, 1961). He hypothesized that the transport of protons across a charge-impermeable membrane in the mitochondrion resulted in an electrochemical gradient which drove the phosphorylation of ADP. Although initially controversial, the research that followed for the next several years lead to the establishment of his theory, resulting in his reception of the 1978 Nobel Prize in chemistry.

The molecular machinery of mitochondrial oxidative phosphorylation consists of a series of inner membrane-bound proteins, localized primarily to the cristae membrane and collectively referred to as the electron transport chain (Figure 2). Upstream metabolic reactions result in the production of NADH and $FADH_2$ from food sources (Wallace, 2007; Ordys et al., 2010). Complexes I and II respectively oxidize these substrates and transfer the electrons to the membrane bound electron carrier ubiquinone (Q) (Cecchini, 2003). Complex I conserves the energy of the oxidation reaction by pumping a proton across the inner membrane (Hirst, 2009). The complex Q-cycle catalyzed by Complex III results in ubiquinol oxidation, cytochrome *c* reduction, and proton translocation into the inner membrane space (Crofts et al., 2008). Complex IV uses the electrons from cytochrome *c* molecules and protons from the matrix to reduce oxygen to water, coupling the reaction to proton pumping (Hosler et al., 2006). The electrochemical gradient

Figure 2

The mitochondrial electron transport chain. Schematic of the components of the electron transport chain. NADH and $FADH_2$ are oxidized to NAD^+ and FAD by complexes I and II, respectively. The electrons from this reaction are transferred to coenzyme Q, which reduces complex III. Complex III reduces the soluble electron carrier cytochrome *c* which is oxidized by Complex IV. Ultimately the electrons are used to reduce O_2 to H_2O. The reactions of Complex I, III and IV result in net translocation of protons from the matrix (or bacterial cytoplasm) to the innermembrane space (or bacterial periplasm). Complex IV, ATP synthase, harnesses the resulting electrochemical gradient to drive the synthesis of ATP from ADP and inorganic phosphate.

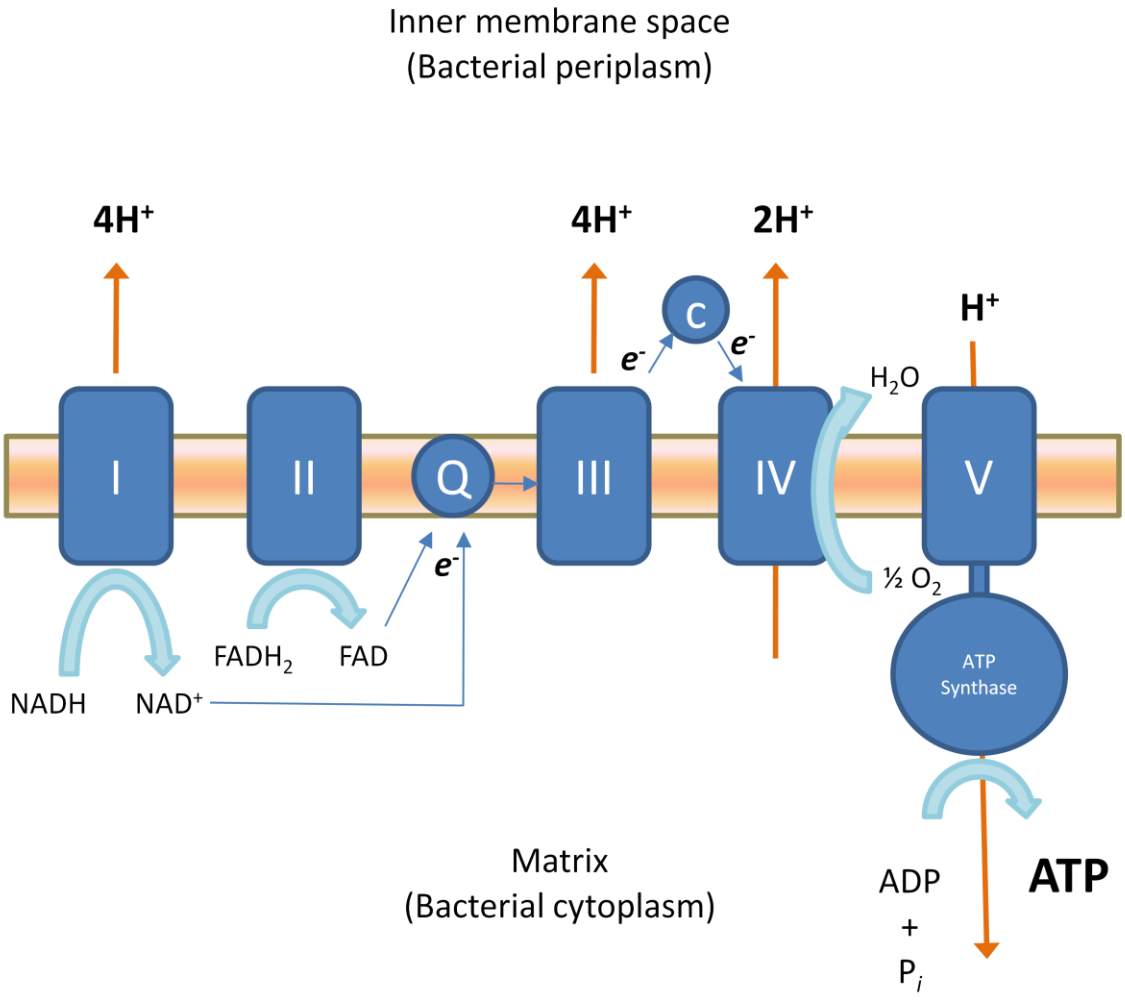
Inner membrane space
(Bacterial periplasm)
4H+
4H+
2H+
H+
C
e-
e-
H2O
I
II
Q
III
IV
V
½ O2
e-
FADH2
FAD
NADH
NAD+
ATP
Synthase
Matrix
(Bacterial cytoplasm)
ADP
+
Pi
ATP

resulting from the proton pumping activities of Complexes I, III and IV is harnessed by Complex V to drive the synthesis of ATP from ADP and inorganic phosphate (von Ballmoos et al., 2009).

Complex I, or NADH:quinone oxidoreductase, consists of 14 core subunits and up to 31 accessory subunits arranged into an L-shape, with an soluble domain extending into the mitochondrial matrix (Radermacher et al., 2006; Sazanov, 2007; Zickermann et al., 2009). The soluble domain contains a catalytic site for NADH oxidation, as well as a bound flavin nucleotide and a series of iron-sulfur centers for transferring the electrons from NADH to the integral membrane domain where ubiquinone (coenzyme Q) reduction and proton translocation occur (Hirst, 2009). A high resolution structure for the hydrophobic domain is still unavailable, which limits the understanding of the reactions it catalyzes. The net result is that for every two electrons extracted from NADH and donated to ubiquinone, four protons are translocated from the matrix to the inner membrane space (Zickermann et al., 2009). Given the low redox potentials of its metal cofactors, Complex I is also a major site of reactive oxygen species generation (Hirst, 2009).

Succinate:ubiquinone oxidoreductase, or Complex II, is involved in both the electron transport chain and in the Krebs cycle (Maklashina and Cecchini, 2010). As a part of the Kreb's cycle, it catalyzes the oxidation of succinate to fumarate, which involves abstracting two electrons and two protons and transferring them to an internally bound FAD, forming $FADH_2$. The electrons are then transferred to ubiquinone via the enzyme's iron-sulfur clusters, and the protons are released back into the matrix (Sun et

al., 2005; Horsefield et al., 2006). Complex II thus increases the pool of ubiquinol within the membrane.

Complex III, also called cytochrome bc_1, catalyzes the oxidation of ubiquinol and the reduction of cytochrome *c*, coupling the reaction to proton translocation across the inner membrane (Crofts, 2004). The complete structure of the mitochondrial form of Complex III consists of 13 subunits, three of which form the catalytic core. The protein catalyzes many metal prosthetic groups for electron transfer, including two heme *b* molecules, a heme *c* molecule, and an iron-sulfer cluster (Iwata et al., 1998). The mechanism by which the oxidoreductive reactions are accomplished involves many catalytic sites and proton and electron transfer pathways (Crofts et al., 2008). The reaction results in two single-electron transfers to two cytochrome *c* molecules, the uptake of two protons from the matrix, and the release of four protons into the inner membrane space (Crofts, 2004). Reduced cytochrome *c* is oxidized by Complex IV, cytochrome *c* oxidase (COX) in a reaction driven by reduction of oxygen and coupled to proton pumping (Hosler et al., 2006). The structure and mechanism of COX is discussed in detail below. The net result of the electron transport activity is that for every two electrons transferred from NADH to ½ O_2 there are ten protons pumped across the inner mitochondrial membrane.

The fifth complex of the electron transport chain is ATP synthase. ATP synthase utilizes the electrochemical proton gradient generated by Complexes I, III and IV to drive the phosphorylation of ADP. ATP synthase is composed of a water soluble F_1 protein complex and a membrane bound F_0 protein complex, joined together by a central and peripheral stalk (von Ballmoos et al., 2009). The F_0 complex facilitates proton transfer

from the inner membrane into the matrix, coupling the process to a physical rotation in a portion of the F_0 complex. The F_0 rotation forces a rotary motion of the F_1 complex, which drives the synthesis of ATP at its nucleotide binding/catalytic sites (Nakanishi-Matsui et al., 2010). The majority of a cell's ATP is synthesized by this mechanism. Thus, the mitochondrial electron transport chain is of central importance to virtually every biochemical pathway and process of life.

The Structure and Function of Cytochrome *c* Oxidase

Cytochrome *c* oxidase (COX) is the terminal oxidase of the mitochondrial electron transport chain and catalyzes the reduction of molecular oxygen to water while concomitantly translocating protons across the inner mitochondrial membrane. The resulting electrochemical proton gradient is used to drive the synthesis of ATP and various other mitochondrial functions. COX is thus indispensible for proper cellular function.

Three Dimensional Structure of Cytochrome c Oxidase

Early structural studies of cytochrome *c* oxidase were complicated by difficulties in crystallization of membrane proteins and in an inability to conduct site-directed mutagenesis studies on the mitochondrially-encoded subunits which constitute the enzyme's functional core. In more recent years, however, three-dimensional crystal structures of COX have been solved for a number of species (Tsukihara et al., 1996; Iwata et al., 2002; Svensson-Ek et al., 2002; Tsukihara et al., 2003). Shown in Figure 3 is the crystal structure of mitochondrial COX from bovine heart (PDB 1V54), which shares

Figure 3

The three dimensional crystal structure of bovine heart COX. Mitochondrial COX is composed of 13 subunits. The functional core of the enzyme consists of the mitochondrial-DNA encoded subunits, SI (cyan), SII (orange) and SIII (pink). In addition there are ten nuclear-DNA encoded subunits (gray). The enzyme crystallizes and functions as dimer. Each monomer contains a Cu_A-Cu_A center (green spheres), a heme *a* center (yellow), and a heme a_3-Cu_B active site (yellow heme, green sphere Cu_B). A) Bovine COX dimer viewed within the plane of the membrane. B) Bovine COX dimer viewed from the inner membrane space, perpendicular to the plane of the membrane. Prepared using Accelrys DS Viewer Pro. PDB 1V54 (Tsukihara et al., 2003).

A)

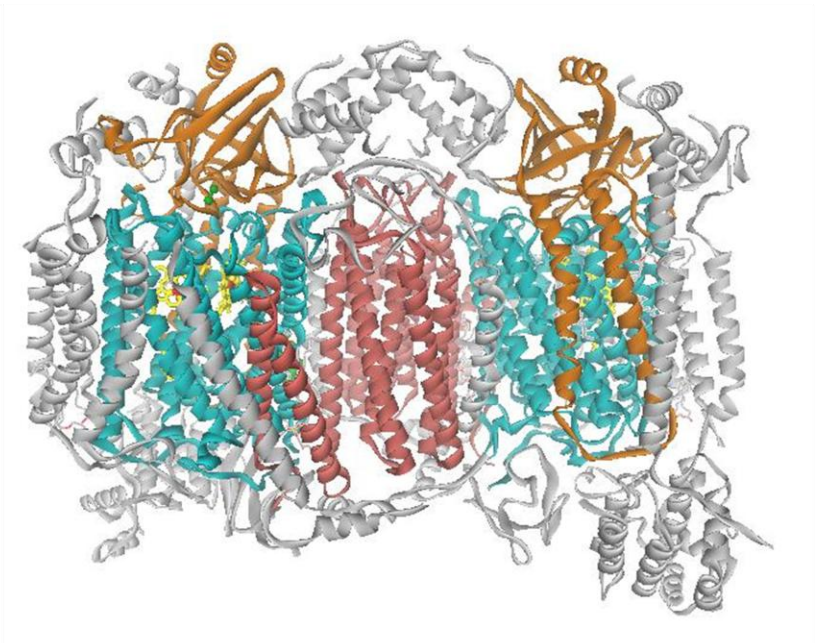

B)

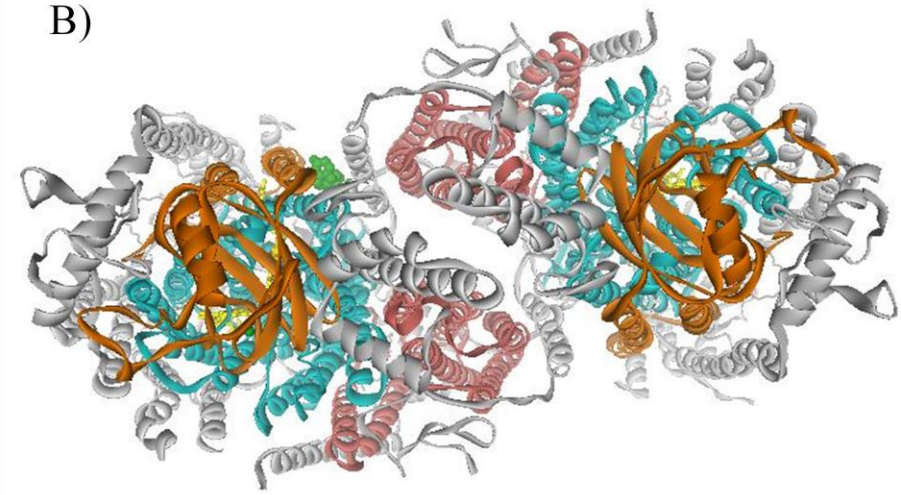

98% sequence identity to human COX. The protein consists of 13 subunits with a combined molecular weight of 205 kDa. Subunits I, II and III are encoded by mitochondrial DNA and are considered the functional core of the enzyme, sharing structural and functional homology across a wide range of species (cyan, subunit I; orange, subunit II; pink, subunit III)(Tsukihara et al., 2003; Hosler, 2004). The functions of the ten remaining nuclear DNA-encoded subunits (shown in gray) are still under investigation with putative roles ranging from complex assembly and stability to regulation of enzymatic activity (Galati et al., 2009; Fornuskova et al., 2010). The bovine form of the enzyme crystallizes as a dimer, and cross-linking and gel filtration studies indicate that this is also its functional oligomeric structure (Estey and Prochaska, 1993; Lee et al., 2001; Sadoski et al., 2001; Musatov and Robinson, 2002).

The "functional core" of COX consists of the mitochondrially encoded subunits, which are experimentally difficult to mutate due to the thousands of mitochondria per cell which each contain their own genome (Brega et al., 2001; Wallace and Fan, 2010). It is therefore necessary to conduct site-directed mutagenesis studies in prokaryotic forms of the enzyme. The two model systems most widely used for such studies are the 124 kD COX from *Parachocus denitrificans* (*P.dent.*) and the 128 kD COX from *Rhodobacter sphaeroides* (*R.sph.*) (Cao et al., 1992; Hosler et al., 1992; Iwata et al., 2002; Svensson-Ek et al., 2002). The three largest subunits of these four subunit bacterial enzymes are structurally and functionally homologous to their mitochondrial counterparts, the functional core of COX. The fourth prokaryotic subunit is not homologous to any mitochondrial subunit and its function is not known. The structural homology of the functional core is shown in Figure 4, a multiple structure alignment of subunits I, II and

Figure 4

Multiple structure alignment of the functional core of cytochrome c oxidase. The aligned x-ray crystal structures of subunits I, II and III are shown for bovine (PDB 1OCC, blue)(Tsukihara et al., 1996), *P.dent.* (PDB 1QLE, green)(Harrenga and Michel, 1999) and *R.sph*. COX (PDB 1M56, red)(Svensson-Ek et al., 2002). Figure from (Geyer, 2007).

III for bovine (blue, PDB 1OCC), *P.dent.* (green, PDB 1QLE), and *R sph.* COX (red, PDB 1M56). *R.sph.* COX is the form of the enzyme used in the studies described herein, as the validity of this model has been well established (Cao et al., 1992; Hosler et al., 1992).

Figure 5 shows the x-ray crystal structure of *R.sph.* COX. The prokaryotic forms of COX crystallize as either a monomer (*P.dent.*) or as a head to tail dimer which would not be structurally possible in the membrane (*R.sph.*). Research suggests that they also function as monomers, although this has not been definitively demonstrated (Shinzawa-Itoh et al., 2007). Subunit I (cyan) is a ~60 kD peptide with 12 transmembrane helices. It contains heme *a* (yellow) and the binuclear active site consisting of heme a_3 (yellow) and Cu_B (green sphere). In addition, there are two conserved proton pathways coordinating a series of conserved water molecules which serve to shuttle protons to the active site and across the membrane. They are designated as the D-pathway (blue, D-pathway residues; red spheres, water molecules) and the K-pathway (magenta, K-pathway residues; pink spheres, waters molecules), named for the conserved residues D132 and K362 in the respective pathways (Brzezinski and Johansson, 2010; Ganesan and Gennis, 2010).

Subunit II (Figure 5, orange) is about 30 kD and contains two transmembrane helices and a large globular beta structure which sits within the mitochondrial innermembrane space or the bacterial periplasm. The subunit II globular domain contains a binding pocket with a number of conserved acidic residues, which facilitate an electrostatic interaction with the conserved lysine residues of cytochrome *c* (Ferguson-Miller et al., 1978). Ferrocytochrome *c* binds at this location and donates its electron to the Cu_A-Cu_A (green spheres) metal center also contained in subunit II. In contrast to the

Figure 5

The x-ray crystal structure of *R.sph.* COX. Subunit I (cyan) consists of 12 transmembrane helices and contains two heme centers (yellow), a Cu_B (green sphere), and the D-pathway and K-pathway for proton transfer. Subunit II (orange) has two transmembrane helices and a globular periplasmic domain which binds and oxidizes cytochrome *c*, receiving the electron onto its Cu_A-Cu_A center (green double sphere). Subunit III (pink) consists of seven transmembrane helices which are separated by a v-shaped cleft into two domains. Subunit IV is a single spanning transmembrane helix (blue). A) Side view in the plane of the membrane with the orientation of the metal centers and proton pathways shown to the right. The blue stick structures and small red spheres are the residues and water molecules of the D-pathway. The magenta stick structures and magenta spheres are the residues and water molecules of the K-pathway. Heme iron is shown as a red sphere with the associated porphyrin ring in yellow. Green spheres are copper atoms. B) Side view showing the v-shaped cleft of subunit III. C) Top view as shown from the periplasmic space, perpendicular to the membrane. Prepared using Accelrys DS Viewer Pro (PDB 1M56)(Svensson-Ek et al., 2002).

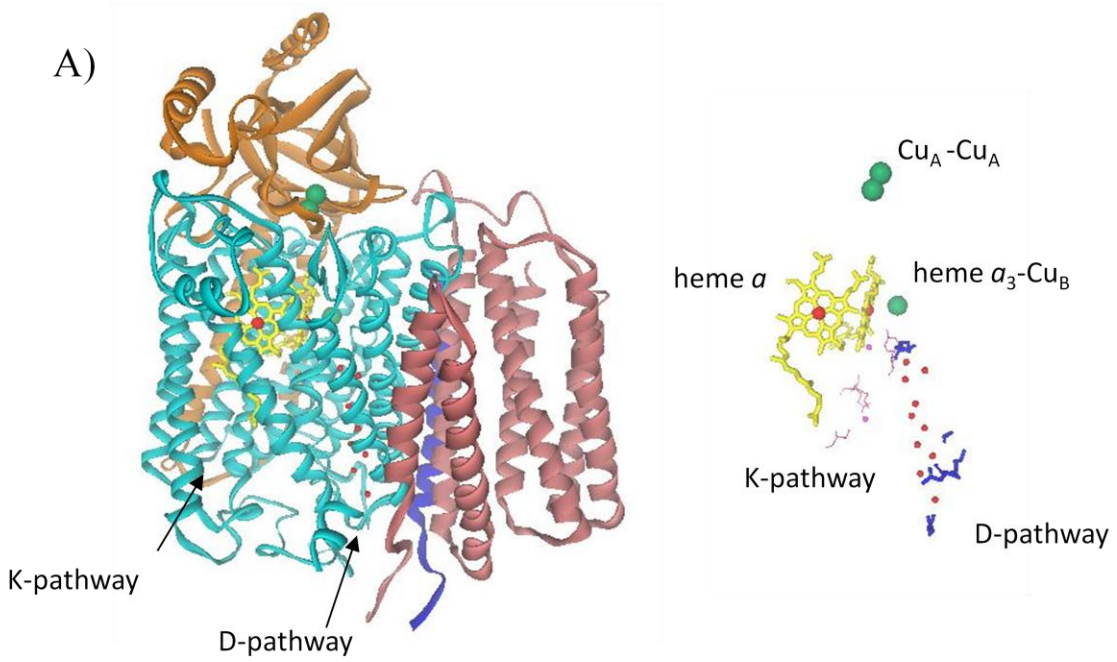
A)
K-pathway
D-pathway
Cu_A-Cu_A
heme *a*
heme a_3-Cu_B
K-pathway
D-pathway

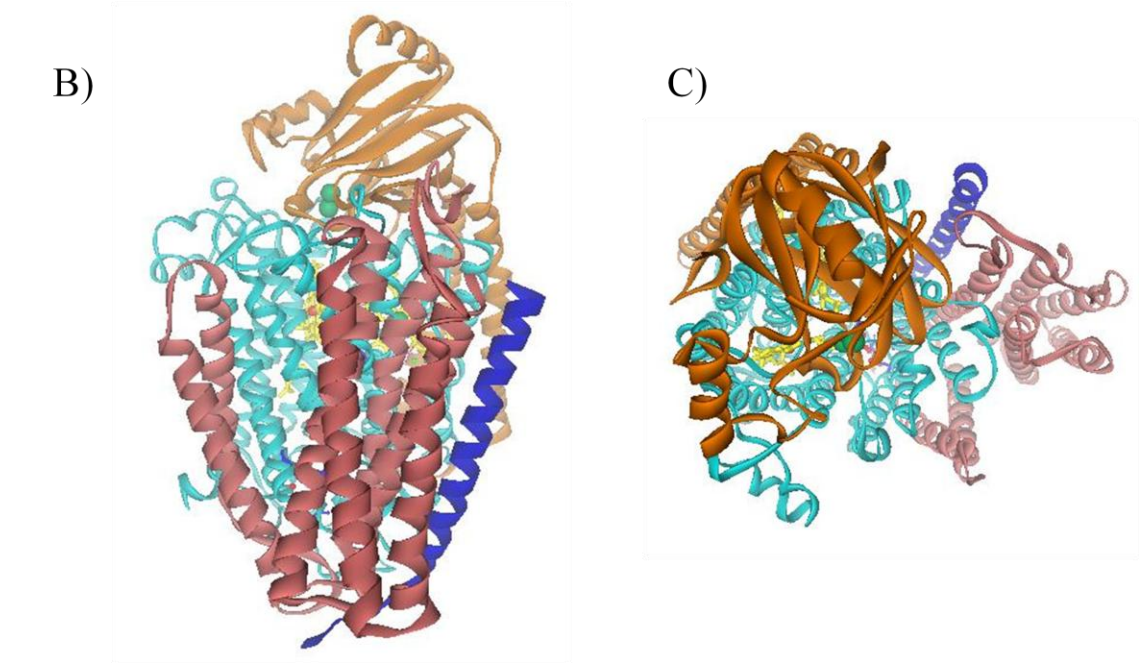
B)
C)

other subunits of the bacterial COX enzyme, subunit IV (blue) is a single spanning transmembrane helix about 5.2 kD in molecular weight and has no homology to any of the mitochondrial subunits.

Subunit III (Figure 5, pink), a 30 kD peptide, shares an extensive interface with subunit I and is composed of seven transmembrane helices which are separated by a v-shaped cleft into two α-helical bundles ((Iwata et al., 2002; Svensson-Ek et al., 2002; Shinzawa-Itoh et al., 2007)). At the n-terminus, two α-helices of subunit III sit along an interface with subunit I in close proximity to the mouth of the D-pathway. There are a number of conserved histidine, acidic and hydrophobic residues on the n-terminus of subunit III that have been proposed to play a functional role (Gilderson et al., 2003; Hosler, 2004). The c-terminal bundle of subunit III, consists of 5 α-helices also containing many conserved residues which seem to be of structural and functional importance (Mather and Rottenberg, 1998; Tiranti et al., 2000; DiMauro and Schon, 2003; DiMauro et al., 2006).

The v-shaped cleft between the two α-helical bundles of subunit III contains two lipids which are resolved in a conserved orientation in the protein x-ray crystal structures of *R.sph.* and bovine COX (Figure 6A)(PDB 1V54 (Tsukihara et al., 2003), PDB 1M56 (Svensson-Ek et al., 2002)). In the bovine structure, these lipids are phosphotidyl glycerols, and in the *R.sph.* structure they are phosphotidyl ethanolamines; the fatty acid tails are 18 carbons long and are singly unsaturated (Varanasi et al., 2006; Shinzawa-Itoh et al., 2007). These lipids are held tightly into place through a variety of ionic

Figure 6

The x-ray crystal structure of *R.sph.* COX showing the resolved lipids contained within the v-shaped cleft of subunit III. Subunits I-IV are shown in the same color scheme as Figure 5. A) Within the v-shaped cleft of subunit III there are two phophotidyl ethanolamines (PL1, dark green; PL2, light green) resolved in the crystal structure. B) The conserved residues in subunits I and III which interact with the phospholipids. The headgroup of PL1 (dark green) is coordinated by R137 of subunit I, and its fatty acid tails interact with a variety of hydrophobic residues conserved in subunits I and III. The headgroup of PL2 (light green) is coordinated by R226 on helix 6 of subunit III, and its fatty acid tails interact with conserved residues on helices 2 and 3 of subunit III. Prepared using Accelrys DS Viewer Pro (PDB 1M56)(Svensson-Ek et al., 2002).

A)

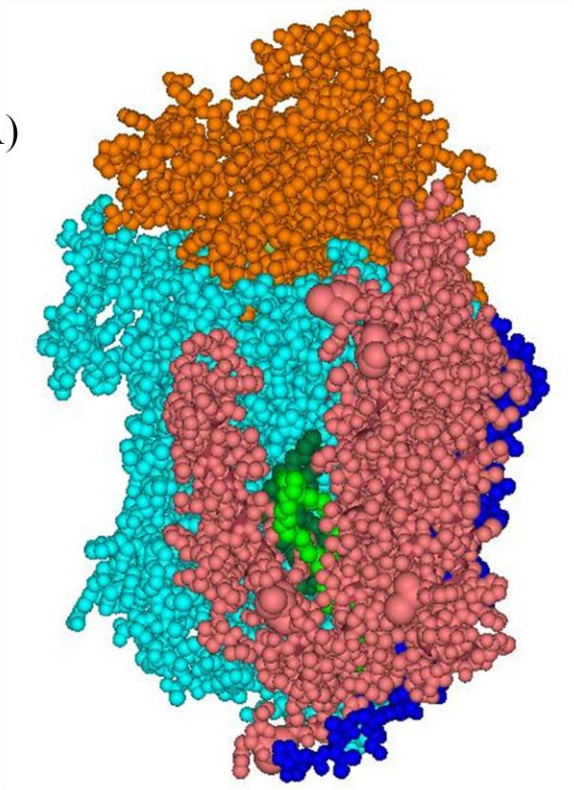

B)

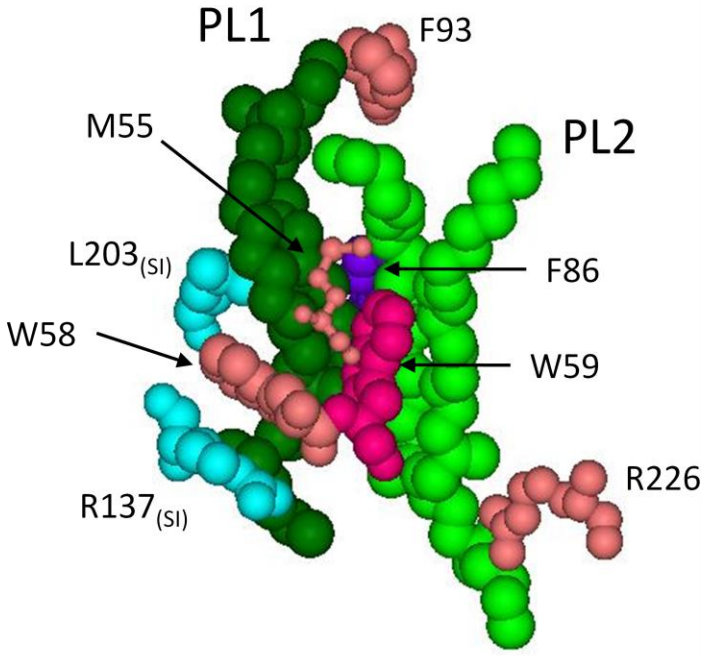

interactions, hydrogen bonds and van der Waals contact with highly conserved residues in subunits I and III. One of the lipids, PL1, sits at the interface with subunit I with its phosphate headgroup being coordinated by R137 in subunit I (Figure 6B, dark green lipid). Its fatty acid tails come into van der Waals contact with several conserved residues on helix 2 and 3 of subunit III, as well as with some conserved residues in subunit I. The headgroup of the second lipid, PL2, forms a strong ionic and hydrogen bond interaction with R226, a highly conserved residue on helix 6 in the c-terminal bundle of subunit III (light green lipid). The fatty acid tail of PL2 forms hydrophobic interactions with several of the conserved residues in helix 2 and 3 of subunit III which also coordinate PL1 (Tsukihara et al., 1996; Svensson-Ek et al., 2002; Shinzawa-Itoh et al., 2007; Varanasi 2006). It has been noted that there is a chain of interactions involving three residues which extends about 16Å from the fatty acid tail of PL1 to H284 of subunit I which is a Cu_B ligand, providing a lipid-mediated structural link between the active site and both domains of subunit III (Varanasi et al., 2006).

Proton and Electron Transfer in Cytochrome c Oxidase

The two enzymatic activities of cytochrome *c* oxidase are to transfer electrons from ferrocytochrome *c* to oxygen and to pump protons across the mitochondrial inner membrane (Hosler et al., 2006; Brzezinski et al., 2008). The reaction stoichiometry is indicated in the following scheme:

$$4 \text{ cytochrome } c^{2+} + O_2 + 8H^+ \rightarrow 2H_2O + 4H^+_{\text{pumped}} + 4 \text{ cytochrome } c^{3+}.$$

Subunits I and II contain the metal centers which are responsible for transferring the electrons necessary for oxygen reduction (Figure 7, blue arrows). Subunit II

Figure 7

Electron and proton pathways in COX. The electron transfer pathway in COX is shown (blue arrows) as well as the D-pathway (red arrow), K-pathway (green arrow) and proton exit pathway (purple hash arrow). Subunit II contains the Cu_A-Cu_A center, which is the initial acceptor of the electron from cytochrome *c*. From here, the electron is transferred to subunit I, first to heme *a* and finally to the heme a_3-Cu_B active site where molecular oxygen binds and is reduced to water. The D-pathway consists of a number of conserved subunit I residues (blue stick structures) which coordinate a series of water molecules (red spheres). The pathway starts at D132 and extends 27Å to E286 where protons are shuttle either to the active site or to a pump site and across the membrane through an unknown exit pathway (purple hash arrow). The K-pathway starts at subunit II residue E101 and extend through conserved residues (magenta stick structure) and coordinated water molecules (magenta spheres) to the active site. Prepared using Accelrys DS Viewer Pro (PDB 1M56)(Svensson-Ek et al., 2002).

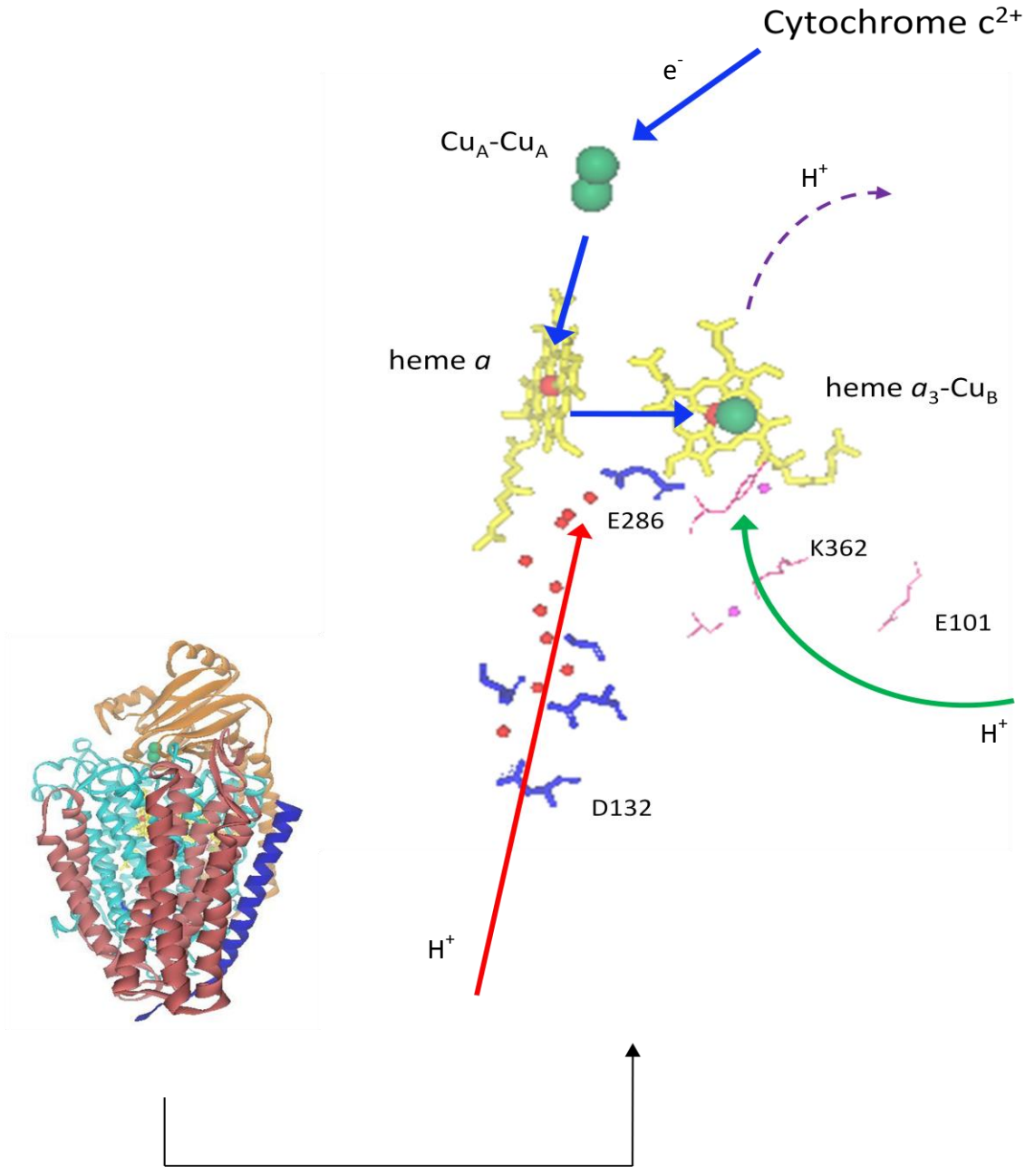
Cytochrome c^{2+}
e^-
Cu_A-Cu_A
H^+
heme *a*
heme a_3-Cu_B
E286
K362
E101
H^+
D132
H^+

electrostatically binds and oxidizes cytochrome c^{2+}, receiving the electron onto its bicupric center (Cu_A-Cu_A). From here, the electron is transferred to subunit I, first to heme *a* and finally to the heme a_3-Cu_B active site where molecular oxygen binds and is reduced to water (Yoshikawa et al., 1998; Jancura et al., 2006).

In addition to its two metal centers, subunit I contains pathways which shuttle protons to the active site and across the membrane (Hosler et al., 2006). The K-pathway provides the protons necessary for the initial reduction of the enzyme prior to oxygen binding (Figure 7, green arrow) (Lepp et al., 2008a; Ganesan and Gennis, 2010). The electrostatic alteration of the active site caused by its reduction drives the uptake of 1-2 protons from the matrix through the K-pathway to the active site. The pathway starts at residue E101 of subunit II which is situated at the interface between subunits I and II. The pathway proceeds to the active site through a series of water molecules, which are coordinated by the conserved residues K362, S299 and Y288 of subunit I (magenta residues). These water molecules (magenta spheres) are resolved in conserved locations in the crystal structures across a range of species and are used to transfer the protons via a Grotthuss mechanism (Brzezinski and Johansson, 2010).

The D-pathway provides from the matrix all protons used for pumping, as well 2-3 of the protons needed to reduce oxygen to water (Figure 7, red arrows) (Lepp et al., 2008b; Brzezinski and Johansson, 2010). The conserved aspartate residue in subunit I (D132) for which the D-pathway is named is putatively the initial proton acceptor of the pathway. An internal water chain extends from D132 approximately 27Å to E286, which is the branch point for protons to be shuttled to the active site or to be pumped to the opposite side of the membrane (Han et al., 2005; Lepp et al., 2008b). The residues which

coordinate this water chain are broadly conserved and are all within subunit I (blue residues). From E286, the protons are either transferred to the active site, or to a proton acceptor in the proton pumping exit pathway (purple hashed arrow). The initial acceptor for the pumped protons has not been identified, but it is thought to involve the heme a_3 propionates and/or H334 (Branden et al., 2005; Pisliakov et al., 2008; Egawa et al., 2009; Lee et al., 2009; Brzezinski and Johansson, 2010).

The mechanism by which COX reduces dioxygen is complex and consists of multiple intermediates, each having characteristic spectroscopic absorbances corresponding to the various oxidation states of the metal centers (Figure 8). The R state is reduced at heme a_3 and Cu_B, and binds O_2 to form the A state with a time constant of τ = 10 μs. Next, two electrons from heme a_3, one electron from Cu_B and an electron and a proton from Y288 are transferred to oxygen, which undergoes molecular scission to form the P state (τ = 200-300 μs) (Gorbikova et al., 2008b). Then, an electron is transferred from heme *a* to the tyrosyl radical and the Cu_B the oxygen ligand is protonated from the D-pathway, resulting in the formation of the F state (τ = 100 μs) (Gorbikova et al., 2008a). The P to F transition is also coupled to a proton pumping event, which involves a second proton uptake through the D-pathway. The decay from F to O is accomplished by a one electron reduction of heme a_3 by heme *a* followed by a protonation of the heme a_3 oxygen ligand via the D-pathway and is coupled to a proton pumping event (τ = 1.5 ms). Another proton is pumped during the subsequent O to E transition, which also involves a displacement of the water molecule at Cu_B, a protonation of Y288 by a K-pathway and a reduction of Cu_B (Adelroth et al., 1997; Jasaitis et al., 1999). The E to R transition is coupled to a proton pumping event and proton uptake through the K-pathway, which

Figure 8

The oxygen reduction catalytic cycle of COX. The oxygen reduction cycle of COX is complex, consisting of multiple intermediates. The redox and ligand states of the heme a_3-Cu_B active site are displayed within the boxes designated with one letter codes for the intermediates. Substrates indicated in blue are utilized or produced in oxygen chemistry. The red protons are those pumped across the membrane. Adapted from (Brzezinski and Johansson, 2010).

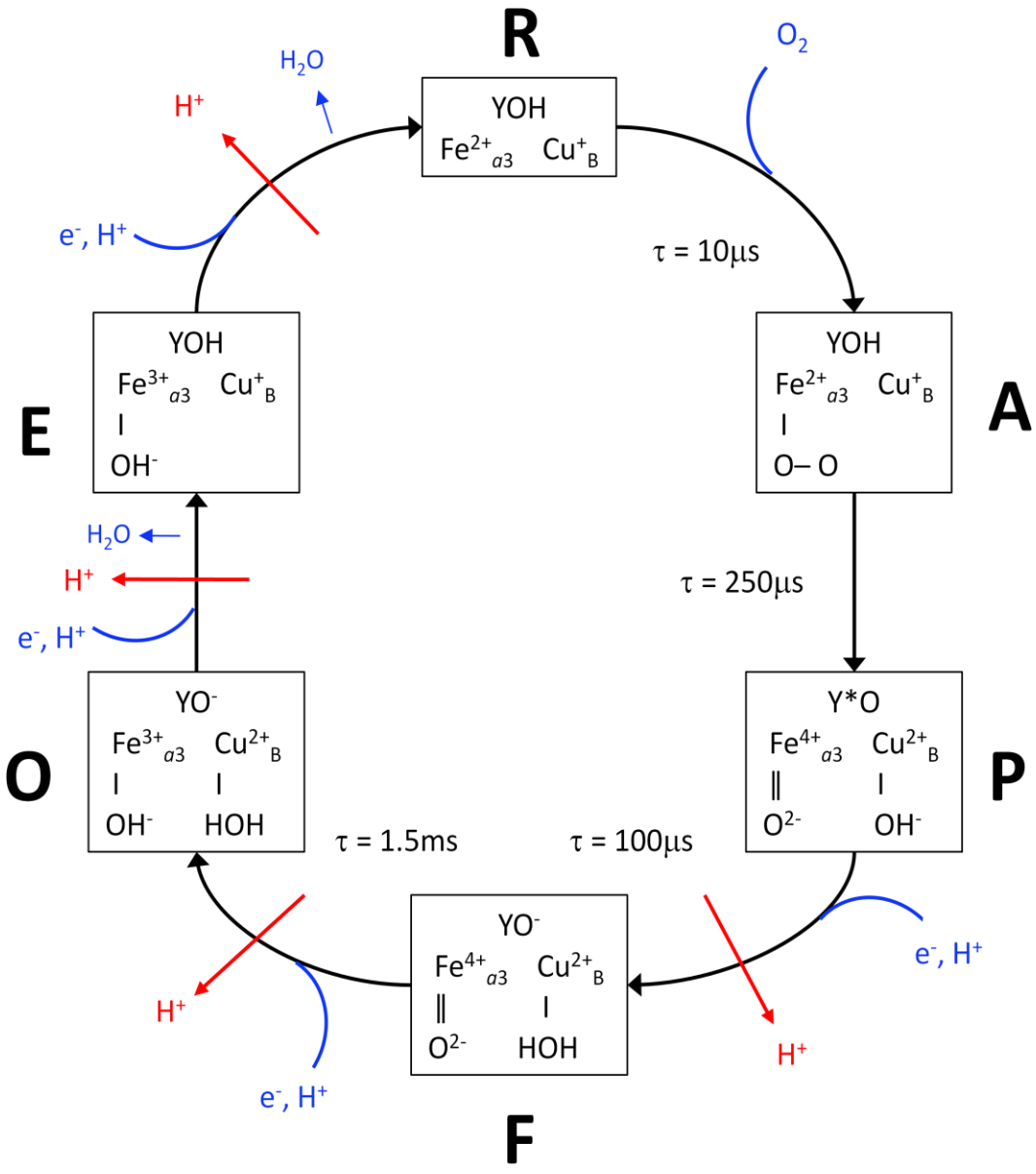
R
YOH
Fe^{2+}_{a3} Cu^{+}_{B}
O_2
H_2O
H^+
e^-, H^+
τ = 10μs
A
YOH
Fe^{2+}_{a3} Cu^{+}_{B}
I
O– O
τ = 250μs
P
Y*O
Fe^{4+}_{a3} Cu^{2+}_{B}
‖ I
O^{2-} OH^-
e^-, H^+
H^+
τ = 100μs
F
YO⁻
Fe^{4+}_{a3} Cu^{2+}_{B}
‖ I
O^{2-} HOH
H^+
e^-, H^+
τ = 1.5ms
O
YO⁻
Fe^{3+}_{a3} Cu^{2+}_{B}
I I
OH^- HOH
H_2O
H^+
e^-, H^+
E
YOH
Fe^{3+}_{a3} Cu^{+}_{B}
I
OH^-
H^+
H_2O
e^-, H^+

provides the proton to the remaining oxygen ligand on heme a_3, allowing it to leave as water (Verkhovsky et al., 2006). The COX molecule has now cycled back to the reduced state and is capable of binding another oxygen molecule (Brzezinski and Gennis, 2008; Brzezinski and Johansson, 2010).

It has been over thirty years since COX was empirically established as a proton pump (Wikstrom, 1977; Krab and Wikstrom, 1978). Since then, much progress has been made toward elucidating the molecular mechanism of the pumping function, although there are still many questions to resolve (Brzezinski and Gennis, 2008). In theory, there are four general components of the current model of the COX proton pump. Firstly, the active site supplies the driving force for proton translocation by the reduction of O_2 to water via the reactions described above. Second, there is a proton loading site for pumped protons which is in some manner coupled to the driving force provided at the active site. Third are the proton pathways necessary to provide protons to the active site and to shuttle protons across the membrane. Finally, there must be a gating mechanism to prevent short circuiting or proton leaks (Brzezinski and Gennis, 2008). Current theories for the mechanism by which the O_2 chemistry at the active site is coupled to the protonation of the proton pump site primarily involve the principle of electroneutrality (see Mitchell and Rich, 1994). In short, it is highly thermodynamically favorable for the negative charge of an electron introduced into the low dielectric environment of the protein interior to be compensated with a positively charged proton. According to this principle, when the electron from cytochrome *c* is transferred from Cu_A to heme *a*, it drives the transfer of a proton from the D-pathway to a pump site, which is in the vicinity of the active site. The subsequent transfer of the electron from heme *a* to heme a_3-Cu_B

drives the transfer of a chemical proton to the active site which in turn expels the proton from the pump site to the exterior of the protein (Salomonsson et al., 2005; Wikstrom and Verkhovsky, 2007; Brzezinski and Gennis, 2008; Sharpe and Ferguson-Miller, 2008). The identity of the pump site is not known, but the most likely current candidates are His 334 or the A-propionate group of heme a_3 (Sharpe and Ferguson-Miller, 2008; Lee et al., 2009; Brzezinski and Johansson, 2010). The gating or valve mechanism must establish unidirectional proton movement from the matrix to the inner membrane space and prevent leaks or short circuits. Multiple mechanisms have been proposed, and the mechanism may include many amino acid residues (Sharpe and Ferguson-Miller, 2008). Given current evidence, E286 which sits at the top of the D-pathway seems to play a predominate role. The mechanism seems to depend upon the proper orientation of water molecules in the vicinity of E286 and may involve a conformation change in the residue side chain (Xu et al., 2007; Sharpe and Ferguson-Miller, 2008; Brzezinski and Johansson, 2010).

The Functional Role of Cytochrome c Oxidase Subunit III

Cytochrome *c* oxidase subunit III is a member of the 3 subunit functional core of the enzyme, although all of the protein's metal centers and proton pathways are contained in subunits I and II. The explicit function of subunit III is not fully understood, but it is highly conserved across all species, sharing 45% sequence identity between the *R.sph.* and human homologs (Saraste, 1990; Varanasi et al., 2006). The severity of *in vivo* mutations in subunit III is further evidence for its importance (Saraste, 1990; Mather and Rottenberg, 1998; Horvath et al., 2002; DiMauro and Schon, 2003; Horvath et al., 2005;

DiMauro et al., 2006), and it has been postulated to play roles in maintaining adequate proton transfer rates in subunit I, in the stabilization of the active site during catalytic turnover, in regulation of oxygen reduction activity, and in the assembly of the COX complex (Bratton et al., 2000; Lincoln et al., 2003; Mills et al., 2003; Mills and Hosler, 2005).

The importance of subunit III in proper COX functioning was demonstrated early on by removing the subunit from the bovine form of the enzyme (Puettner et al., 1985; Prochaska and Reynolds, 1986). The subunit III deficient enzyme had decreased electron transfer activity and its proton pumping efficiency was reduced to an even greater extent (Prochaska and Reynolds, 1986). A similar effect was also observed when the conserved subunit III residue E90 was labeled with DCCD (Prochaska et al., 1981). The deleterious effects caused by DCCD labeling were shown to be accompanied by a conformational change in subunit III which was likely caused by a disruption in hydrogen bonds within the subunit (Ogunjimi et al., 2000).

In more recent years, the functional role of subunit III has been examined by studies that remove the subunit from the bacterial forms of the enzyme, *R.sph.* or *P.dent.* COX, leaving only subunits I and II of the functional core (I-II OX). The removal of subunit III results in a reduction of the enzyme's catalytic lifetime to only about 0.5% of that of four subunit COX (Bratton et al., 1999; Gilderson et al., 2003; Hosler, 2004; Mills and Hosler, 2005; Varanasi et al., 2006). This shortened catalytic lifetime is the result of the phenomenon termed turnover-induced inactivation, which is a spontaneous and irreversible inactivation of the enzyme which takes place only during catalytic turnover and is accompanied by structural alteration of the heme a_3-Cu_B active site. Specifically,

the heme a_3 center of the inactivated enzyme is in a more flexible structural environment and Cu_B is depleted from the active site which displays decreased binding to oxygen-intermediate analogs (Bratton et al., 1999). At low pH (6.5), the initial rate of O_2 reduction activity of I-II OX is unimpeded, however the pH dependence of its activity is altered such that at physiological pH it is only about half that of normal COX, corresponding to a decrease in the rate of proton uptake in the D-pathway from bulk solution through D132 to E286 (Gilderson et al., 2003). I-II OX also shows a decrease in proton pumping efficiency to about half that of normal COX, which could be due to impeded proton flow through the D-pathway and through the proton exit pathway and/or due to a structural alteration in the environment of subunit I E286, which could hinder its ability to protonate the pump site (Gilderson et al., 2003; Mills et al., 2003). The mechanism of turnover-induced inactivation is not known, but the impedance of D-pathway proton uptake increases the lifetimes of the reactive oxoferryl intermediates P and F (see Figure 8), allowing for the possibility of a hydroxylation reaction in the vicinity of the active site (Mills et al., 2003; Mills and Hosler, 2005).

The preceding results suggest a role for subunit III in maintaining adequate proton uptake through the D-pathway. Indeed, direct measurement of D-pathway proton uptake in the absence of subunit III shows a rate that is only about 3-4% of four subunit COX (Gilderson et al., 2003). One mechanism by which subunit III might facilitate D-pathway proton uptake is by the function of a putative proton antenna on its n-terminus. D132 is surrounded by a number of conserved protonatable residues in subunit III which are thought to collect protons and transfer them to D132 at a rate faster than simple diffusion from bulk solution allows, thus serving as a putative “proton collection antennae” (Mills

et al., 2003; Hosler, 2004; Adelroth and Hosler, 2006). In addition, the shift in pH profile of proton uptake through the D-pathway seen in the absence of subunit III suggests an alteration in a protonateable residue within the pathway, perhaps D132 itself. The n-terminus of subunit III also contains a stretch of conserved hydrophobic residues which may play a role in fine tuning an optimal pKa of D132 for maximal D-pathway uptake (Gilderson et al., 2003; Hosler, 2004).

Subunit III may also serve to stabilize the structure of the subunit I active site during catalytic turnover. Even when proton uptake through the D-pathway is completely abolished by the mutation of D132 to an alanine, the removal of subunit III from D132A still results in a 10 fold decrease in its catalytic lifetime (Mills and Hosler, 2005; Adelroth and Hosler, 2006). This suggests that there is an additional protective mechanism against turnover-induced inactivation provided by subunit III, such as structural stabilization, which does not depend upon the rate of proton uptake through the D-pathway. The presence of subunit III could decrease the degree of structural oscillations in the active site thereby lowering the probability of a hydroxylation reaction. Stabilization would be mediated via long range protein-protein interactions, and may be enhanced by the presence of the structural lipids within the v-shaped cleft of subunit III (Hosler, 2004; Varanasi et al., 2006). Mutagenesis of the conserved residues which bind the cleft lipids increases the propensity of the enzyme to undergo turnover-induced inactivation without slowing proton uptake through the D-pathway (Varanasi et al., 2006). It has been proposed that the structural lipids act as a "flexible buttress," allowing small catalysis-associated motions within the active site while preventing larger scale motions which

could increase the probability of turnover-induced inactivation (Hosler, 2004; Varanasi et al., 2006).

Finally, subunit III might be involved in facilitating proper assembly of COX (Bratton et al., 2000; Tiranti et al., 2000). One of the early assembly intermediates of COX is a form of subunit I which contains a heme *a* center but not the heme a_3-Cu_B active site. This form of subunit I, denoted subunit I*a*, appears to accumulate in the membrane in the initial stages of assembly (Bratton et al., 2000; Fontanesi et al., 2008; Fernandez-Vizarra et al., 2009). The next step in assembly of *R.sph.* COX involves the insertion of the heme a_3-Cu_B active site and requires the presence of subunit II and some additional assembly factors (Bratton et al., 2000; Smith et al., 2005). When subunit III has been genetically deleted from the *R.sph.* genome, COX subunits I and II are capable of folding correctly with proper insertion of all their metal centers. However, there is a significant enrichment of subunit I*a* in these cells, suggesting that although subunit III is not required for proper assembly of subunits I and II, it does participate in the process, perhaps by increasing the rate of assembly by stabilizing an assembly intermediate (Bratton et al., 2000). Proper assembly of COX is also aided by various proteases which degrade improperly folded subunits (Stiburek and Zeman, 2010). These proteases are located in both the matrix and inner-membrane space and are conserved from prokaryotes to mammalian mitochondria (Tatsuta and Langer, 2009).

Specific Aims

The research designs of this dissertation are aimed at elucidating the structural and functional properties of *Rhodobacter sphaeroides* cytochrome *c* oxidase (*R.sph.* COX). The dissertation is divided into two parts, each with different aims:

Specific Aim 1: To examine the functional oligomeric structure of *R.sph.* COX via discontinuous sucrose gradient ultracentrifugation.

Mitochondrial COX crystalizes as a dimer and has been shown to exist in the dimeric state under mild detergent concentration and within a phopholipid bilayer (Estey and Prochaska, 1993; Tsukihara et al., 1996; Nguyen et al., 2002). *R.sph.* COX does not crystallize in a functional dimeric state, and its oligomeric structure within a phospholipid bilayer is unknown (Svensson-Ek et al., 2002). In this aim, discontinuous sucrose gradient ultracentrifugation was used to purify phospholipid vesicles containing COX from those lacking protein. The biophysical and biochemical characterization of these purified vesicles containing *R.sph*. sheds insight into its oligomeric structure in a membrane environment.

Specific Aim 2: To examine the structural and functional significance of a c-terminal truncation in subunit III of *R.sph.* COX.

A human mitochondrial disease resulting in severe lactic acidosis episodes has been shown to result from a mutation in which the four c-terminal helices of subunit III have been genetically deleted by a stop codon introduced into the mitochondrial DNA (Tiranti et al., 2000). In order to assess the structural and functional importance of the c-

terminal domain of COX subunit III, the corresponding mutation was made in *R.sph* COX (Δ114). This mutation removes the bulk of the c-terminal helical bundle while retaining the v-shaped lipid-binding cleft, the subunit I-subunit III interface, and the residues conserved in the putative D-pathway proton antenna of subunit III. The structural and functional properties of this mutant were compared to wildtype COX and to two forms of COX in which subunit III has been genetically or biochemically removed. Characterization of this mutant can shed insight into the functional importance of n-terminal and c-terminal domains of subunit III as well as into the importance of its lipid-binding cleft.

II. Materials and Methods

Mutagenesis of R.sph. COX Subunit III

A c-terminal truncation of *R.sph.* COX subunit III was created to model a human mitochondrial disease mutation (Tiranti et al., 2000). Figure 9A shows the protein sequence alignment of *R.sph*. and human COX subunit III. The stop codon introduced in the human sequence at Q111 corresponds to I115 in *R.sph.* COX. Site-directed mutagenesis of subunit III was conducted using a Stratagene QuickChange kit. Figure 9B shows the DNA and protein sequences of *R. sphaeroides* COX subunit III, highlighting the location of I115 which was mutated to a stop codon to form Δ114 COX. The primers used to mutagenesis are shown in Figure 9C. The template DNA of subunit III used for mutagenesis was incorporated into a plasmid termed pMB301, shown in Figure 10A (Bratton et al., 2003). For mutagenesis, 20 ng of pMB301 was mixed with 125 μg of the forward and reverse primers in addition to reaction buffer, dNTP mix, and Pfu DNA polymerase provided with the Stratagene kit (50 μL final volume). Following an initial 30 second melting phase at 95˚C, sixteen thermocycles were conducted in a PCR thermocycler, each consisting of a 30 second melting phase (95˚C), a 1 minute annealing phase (55˚C) and 5 minutes of polymerase extension (68˚C). Parental DNA was selectively degraded by adding the restriction enzyme DpnI and digesting at 37˚C for 1 hour. This reaction was used to transform Stratagene XLI-Blue Supercompetent cells

Figure 9

DNA, protein and primer sequences used for site-directed mutagenesis of *R.sph.* COX subunit III. A) Protein sequence alignment of the n-terminus of subunit III in *R.sph.* and human COX showing the location of the truncation in red. Human Q111 aligns with I115 in the *R.sph.* sequence. B) The DNA and protein sequence of *R.sph.* COX subunit III. Pink shading indicates the binding region of the PCR primers used for site-directed mutagenesis. The residue mutated to a stop codon (I115) in the Δ114 truncation mutation is shaded blue. B) The sequence of the forward and reverse primers used for site-directed mutagenesis. The underlined residues are mismatched from the original sequence.

A)

```
R.sph.MAHAKNHDYHILPPSIWPFMASVGAFVMLFGAVLWMHGSGPWMGLIGLVVVLYTMFGWWS 60
Human MTHQS-HAYHMVKPSPWPLTGALSALLMTSGLAMWFHFHSMTLLMLGLLTNTLTMYQWWR 59

R.sph.DVVTES-LEGDHTPVVRLGLRWGFILFIMSEVMFFSAWFWSFFKHALYPMGPESPIIDGI 119
Human DVTRESTYQGHHTPPVQKGLRYGMILFITSEVFFFAGFFWAFYHSSLAPT----PQLGGH 115
```

B)

atg	gcc	cac	gcc	aag	aac	cac	gac	tac	cac	atc	ctg	ccg	ccc	tcg	atc	tgg	ccc
M	A	H	A	K	N	H	D	Y	H	I	L	P	P	S	I	W	P18
ttc	atg	gcc	tcg	gtc	gga	gcc	ttc	gtc	atg	ctg	ttc	ggc	gcc	gtg	ctc	tgg	atg
F	M	A	S	V	G	A	F	V	M	L	F	G	A	V	L	W	M36
cac	ggc	tcg	ggg	ccc	tgg	atg	ggg	ctg	atc	ggg	ctc	gtc	gtc	gtg	ctc	tac	acg
H	G	S	G	P	W	M	G	L	I	G	L	V	V	V	L	Y	T54
atg	ttc	ggc	tgg	tgg	tcc	gac	gtg	gtg	acg	gaa	agc	ctc	gag	gcg	acc	aca	cgc
M	F	G	W	W	S	D	V	V	T	E	S	L	E	G	D	H	T72
cgg	tgg	tgc	gtc	tgg	gcc	tgc	gct	ggg	gct	tca	tcc	tct	tca	tc	atg	tcc	gag
P	V	V	R	L	G	L	R	W	G	F	I	L	F	I	M	S	E90
gtg	atg	ttc	ttc	tcg	gcc	tgg	ttc	tgg	agc	ttc	ttc	aag	cac	gcg	ctc	tat	ccg
V	M	F	F	S	A	W	F	W	S	F	F	K	H	A	L	Y	P108
atg	ggg	ccc	gag	agc	ccg	atc	atc	gac	ggg	atc	ttt	ccg	ccc	gag	ggg	atc	atc
M	G	P	E	S	P	I	I	D	G	I	F	P	P	E	G	I	I126
acc	ttc	gat	ccg	tgg	cat	ctg	ccg	ctc	atc	aac	acg	ctg	atc	ctg	ctc	tgc	tcg
T	F	D	P	W	H	L	P	L	I	N	T	L	I	L	L	C	S144
ggc	tgc	gcg	gcc	acc	tgg	gcg	cac	cat	gcg	ctg	gtg	cat	gag	aac	aac	cgc	cgc
G	C	A	A	T	W	A	H	H	A	L	V	H	E	N	N	R	R162
gac	gtg	gcc	tgg	ggg	ctg	gcg	ctc	gcc	atc	gcg	ctc	ggc	gcg	ctc	ttc	acg	gtg
D	V	A	W	G	L	A	L	A	I	A	L	G	A	L	F	T	V180
ttc	cag	gcc	tac	gaa	tac	agc	cac	gcg	gcc	ttc	ggc	ttc	gcg	ggc	aac	atc	tat
F	Q	A	Y	E	Y	S	H	A	A	F	G	F	A	G	N	I	Y198
ggc	gcc	aac	ttc	ttc	atg	gcg	acg	ggc	ttc	cac	ggc	ttc	cac	gtc	atc	gtg	ggc
G	A	N	F	F	M	A	T	G	F	H	G	F	H	V	I	V	G216
acg	atc	ttc	ctg	ctc	gtc	tgc	ctg	atc	cgg	gtg	cag	cgc	ggc	cac	ttc	acc	ccc
T	I	F	L	L	V	C	L	I	R	V	Q	R	G	H	F	T	P234
gag	aag	cat	gtc	ggc	ttc	gag	gcg	gcg	atc	tgg	tac	tgg	cac	ttc	gtc	gat	gtg
E	K	H	V	G	F	E	A	A	I	W	Y	W	H	F	V	D	V252
gtc	tgg	ctg	ttc	ctc	ttc	gcc	tcg	atc	tac	atc	tgg	ggc	cag	taa			
V	W	L	F	L	F	A	S	I	Y	I	W	G	Q	STOP			

C)

```
Forward 5′-GGGCCCGAGAGCCCGTAAATCGACGGGATCTTTC-3′
Reverse 3′-CCCGGGCTCTCGGGCATTTAGCTGCCCTAGAAAG-5′
```

Figure 10

Schematic of site-directed mutagenesis protocol for constructing *R.sph.* COX subunit III mutants. Site directed mutagenesis was conducted on COX subunit III using pMB301 as the template DNA. A) Mutated pMB301 and pMB307 were digested with XmaI, and the 0.9 kb fragment from pMB301 containing mutant subunit III was ligated into the linearized pMB301 vector. B) pMB307+III and pRK415 were digested with HindIII and EcoRI, and the 5.2 kb fragment from pMB307+III was ligated into the linearized pRK415 vector. C) The pRK415+COX plasmid contains genes for COX Subunit II, cox10, cox11, mutant subunit III, and COX subunit I with a poly histidine tag. Arrows indicate the direction of transcription.

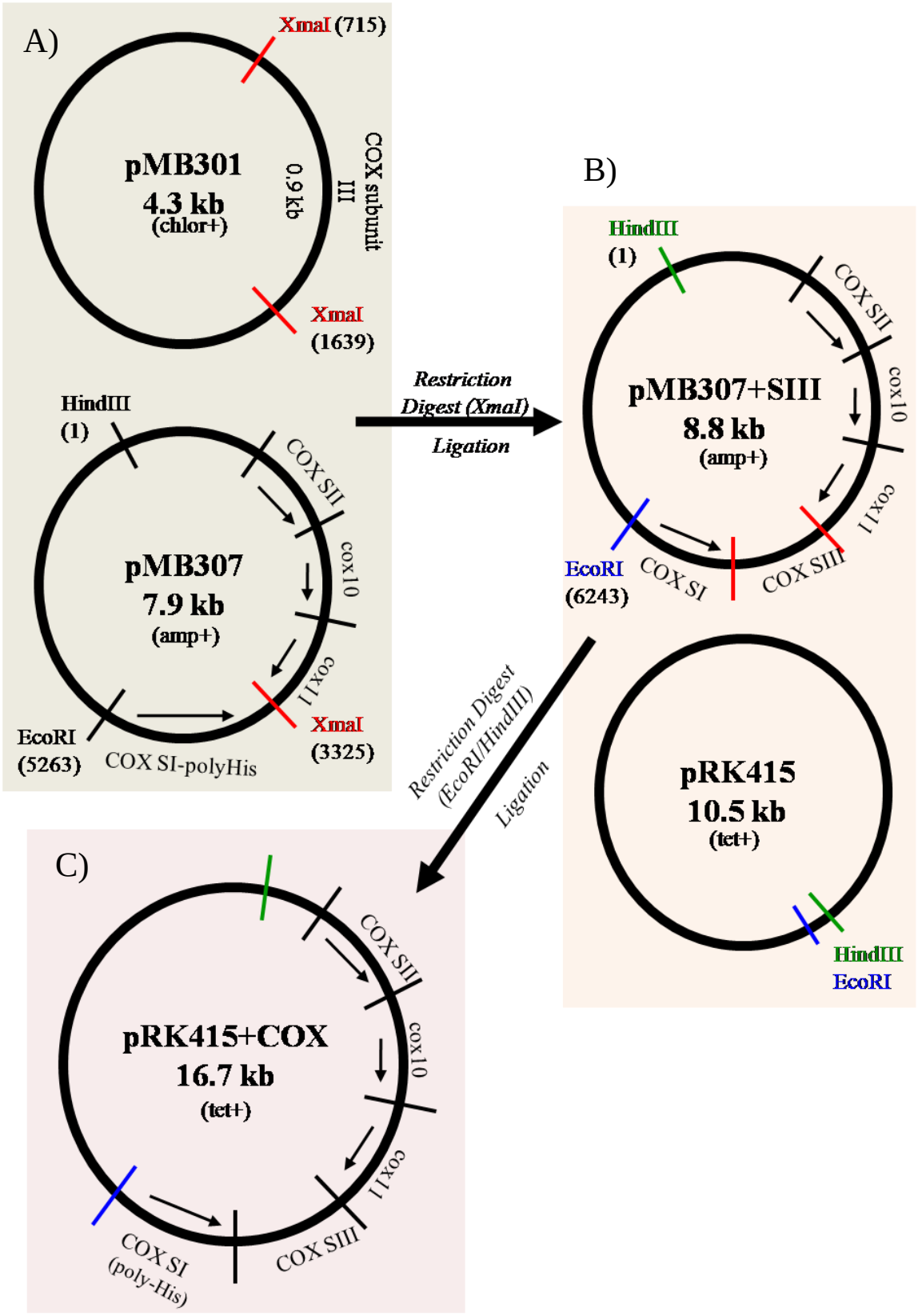
A)
XmaI (715)
pMB301
4.3 kb
(chlor+)
0.9 kb
COX subunit III
XmaI
(1639)
HindIII
(1)
COX SII
cox10
pMB307
7.9 kb
(amp+)
cox11
EcoRI
(5263)
COX SI-polyHis
XmaI
(3325)
Restriction
Digest (XmaI)
Ligation
B)
HindIII
(1)
COX SII
cox10
pMB307+SIII
8.8 kb
(amp+)
cox11
EcoRI
(6243)
COX SI
COX SIII
Restriction Digest
(EcoRI/HindIII)
Ligation
pRK415
10.5 kb
(tet+)
HindIII
EcoRI
C)
COX SIII
cox10
pRK415+COX
16.7 kb
(tet+)
cox11
COX SI
(poly-His)
COX SIII

which were subsequently spread onto LB plates containing 10 μg/mL chloroamphenicol and incubated overnight at 37˚C. Resulting colonies were used to inoculate 3 mL LB cultures (10 μg/mL chloro), which were grown with shaking for 12-16 hours at 37˚C. A Qiagen QIAprep Spin Miniprep kit was used to isolate the pMB301 plasmid, which was sequenced by Davis Sequencing (Davis, CA) for verification of the desired mutation.

Mutated pMB301 (pMB301-Δ114) and the plasmid pMB307 (see Figure 10A) were digested with XmaI for 45 minutes at 37˚C, and the digestion fragments were separated by 1% agarose gel electrophoresis (Tris-Acetate-EDTA buffer, 60 volts for 1 hour). The 0.9 kb subunit III insert from pMB301-Δ114 and the 7.9 kb linearized vector from pMB307 were purified by gel extraction using a Qiagen QIAquick Gel Extraction kit. Ligation was performed using a New England BioLabs Quick Ligation kit, using approximately 50 ng of vector and 500 ng of insert in a total volume of 20 μL. The entire ligation reaction was used to transform Stratagene XL-10 Gold Ultracompetent cells, which were incubated overnight on LB plates at 37˚C (40 μg/mL ampicillin). Colonies were used to inoculate 3 mL cultures (LB, 40 μg/mL amp, 12-16 hours, 37˚C, shaking), and the pMB307-Δ114 plasmids were isolated via miniprep. In order to screen for proper insertion orientation, pMB307-Δ114 plasmid DNA was digested with XhoI for 1 hour at 37˚C, and the fragments were separated by 1% agarose gel electrophoresis. Plasmids with the correct insertion orientation resulted in fragment sizes of 6.2 kb and 2.6 kb.

pMB307-Δ114 and the broad-host range vector pRK-415 (see Figure 10B) were digested with EcoRI and HindIII for 40 minutes at 37˚C. The 6.2 kb fragment from pMB307-Δ114 which contained COX subunits I, II and III-Δ114 and two requisite accessory genes was purified via gel extraction. This insert was ligated into the gel

extracted 10.5 kb EcoRI/HindIII vector from pRK415. The ligation was conducted as above utilizing approximately 50 ng of vector and 250 ng of insert (20 μL final volume). This ligation reaction was used to transform Stratagene JM109 cells, which were incubated overnight at 37˚C on LB plates containing 2.5 μg/mL tetracycline. Resultant colonies were used to inoculate 3mL cultures grown as above, and the plasmids were isolated by miniprep and checked for proper ligation via an EcoRI/HindIII double digest and gel electrophoresis which yields fragments of 6.2 kb and 10.5 kb if correct.

Triparental conjugation was used to create a strain of *R. sphaeroides* that expressed the subunit III-Δ114 mutant form of COX (Figurski and Helinski, 1979). JM109 cells containing pRK415-Δ114 and HB101 cells containing the helper plasmid pRK2013 were grown for 16 hours at 37˚C in 3 mL LB cultures containing 2.5 μg/mL tetracycline and 30 μg/mL kanamycin, respectively. Concurrently, *R. sphaeroides* YZ-200 cells – a strain in which the genes for subunits II and III have been deleted from the genome – were grown to an OD_{660} of 1.0-1.2 in 3 mL Sistrom's media containing both 50 μg/mL spectinomycin and 50 μg/mL streptinomycin (Sistrom, 1962; Zhen et al., 1998). Two milliliters of the YZ-200 culture, 1 mL of the JM109 culture, and 1 mL of the HB101 culture were separately spun down in sterile eppendorf tubes using a lab bench microcentrifuge. The pellets were each washed 3 times in 1 mL of sterile 1x Phos Buffer (30 mM potassium phosphate, pH 7.0) and then combined in 100 μL of the same buffer. The mixture was pipetted onto a Peptone-Yeast Extract agar plate which contained no antibiotics and was incubated upside down 12-16 hours at 30-32˚C. The cells were collected, suspended in 100 μL of sterile 1x Phos Buffer and spread onto a Sistrom's agar plate containing 50 μg/mL spectinomycin, 50 μg/mL streptinomycin and 1 μg/mL

tetracycline. Colonies began to develop after 3-4 days of incubation at 30-32˚C and were restreaked on fresh Sistrom's plates containing the three antibiotics. Colonies that formed were used to overexpress COX-Δ114 as described below.

Expression and Purification of COX from R. sphaeroides

R. sphaeroides cytochrome *c* oxidase was expressed in a strain of the bacterium in which genomic subunit II and subunit III have been deleted (termed YZ-200). The strain also contains resistance genes to spectinomycin and streptomycin (Zhen et al., 1998). These cells are conjugated with a plasmid (pRK415, see Figure 10C) containing genes for subunit II, for the assembly accessory genes cox10 and cox11, for tetracycline resistance, for wildtype or mutant subunit III, and for subunit I, which has been genetically engineered to contain a 6 histidine tag at the c-terminus. A form of oxidase in which subunit III is genetically deleted ($I\text{-}II_{GD}$) can also be expressed by using the pRK415 plasmid without the subunit III insertion.

Three milliliters of Sistrom's media was inoculated with 100 μL of the appropriate YZ-200 glycerol stock, and the cells were grown in a shaking incubator at 30-32ºC (300 rpm) to an OD_{660} of 0.8-1.0 in the presence of 50 μg/mL spectinomycin, 50 μg/mL streptomycin and 1 μg/mL tetracycline. Entire 3 mL cultures were used to inoculate 100 mL cultures, which were grown in baffled flasks under the same conditions. When the cultures reached an OD_{660} of 0.8-1.0, 12-15 mL were used to inoculate 250 mL cultures grown in 1 L baffled flasks. Cultures typically reached an OD_{660} of 1.0-1.2 within 20-24 hours at which point they were harvested by centrifugation

at 11,300 x *g* and stored at minus 80ºC after washing the pellet in 50 mM potassium phosphate, 1 mM EDTA, pH 7.2.

Frozen pellets were resuspended in BioNeb Buffer (10 mM Tris, 10 mM EDTA, 10 mM $MgCl_2$, 20% glycerol, pH 8.0). Phenylmethylsulfonylfluoride (PMSF, 1mM), lysozyme (25 mg/mL) and DNAse I (50 μg/mL) were added, and the suspension was homogenized and passed through a Bio-Neb (Bio-Rad) apparatus 5-7 times at 100 psi. Centrifugation at 24,000 x *g* removed unlysed cells, and the supernatant was decanted and analyzed for heme aa_3 concentration on a Hewlett Packard 8453 UV/Visible diode array spectrophotometer using the reduced *minus* oxidized spectrum, which has an extinction coefficient of $\varepsilon = 24{,}000\ M^{-}cm^{-}$ at 606-630 nm (van Gelder, 1966). The supernatant was supplemented with 100 μL of 100 mM PMSF and subjected to 153,000 x *g* for 1.5 hours at 4ºC using a Ti50.2 rotor in a Beckman Optima LE-80K preparative ultracentrifuge. The resulting membrane pellet was washed in 50 mM potassium phosphate, 1 mM EDTA, pH 7.2, and the ultracentrifuge step was repeated after adding PMSF to 1 mM. The membrane pellet was stored at minus 80ºC after decanting the supernatant (Zhen et al., 1998).

Purification of *R.sph.* COX was accomplished via Ni^{2+}-NTA chromatography utilizing the poly-histidine tag on subunit I. The membrane pellet was resuspended in 10 mM Tris-KOH, 40 mM KCl, pH 8.0. Dodecyl maltoside (DM) was added to 2% and the mixture was stirred for 15 minutes at 4ºC and then centrifuged at 37,000 x *g* for 20 minutes at 4ºC. The supernatant was transferred to a polycarbonate tube; imidazole was added to 10 mM, and 0.8 mL of Ni^{2+}-NTA resin (Qiagen) was added per mg of COX. The mixture was rocked on a platform at 4ºC for 1 hour and then poured into a Bio-Rad

glass econo-column (0.7 cm inner diameter, 30-50 cm length) and allowed to settle without flow for 10-15 minutes. Gravity flow at a rate of 0.2-0.3 drops/second was used to pack the column after which it was washed with 5-10 bed volumes of running buffer (10 mM Tris-KOH, 40 mM KCl, 10 mM Imidazole, 0.1% DM, pH 8.0). Once the flow through was clear, 2-3 bed volumes of elution buffer was layered onto the column (10 mM Tris-KOH, 40 mM KCl, 100 mM histidine, 0.1% DM, pH 8.0) and the flow rate was slowed to 0.1-0.2 drops/second in order to keep the enzyme concentrated. The green tinted fractions in the eluent were pooled and concentrated using 2 mL Millipore YM-100 Centricon devices at 4ºC. Multiple dilution and concentration steps were employed to lower the histidine concentration below 1 mM using resuspension buffer (10 mM Tris-KOH, 40 mM KCl, pH 8.0).

Biochemical Depletion of Subunit III from R.sph. COX

In order to remove subunit III, purified *R.sph.* COX incorporating a subunit I histidine tag was incubated on a rotating platform at 4°C in 20 mM Tris, 150 mM KCl and 12-15% Triton X-100 for 30 minutes. The ratio of Triton X-100 to COX was 100 mg detergent to 1 mg protein. Imidazole was added to 10 mM and 0.8 mL of Ni^{2+}-NTA resin (Qiagen) was added for each milligram of oxidase. The slurry was incubated at 4°C on a rocker platform for 15-30 minutes and then poured into an empty column and packed at a fast flow rate. The column was washed with 10 bed volumes of Triton wash buffer (20 mM Tris, 150 mM KCl, 10 mM Imidazole, 0.05% Triton X-100, pH 7.5), and then 10 bed volumes of DM wash buffer (20 mM Tris, 150 mM KCl, 10 mM Imidazole, 0.05% DM, pH 7.5). The enzyme was eluted with elution buffer (20 mM Tris, 150 mM KCl,

100 mM Histidine, 0.05% DM, pH 7.5), and the entire procedure was repeated. After the second elution, 2 mM EDTA was added to remove surface metal from the enzyme. To reduce the histidine concentration below 1 mM, the sample was repeatedly washed and concentrated in Millipore YM-100 Microcon filter devices using filtration wash buffer (20 mM Tris, 50 mM KCl, 0.05% DM, pH 7.5). The approximate yield of I-II_{BD} was 35%.

Two Dimensional PAGE of Wildtype and Mutant R.sph COX

Blue Native Polyacrylamide Gel Electrophoresis (BN-PAGE) was conducted using a modification of Schagger's method for membrane protein complexes (Schagger and von Jagow, 1991). *R. sphaeroides* COX stock enzyme was diluted to 0.7 μg/μL in 16% glycerol, and 7 μg of sample was loaded per well onto a 4-15% gradient polyacrylamide gel (Bio-Rad Ready Gel Tris-HCl, pH 8.8, Mini-PROTEAN). Electrophoresis at 40 V for 30 minutes was followed by electrophoresis at 80 V for 4 hours at 4°C, using a discontinuous buffer system (Cathode Buffer = 50 mM Tricine, 15 mM BisTris, 0.002% Serva Blue, pH 7.0 at 4°C; Anode Buffer = 50 mM BisTris-HCl, pH 7.0 at 4°C). The Serva Blue contained in the cathode buffer induced a charge shift in the enzyme, so separation of the native enzyme forms was based primarily on size. Following electrophoresis, an image of the gel was taken on a Fuji LAS-4000 imager in precision mode.

SDS-PAGE was used to separate the native bands into their denatured components along a second dimension. The selected bands, detected as areas of stain, were excised from the native gel with a razor blade and incubated in 2% SDS at 37°C for

30 minutes. The incubated bands were placed in a slot well within a 1 cm 6% stacking layer of a 16% polyacrylamide gel (pH 8.8) containing 6 M urea and secured with 1% agarose (Fuller et al., 1981). Electrophoresis was performed at 60 V for 25 minutes and then 120 V for 2.5 hours. The gel was then stained with Coomassie G-250 according to manufacturer's directions (Bio-Rad) and subsequently silver stained according to the method described below. Images of the Coomassie stained and silver stained gels were captured on a Fuji LAS-4000 imager in the precision mode.

Silver Staining Polyacrylamide Protein Gels

Silver staining of PAGE protein gels was used to visualize protein bands with 10 ng/band sensitivity. In a glass container, the gels were soaked in 7% acetic acid for 7 minutes followed by two 20 minute washes in 50% methanol and two 10 minute washes in Milli-Q water. The gels were soaked for 15 minutes in staining solution (0.8% silver nitrate, 0.36% NaOH, 0.2 M NH_4OH) and then washed twice for 5 minutes each with Milli-Q water before swirling in developing solution (0.005% citric acid, 0.02% formaldehyde) until the bands were of the desired intensity (about 3 minutes). Development was stopped by three rinses in Milli-Q water. Gels were immediately imaged on a Fuji LAS-4000 imager in the precision mode.

Estimating Subunit III Content of R.sph. Δ114 COX from Two Dimensional PAGE

Two dimensional PAGE was conducted on wildtype and mutant forms of COX as described above. Silver stained second dimension SDS-PAGE gels were used to estimate

the subunit III stoichiometry of the Δ114 truncation mutation. The density of the subunit bands were quantified using Fujifilm MultiGuage V2.2 software.

Protein Immunoblotting of R.sph. COX Subunit III

In order to conduct immunoblot analysis of COX subunit III, a polyclonal antibody was raised against the peptide corresponding to residues 64-77 of subunit III. These residues are situated on the short loop between transmembrane helices 2 and 3 at the bottom of the v-shaped cleft and are retained in the Δ114 truncation mutation. The antibody was created as described previously (Geyer, 2007).

SDS-PAGE was conducted on wildtype and mutant COX using a 16% acrylamide (37.5:1 acrylamide:bis) gel containing 6 M urea and 0.1% SDS (Fuller et al., 1981). Seven μg of COX were denatured in 3% SDS and Laemmli buffer (30 mM Tris-HCl, 15% glycerol, 0.005% bromophenol blue, pH 6.8) and then loaded into the gel. After stacking in the 1 cm 6% stacking layer at 60 V for 20 minutes, the subunits could be adequately separated by electrophoresis at 120 V for 2.5 hours. The gel and two sheets of nitrocellulose were then soaked for 10-15 minutes in transfer buffer (10 mM CAPS, 10% methanol, pH 11.0). A sandwich was prepared consisting of a sheet of filter paper (Bio-Rad), 2 sheets of nitrocellulose, the gel, and another sheet of filter paper. The sandwich was placed between two sponges and secured into a tank transfer apparatus (Bio-Rad) filled with transfer buffer. A constant 200 mA current was applied for 90 minutes, followed by 30 minutes at 500 mA. After transfer, the gel was stained with Coomassie G-250 to evaluate transfer efficiency. The nitrocellulose sheets were briefly rinsed in Milli-Q water before proceeding to immunoblotting.

Non-specific binding was blocked by incubating the nitrocellulose membranes at room temperature on an orbital platform for 1 hour with 3 changes of Tris-Buffer-Saline (TBS-B: 50 mM Tris-HCl, 170 mM NaCl, 5% milk, pH 7.5). The cleft antibody was diluted 1:250 in 25 mL of TBS-B for each nitrocellulose membrane. Primary antibody incubation was conducted at room temperature for 1 hour on an orbital platform. The blots were subsequently washed 3 times for 10 minutes each in TBS-B. The secondary antibody was a Goat-Anti-Rabbit-IgG conjugated to Horse Radish Peroxidase used at a 1:3000 titer (Bio-Rad). Secondary antibody incubation for 1 hour at room temperature was followed by washing the blots 3 times for 10 minutes each with TBS-B before placing them in 0.1% TBS-B. The blots were developed by soaking for 3 minutes in freshly prepared renaissance chemiluminescence reagent (100 mM Tris, 1.25 mM luminol, 0.2 mM p-coumaric acid, 0.03% H_2O_2, pH 8.5). The blots were transferred to a sheet protector and images were recorded on a Fuji LAS-4000 in increment mode.

MALDI-TOF Mass Spectrometry of Wildtype and Mutant R.sph. COX

MALDI-TOF mass spectrometry was used to assess the purity and subunit composition of wildtype and mutant forms of COX. Samples were washed in 30 mM Tris, pH 8.8 and concentrated to 2-3 μg/μL using Millipore YM-100 Microcon filter devices. One microliter of sample was mixed with 1 μL of the appropriate EAM matrix and spotted onto a Bruker MTP-384 Ground Steel Target Plate. A 10 mg/mL SPA-EAM matrix in 54% acetone/10% acetone/0.5% TFA was used to assess high molecular weight peptides (>15 kD). For lower molecular weight peptides (<15 kD), 1 mg/mL CHCA-EAM matrix in 5.4% acetonitrile/10% acetone/0.5% TFA was used. A Bruker Autoflex

III MALDI-TOF/TOF mass spectrometer was used in the positive reflector mode to analyze the samples.

Measuring the Activity and Catalytic Lifetime of R.sph. COX

To determine the maximum catalytic activity of solubilized *R. sphaeroides* COX, enzyme was diluted to 2-5 μM in 50 mM potassium phosphate, pH 7.4 containing 0.1% DM and allowed to incubate on ice for at least 15 minutes prior to the assay. The rate of oxygen consumption was measured in a water jacketed chamber at 25°C with a Clark electrode (Yellow Springs Instrument Company Model 17372). The typical activity assay buffer used was 50 mM potassium phosphate, 0.1% DM, pH 7.4, although in some cases the assay buffer was supplemented with 1 mg/mL asolectin (L-α-phosphatidylcholine from soybean, Type II-S, Sigma), which was sonicated to clarity prior to adding the DM. Before enzyme addition, 50 μM cytochrome *c* (type III), 18 mM ascorbate, and 0.6 mM TMPD were incubated in assay buffer for 2-3 minutes to determine the auto-oxidation rate of the reductants. Then, 2-10 picomoles of COX were added and the maximum rate of oxygen consumption was measured. When measuring the maximal catalytic activity of reconstituted COX in liposomes (COV), DM was omitted throughout. The auto-oxidation was recorded as above with the addition of 6 μM valinomycin and 6 μM CCCP, to dissipate the electrochemical gradient in the COVs. Then 2-10 picomoles of COVs were added to measure the maximum uncoupled rate of oxygen reduction. To determine the catalytic lifetime of forms of COX which undergo turnover induced inactivation, the solubilized or reconstituted activity was measured over the course of 10-15 minutes in order to record the entire inactivation curve.

Measurement of the pH Dependence of R.sph. COX Activity and Catalytic Lifetime

To determine the pH dependence of oxygen reduction activity, activity assays were conducted at pH values ranging from 6.0 to 10.0. Buffers suitable to the assay pH were selected (pH 6.0-6.5, 25 mM MES; pH 7.0-8.5, 25 mM HEPES; pH 9.0-10.0, 25 mM CHES). Each buffer contained 0.1% DM and in some cases 1 mg/mL asolectin. The ionic strength of the buffers was adjusted to I = 100 mM using an appropriate amount of KCl as determined using an online buffer calculator (http://www.liv.ac.uk/buffers/buffercalc.html). Solubilized enzyme was diluted to 2-5 μM in 25 mM HEPES, 0.1% DM, I = 100 mM, pH 7.5, and was incubated on ice for at least 15 minutes prior to the assays. Auto-oxidation rates using the appropriate buffer were measured as described above for solubilized COX, and the amount of COX subsequently added was adjusted for each pH value (2-30 picomoles) so as to maintain a linear instrument response throughout the range of activity. Activity was measured for 10-15 minutes after adding COX to obtain the complete inactivation curve of those forms of COX subject to turnover induced inactivation.

Calculating Turnover Induced Inactivation of Mutant R.sph. COX

The solubilized or reconstituted COX activity was measured over the course of 10-15 minutes in order to determine the catalytic lifetime of COX mutants which undergo turnover induced inactivation. The increasing proportion of inactivated enzyme was reflected by an exponential decay in the catalytic activity with respect to time. The enzyme's CC_{50} is defined as the number of catalytic turnovers undergone before the rate reaches half maximal activity, and it was calculated as diagrammed in Figure 11 (also

Figure 11

Calculation of CC_{50} value for *R.sph.* COX mutants undergoing turnover induced inactivation. The auto-oxidation rate obtained in the absence of COX is extrapolated (line 1), and a parallel line along the decay curve is drawn (line 2). This tangent intersects the decay curve at the point of complete enzyme inactivation (point A). From point A, a line is drawn vertically to intersection with line 1 (point B). The magnitude of line AB is bisected (at point *m*), and a line perpendicular to line AB is drawn to the intersection with the decay curve (point C). A vertical line is drawn from C to the intersection with line 1 (point D). The magnitude of line CD is used to calculate the number of catalytic turnovers undergone before the enzyme population reaches half maximal activity. This value, CC_{50}, is the catalytic lifetime of the enzyme.

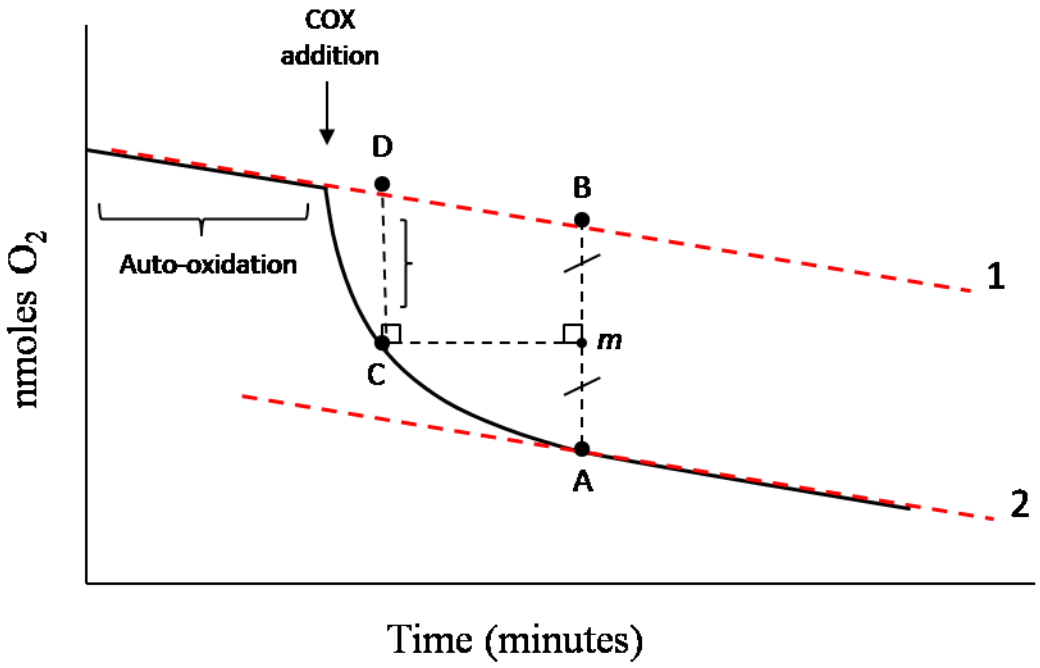

line 1 ‖ line 2
***m* is midpoint of line AB**

see (Bratton et al., 1999; Mills et al., 2003; Mills and Hosler, 2005)). Briefly, the tangent parallel to the extrapolated auto-oxidation rate was drawn along the exponential decay curve. This tangent intersects the curve at the point of complete enzyme inactivation (point A). A vertical line from point A to the extrapolated auto-oxidation rate (point B) was bisected (at point *m*) and a perpendicular line was drawn from *m* to intersection with the decay curve. This is the point of half maximal activity (point C). The magnitude of the vertical line from half maximal activity to the extrapolated auto-oxidation rate (line CD) is proportional to the number of moles of oxygen consumed, and it is used to calculate the number of catalytic cycles the enzyme has undergone before reaching half maximal activity, given that one catalytic turnover consumes one molecule of O_2.

Reconstitution of R.sph. COX into Small Unilamellar Phospholipid Vesicles

R. sphaeroides COX was reconstituted into small unilamellar vesicles using the cholate dialysis technique diagrammed in Figure 12 (Wilson and Prochaska, 1990). Soybean asolectin (80 mg/mL, Sigma) was dispersed into 56 mM HEPES, pH 7.2, 7.2% cholate (3x re-crystallized) using a Branson Sonifier 250 at a 50% duty cycle and 50% power output for 7-10 cycles of 1 minute each. The lipids were kept on ice and the sonicator tip was allowed to cool between cycles. The clarified phospholipid/cholate mixture was centrifuged at 20,000 x *g* for 10 minutes to remove traces of titanium fragments from the sonicator tip. COX was incubated on ice in Triton X-100 for 15-20 minutes to make the preparation monodisperse (3 mg detergent per mg COX). Then, 500 μL of phospholipid/cholate was added to the COX incubation, followed by the addition

Figure 12

Cholate dialysis technique for reconstituting COX into small unilamellar vesicles (COV). *R. sphaeroides* COX was incubated with Triton X-100 (3 mg Triton/mg COX) on ice for 15-30 minutes to achieve a monodisperse population of COX. Asolectin (80 mg/mL), cholate (7.2%) and HEPES (56 mM, pH 7.2) were sonicated to clarity, forming mixed detergent/lipid micelles. The pre-incubated COX was mixed with the lipid mixture and then an equal volume of 100 mM HEPES, pH 7.2 was added. Dialysis against 100 mM HEPES (pH 7.2) using a 10-14 kD molecular weight cutoff membrane removed the cholate and drove the formation of COX vesicles (COV's) which have an intravesicular volume containing 100 mM HEPES, pH 7.2.

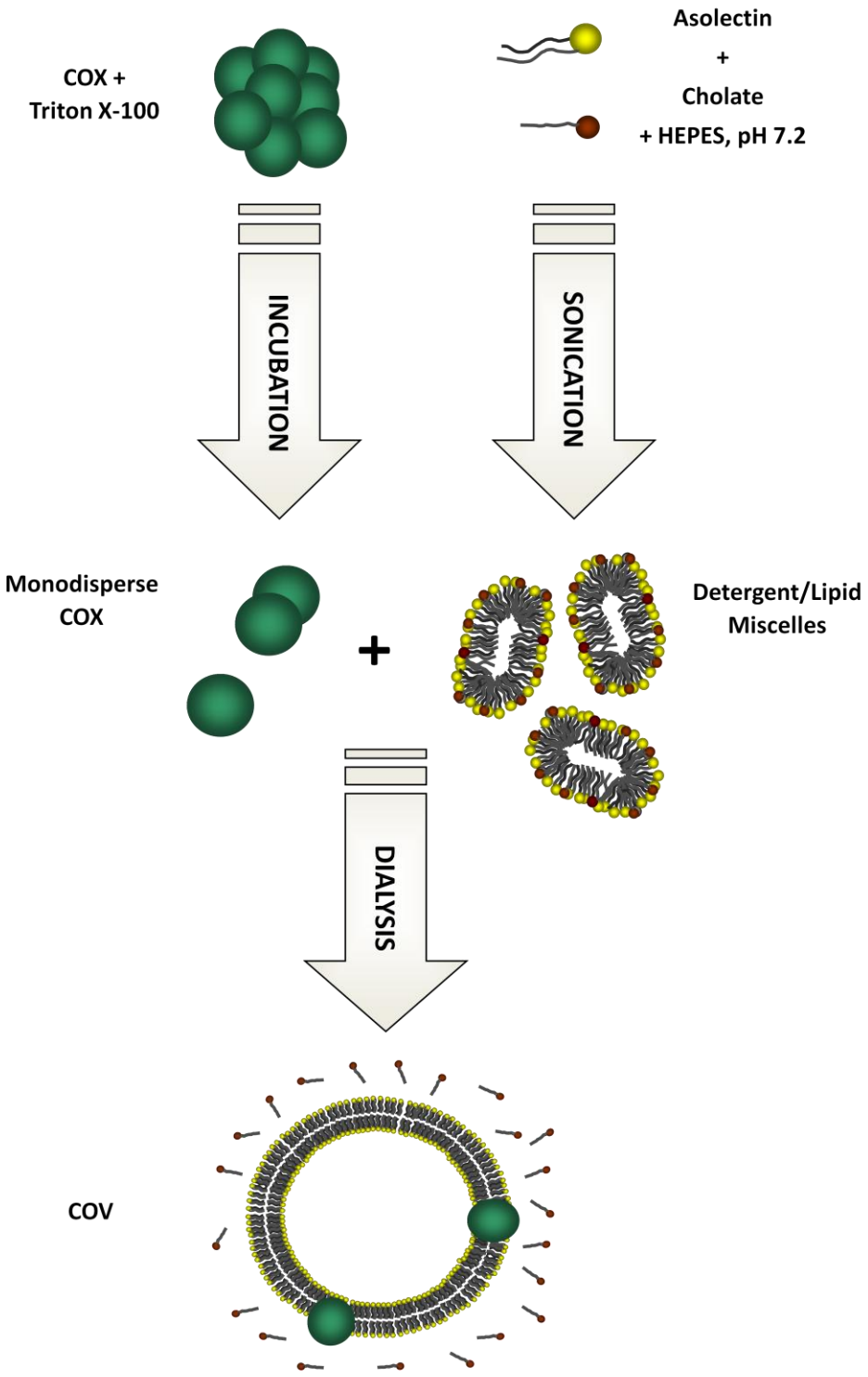
COX +
Triton X-100
Asolectin
+
Cholate
+ HEPES, pH 7.2
INCUBATION
SONICATION
Monodisperse
COX
+
Detergent/Lipid
Miscelles
DIALYSIS
COV

of 500 μL of 100 mM HEPES, pH 7.2. The solution was injected into a Slide-a-Lyzer dialysis cassette (10,000 kD cut off) and dialyzed against 100 mM HEPES, pH 7.2 for 4 hours, resulting in cytochrome *c* oxidase vesicles (COV) with an intravesicular buffer of 100 mM HEPES, pH 7.2. External buffer was exchanged by a series of buffer changes: 1) 10 mM HEPES, 50 mM Sucrose, 50 mM KCl pH 7.2 (6-8 hours), 2) 1 mM HEPES, 50 mM Sucrose, 50 mM KCl pH 7.2 (12 hours), and if necessary, 3) 50 μM HEPES, 50 mM Sucrose, 50 mM KCl pH 7.2 (16 hours) (Cvetkov and Prochaska, 2007).

Respiratory Control Ratios of Reconstituted R.sph. COX

The respiratory control ratio (RCR) is a measure of the endogenous proton permeability of the COVs (DiBiase and Prochaska, 1985; Wilson and Prochaska, 1990). To measure the RCR of wildtype COVs, cytochrome *c* (50 μM), ascorbate (18 mM) and 50 mM potassium phosphate (pH 7.4) were incubated with stirring for 2-3 minutes in the water jacketed chamber of a Clark type oxygen electrode apparatus (Yellow Springs Instruments). This rate of oxygen consumption in the absence of COVs, the auto-oxidation rate, was subtracted from all subsequent rates. Then 5-10 pmole of COVs were added and the controlled rate was measured for 2 minutes. The addition of valinomycin (6 μM) allowed the valinomycin-stimulated rate to be measured for 2 minutes. Finally, CCCP (6 μM) was added and the fully uncoupled rate was measured. The RCR was calculated as the ratio of the fully uncoupled rate (valinomycin and CCCP added) to the rate in the controlled state wherein no ionophores are added. RCR_{val} is the ratio of the fully uncoupled rate to the valinomycin-stimulated rate (Wilson and Prochaska, 1990; Cvetkov and Prochaska, 2007).

In COX forms that undergo turnover induced inactivation, the RCR was measured in three separate assays. The controlled rate was measured by incubating only cytochrome *c* (50 μM) and ascorbate (18 mM) in the reaction chamber during the auto-oxidation measurement. 5-10 pmole COVs were added and the controlled rate was measured. The valinomycin-stimulated rate was measured by adding valinomycin (6 μM) in addition to cytochrome *c* and ascorbate during the auto-oxidation measurement. The same amount of COVs as used for the controlled rate measurement was added to obtain the valinomycin-stimulated rate. Finally, the fully uncoupled rate was obtained in a third assay by adding both valinomycin and CCCP (6 μM) to the cytochrome *c* and ascorbate auto-oxidation measurement. The same amount of COVs was added as before, and the fully uncoupled rate was measured. RCR and RCR_{val} were calculated from the rates as described above after subtracting the auto-oxidation rates.

Stopped Flow Measurement of R.sph. COV Proton Pumping Efficiency

An Applied Photophysics SV.20 Stopped-Flow Absorbance Analyzer was used to measure the proton pumping efficiency of wildtype and mutant cytochrome *c* oxidase. COX was reconstituted as described previously, and the external buffer was exchanged via dialysis to low pumping buffer (50 μM HEPES, 50 mM Sucrose, 50 mM KCl, pH 7.2) (Cvetkov and Prochaska, 2007). Stopped flow absorbance spectroscopy allowed millisecond absorbance changes to be monitored upon mixing equal volumes of solutions containing COVs or ferrocytochrome *c*. The electron transfer induced pH changes due to proton pumping were monitored by inclusion of the membrane-impermeable, pH-sensitive dye, phenol red. Specifically, the COVs were diluted with low pumping buffer

to a heme aa_3 concentration of 0.1 μM, and phenol red was added to 100 μM. A separate solution of ferrocytochrome *c* (1.6 - 4 μM) was prepared in low pumping buffer and 100 μM phenol red. The solutions were titrated with 10-50 mM NaOH to a pH of 7.200 ± 0.005 using an Scientific Instruments IQ240 pH meter equipped with a stainless steel probe. To monitor the extravesicular acidification due to proton pumping, 5 μM valinomycin was added to both solutions in order to dissipate the membrane potential. The samples were loaded into two separate syringes and injected into the sample handling unit of the stopped flow analyzer, and the absorbance at 558 nm through a 2 mm path length cell was monitored upon sample mixing (an isosbestic point for ferrocytochrome *c* oxidation). Averages of 10 reaction traces were taken per sample. The magnitude of the decreases in dye absorbance due to acidification is proportional to the number of protons pumped in the reaction. In order to calibrate the magnitude of the pH changes, a separate set of samples were prepared which contained both 5 μM CCCP and 5 μM valinomycin. This dissipates both the charge and the proton gradients, so the magnitude of the alkalinization changes observed is proportional to the number of electrons consumed in the reaction (in order to reduce oxygen, one proton and one electron is consumed). The proton pumping ratio (H^+/e^- ratio) indicates the number of protons pumped for each input electron, with a theoretical value of 1.0. This value is calculated as the ratio of the magnitude of the acidification traces (only valinomycin present) to the magnitude of the alkalinization traces (both valinomycin and CCCP present) (see Cvetkov and Prochaska, 2007).

Discontinuous Sucrose Gradient Ultracentrifugation of R.sph. COX Vesicles

Discontinuous Sucrose Gradient Ultracentrifugation was used to separate liposomes containing protein (pCOV) from vesicles devoid of COX. Solutions of varying sucrose concentration were made in 10 mM Tris-HCl, pH 7.4, and correct sucrose concentration was verified by their refractive indices. Two milliliters of cold 13% sucrose solution was placed in the bottom of a Beckman centrifuge tube (13 x 51 mm), and 1 mL of 12% sucrose, then 1 mL of 11% sucrose, and finally 1 mL of COV sample were layered on top. The tubes were placed in a Beckman SW 50.1 swinging bucket rotor and subjected to 300,000 x *g* for 22 hours at 4°C in a Beckman Optima LE-80K Ultracentrifuge. Centrifugation resulted in the formation of two distinct bands: a yellowish band near the bottom of the 13% layer (pCOV), and a white, cloudy band in the 12% sucrose layer (Light COV) (see Figure 13). These bands were separately collected with a blunt end needle (Cvetkov and Prochaska, 2007).

Estimation of the Number of R.sph. COX Molecules per Phospholipid Vesicle

Small unilamellar vesicles containing COX (pCOV) were separated from liposomes devoid of enzyme via discontinuous sucrose density ultracentrifugation. The pCOV fraction was analyzed for its heme and lipid content in order to estimate the number of COX molecules per vesicle. The concentration of COX was calculated from the reduced *minus* oxidized absorbance at 605 nm using an extinction coefficient of 24,000 $M^{-}cm^{-}$ (van Gelder, 1966). To determine the lipid concentration, the pCOV fraction was digested in 70% perchloric acid at 100°C for 1 hour. The inorganic

Figure 13

Purification of COV's using discontinuous sucrose gradient ultracentrifugation. Two milliliters of ice-cold 13% sucrose was placed in the bottom of a Beckman centrifuge tube. Upon this layer, 1 mL of 12% sucrose and then 1 mL of 11% sucrose were carefully layered. All sucrose solutions contained 10 mM Tris-HCl, pH 7.2. Finally, 1 mL of COVs was layered on top of the sucrose gradient. The sample was subjected to 300,000 x *g* for 22 hours at 4°C. Two bands resulted: a yellowish band in the 13% sucrose layer (pCOV), and a white, cloudy band in the 12% layer (light COV). The bands were collected with a blunt-tipped needle.

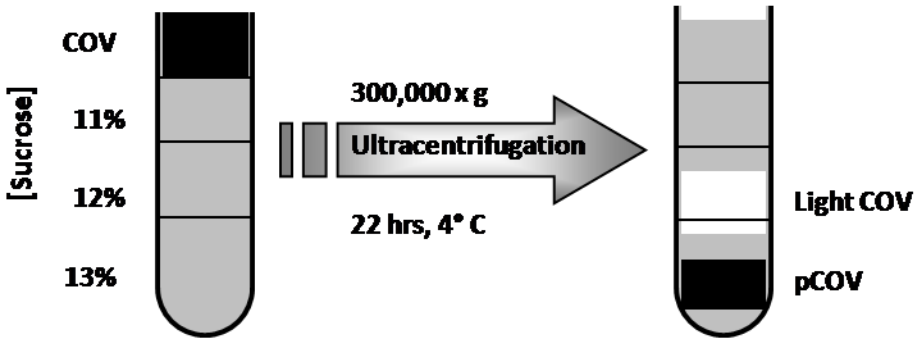
COV
[Sucrose]
11%
12%
13%
300,000 x g
Ultracentrifugation
22 hrs, 4° C
Light COV
pCOV

phosphate concentration was then measured via a colorimetric assay (Organisciak and Noell, 1976; Nguyen et al., 2002; Cvetkov and Prochaska, 2007).

Small unilamellar vesicles made via cholate dialysis have diameters ranging from 250 to 300 Å (Muller and Azzi, 1985). Given headgroup sizes for phospholipids in the outer (74 Å) and inner (61 Å) monolayer (Huang and Mason, 1978), the number of lipids per vesicle was calculated to be between 4250 (250 Å vesicle) and 6450 (300 Å vesicle). The number of COX molecules per vesicle was calculated by dividing the aa_3 concentration by the lipid concentration and then multiplying by the number of lipids per vesicle.

III. Results

Part One: Biophysical and Biochemical Characterization of Purified *R.sph.* COX Vesicles

Measurement of the vectorial proton pumping activity of COX requires reconstituting the enzyme into phospholipid vesicles using techniques which typically result in preparations containing an excess number of liposomes devoid of enzyme. Discontinuous sucrose gradient ultracentrifugation was used to separate these empty liposomes from those containing *R.sph.* COX, and the purified COX vesicles (pCOV) were characterized for their biophysical and biochemical properties.

Purification of R.sph. COV via Discontinuous Sucrose Gradient Ultracentrifugation

When reconstituting COX into phospholipid vesicles, an excess lipid to COX stoichiometry is used to maximize reconstitution efficiency. This results in a heterogeneous preparation consisting of both proteoliposomes and also many liposomes devoid of enzyme. These liposomes lacking enzyme can cause technical problems such as light scattering and increased net buffering capacity of the solution. In previous work, liposomes lacking enzyme were removed from bovine COVs by discontinuous sucrose density ultracentrifugation (Nguyen et al., 2002). In this study, the suitability of the technique for *R.sph.* COVs was assessed and found to be applicable. Following ultracentrifugation on a discontinuous sucrose gradient, two bands resulted from the

R.sph. COV sample (see Figure 13). The yellowish band in the 13% sucrose layer (pCOV) contained 80% of the COX recovered, while the white cloudy band in the 12% sucrose layer (Light COV) contained some COX and lipid concentrations 6-8 fold higher than the pCOV band. The total enzyme yield for *R.sph.* COVs was about 40%, compared to a 60% yield obtained for bovine COVs. The *R.sph.* pCOV band was also more diffuse than that seen for bovine. Overall, however, the data demonstrates that sucrose gradient ultracentrifugation is a viable means of separating *R.sph.* COVs from empty liposomes (see Discussion).

Functional and Biophysical Properties of R.sph. COV and pCOV

The usefulness of the purification technique requires minimal disruption of the functional properties of COX and of the biophysical properties of the liposomes. These properties were therefore assessed in the purified fraction of *R.sph*. COX liposomes (pCOV) and compared to liposomes which had not undergone purification (COV). Unpurified COVs displayed a steady-state activity of 708 ± 180 sec^{-1} (see Table I). The pCOV fraction maintained steady-state activity at ~75% of the COV (535 ± 130 sec^{-1}), similar to the percent activity maintained for bovine pCOV (Nguyen et al., 2002). Therefore, electron transfer rates were largely maintained in the pCOV preparations relative to COVs.

Potential damage to the phospholipid vesicles caused by ultracentrifugation was assessed by measuring the respiratory control ratio of pCOVs and COVs. The respiratory control ratio is a measure of the endogenous proton permeability of COX vesicles

Table I

Functional and Biophysical Properties of Unpurified (COV) and Purified (pCOV) *R.sph.* COX Phospholipid Vesicles

	R.sph. COV	*R.sph.* pCOV
TN (s^{-1}) [a]	708 ± 180	535 ± 130
RCR[b]	8.6 ± 1.6	6.0 ± 1.3
RCR_{val}[c]	3.5 ± 0.7	2.4 ± 0.4
H^+/e^- (20 e^-) [d]	0.9 ± 0.2	0.7 ± 0.2
H^+/e^- (40 e^-)[e]	0.9 ± 0.1	0.5 ± 0.1

[a] The maximum rate of electron transfer at pH 7.4 (e^-/s*mol COX) was measured polarographically by an oxygen electrode under saturating substrate conditions and in the presence of uncoupling ionphores (50 μM cytochrome *c*, 18 mM ascorbate, 6 μM CCCP, 6 μM valinomycin).
[b] The ratio of the uncoupled activity (valinomycin and CCCP included) to the controlled activity (in the absence of ionophores).
[c] The ratio of the uncoupled activity to valinomycin-stimulated activity.
[d] Proton pumping stoichiometry (H^+/e^-) indicates the number of protons pumped per electron transferred to COX. To achieve 5 catalytic turnovers, 20 electrons/COX are supplied (0.05 μM COX, 1 μM ferrocytochrome *c*).
[e] 40 electrons/COX results in 10 catalytic turnovers (0.05 μM COX, 2 μM ferrocytochrome *c*).

(Wilson and Prochaska, 1990). It is calculated as the ratio of the uncoupled rate of electron transfer (in the presence of valinomycin and CCCP) to the rate of electron transfer in the presence of an electrochemical proton gradient (no ionophores included). A higher ratio can indicate vesicles which are more impermeable to protons, or less "leaky" (Wilson and Prochaska, 1990). Unpurified COVs had RCR values of 8.6 ± 1.6 (see Table I). This value was maintained at ~70% in the pCOV fraction (6.0 ± 1.3). The RCR_{val} is the ratio of the uncoupled activity to the valinomycin-stimulated rate and reflects the proton permeability of the membrane under the conditions used for proton pumping (Wilson and Prochaska, 1990). Unpurified COVs had RCR_{val} values of 3.5 ± 0.7, and pCOV maintained this value at ~70% (2.4 ± 0.4). As will be discussed further, these results indicate that ultracentrifugation does not severely damage the ability of the phospholipid vesicles to maintain an electrochemical gradient.

Finally, the proton pumping activity of pCOV was compared to unpurified COVs by stopped-flow absorbance spectroscopy. The traces displayed in Figure 14 show that the proton pumping activity of pCOV is maintained to a high degree relative to unpurified COVs. The pH-induced absorbance changes at a cytochrome *c* isosbestic point (556 nm) are monitored by the inclusion of phenol red in the assay buffer. The magnitude of the decreases in absorbance (acidification) is proportional to the number of protons pumped during the reaction, while the magnitude of the increases in dye absorbance (alkalinization) is proportional to the number of electrons used (see Materials and Methods). The proton pumping efficiency (H^+/e^-) is calculated by the ratio of the absorbance decrease to that of the absorbance increase and has a theoretical value of one (Krab and Wikstrom, 1978). The H^+/e^- ratios for *R.sph.* COVs and pCOVs are presented

Figure 14

Proton pumping traces of *R.sph*. COV and pCOV. Proton pumping activity was measured by stopped-flow absorbance spectroscopy on an Applied Photophysics SV.20 reaction analyzer. The reaction commenced upon mixing reconstituted COX with reduced cytochrome *c*. Phenol red was included as a pH indicator to monitor pH-induced changes in absorbance at 556 nm, an isosbestic point for cytochrome *c* reduction. Acidification induced by the proton pumping activity of reconstituted COX in the presence of valinomycin is shown in the lower traces. The alkalinization phase (upper traces) results from the consumption of protons when reconstituted COX undergoes turnover in the presence of CCCP and valinomycin. This trace is proportional to the number of electrons transferred to COX. The H^+/e^- ratio is calculated from the extents of the lower and upper traces. Displayed are representative traces for a 5 turnover experiment (0.05 μM COX, 1 μM ferrocytochrome *c*, 5 μM CCCP and/or 5 μM valinomycin, pH 7.2). A) unpurified COX vesicles (COV) had H^+/e^- ratios of 0.9 ± 0.2 (5 turnovers). B) purified COX vesicles (pCOV) had H^+/e^- ratios of 0.7 ± 0.1 (5 turnovers).

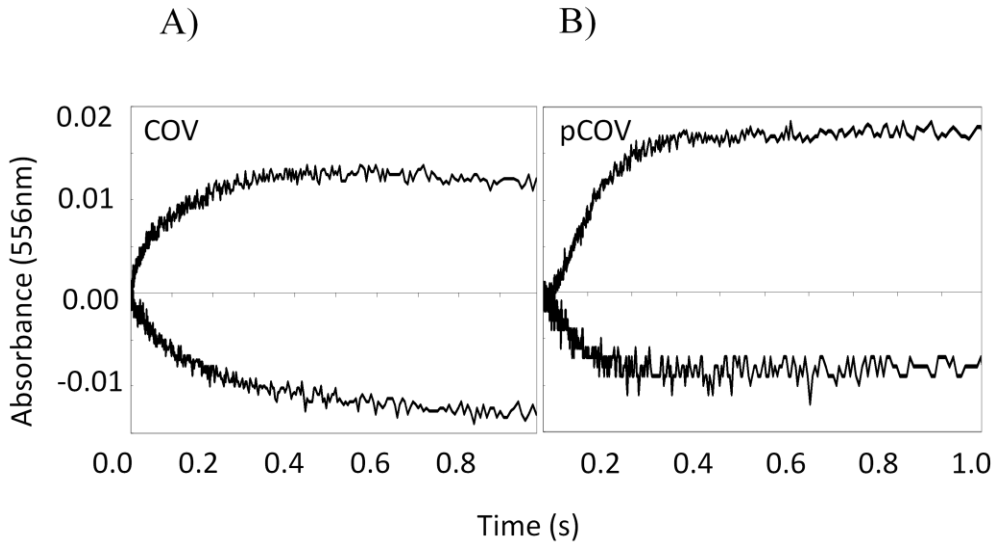
A)
B)
COV
pCOV
0.02
0.01
0.00
-0.01
Absorbance (556nm)
0.0
0.2
0.4
0.6
0.8
0.2
0.4
0.6
0.8
1.0
Time (s)

in Table I. The unpurified COVs had H^+/e^- ratios of 0.9 ± 0.2 when the enzyme was supplied with enough electrons for both 5 and 10 enzymatic turnovers (5 turnovers = 20 electrons/COX, 10 turnovers = 40 electrons/COX). When pCOVs were supplied with enough electrons for 5 catalytic turnovers, the H^+/e^- ratio relative to COVs was maintained at ~80% (0.7 ± 0.1). When pCOVs underwent 10 catalytic turnovers, they maintained about 55% the efficiency of unpurified COVs (0.5 ± 0.1). This reduction in proton pumping efficiency will be discussed, but the substantial pumping efficiency maintained in low turnover experiments demonstrates the usefulness of ultracentrifugation purification.

Two incentives for removing the liposomes devoid of enzyme are that their presence increases the buffering capacity of the solution and that they increase light scatter. Proton pumping assays are conducted in low buffer solution in order to monitor pH changes caused by proton pumping. Given an equal number of turnovers, the extent of the absorbance changes observed will depend on the buffering capacity of the solution. In a less buffered solution, pH can change more easily and corresponding absorbance changes will be greater. Therefore, it is notable that the absorbance change in the upper trace of Figure 14 is greater for pCOV (B) than it is for the COVs (A), suggesting a decrease in the buffering capacity resulting from the removal of the empty liposomes. The degree of light scatter was analyzed by absorbance spectroscopy, and pCOV scattered 50% less light at 550nm than did unpurified COVs. These results indicate the usefulness of ultracentrifugal purification for decreasing the lipid-induced buffering capacity and light scatter of solution.

Estimation of the Number of COX Molecules per pCOV

In previous work, characterization of bovine pCOV revealed that there were on average 2-3 COX molecules per liposome, a result consistent with the evidence that bovine COX dimerizes in the membrane (Nguyen et al., 2002). The oligomeric state of *R.sph*. in the membrane had not been previously examined, so the number *R.sph* COX molecules per vesicles was estimated in the pCOV fraction. To do so, the COX and lipid concentrations were determined by analysis of heme aa_3 and inorganic phosphate content, respectively. Liposomes made by the cholate dialysis technique have known vesicular diameters (250-300 Å) and lipid packing constraints (Huang and Mason, 1978; Muller and Azzi, 1985), which allows the number of COX molecules per vesicle to be estimated. The results displayed in Table II indicate that *R.sph.* pCOV contained approximately one COX molecule per phospholipid vesicle, in contrast to the 2-3 bovine COX molecules estimated for bovine pCOV isolated by the same technique. This result sheds insight into the oligomeric state of *R.sph*. in the lipid membrane, as will be discussed.

Table II

Estimation of the Number of COX Molecules per Phospholipid Vesicle in Purified Liposomes[a]

	R.sph. pCOV	Bovine pCOV[b]
COX/COV 250Å	0.72 ± 0.19	1.84 ± 0.36
COX/COV 300Å[b]	1.09 ± 0.28	2.88 ± 0.56

[a] Calculation was based on lipid and COX concentrations and known vesicular curvatures and sizes (250-300 Å). COX concentration was determined by heme aa_3 absorbance at 606 nm using an extinction coefficient of 24 $mM^{-1}cm^{-1}$. Lipid concentration was determined by digesting pCOV in perchloric acid and then using a colometric assay to determine phosphate concentration with nanomolar sensitivity. $N = 6$

[b] These measurements are in agreement with published values (Nguyen et al., 2002).

Part Two: Structural and Functional Characterization of *R.sph.* Δ114 COX

A pathogenic mitochondrial DNA mutation resulting in severe, episodic lactic acidosis introduces a premature stop codon in COX subunit III at residue Q111 after the third helix of subunit III (Tiranti et al., 2000). Protein sequence alignments indicate that human Q111 aligns with I115 in the *R. sphaeroides* COX (see Figure 9A). A stop codon was introduced at position 115 of subunit III in *R.sph.* COX, creating *R.sph.* Δ114 COX to model the mitochondrial mutation. As shown in Figure 15, this mutation removes the four c-terminal helices of subunit III while retaining the v-shaped lipid-binding cleft, the subunit I-subunit III interface, and the residues conserved in the putative D-pathway proton antenna of subunit III. The structural and functional properties of this mutant were compared to wildtype COX and to two forms of COX in which subunit III has been genetically or biochemically removed (I-II_{GD} and I-II_{BD} COX, respectively). Characterization of this mutant shed insight into the functional importance of n-terminal and c-terminal domains of subunit III as well as into the importance of its lipid-binding cleft.

Expression and Purification of R.sph. Δ114 COX

R.sph. COX subunit III was mutated by replacing the codon for I115 with a stop codon in order to truncate the subunit after 114 residues (Δ114). The mutation was modeled after a human mitochondrial disease mutation in which the four c-terminal helices of the seven-helical subunit III are genetically removed (Tiranti et al., 2000). The

Figure 15

The x-ray crystal structure of *R.sph.* COX showing the truncation of subunit III in the Δ114 COX mutant. Subunit I (cyan) is shown with heme centers in yellow and the mouth of the D-pathway indicated by D132 (red structure), surrounded by conserved subunit III residues putatively acting as a proton antenna (pink structures). Subunit II is in orange and subunit IV is in blue. Copper atoms are green spheres. The three n-terminal helices of subunit III which are retained in the Δ114 mutant are shown in pink. In gray are the helices of subunit III which are removed in the mutation (beginning with I115). F101 is indicated in magenta at the top of subunit III helix 3. The 13 amino acid stretch between F101 and I115 is colored in magenta. Within the v-shaped cleft of subunit III are two phosphotidyl ethanolamine molecules designated PL1 (light green) and PL2 (dark green). A) Side view in the plane of the membrane B) Top view shown from the periplasmic space perpendicular to the membrane. Prepared using Accelrys DS Viewer Pro (PDB 1M56 (Svensson-Ek et al., 2002)).

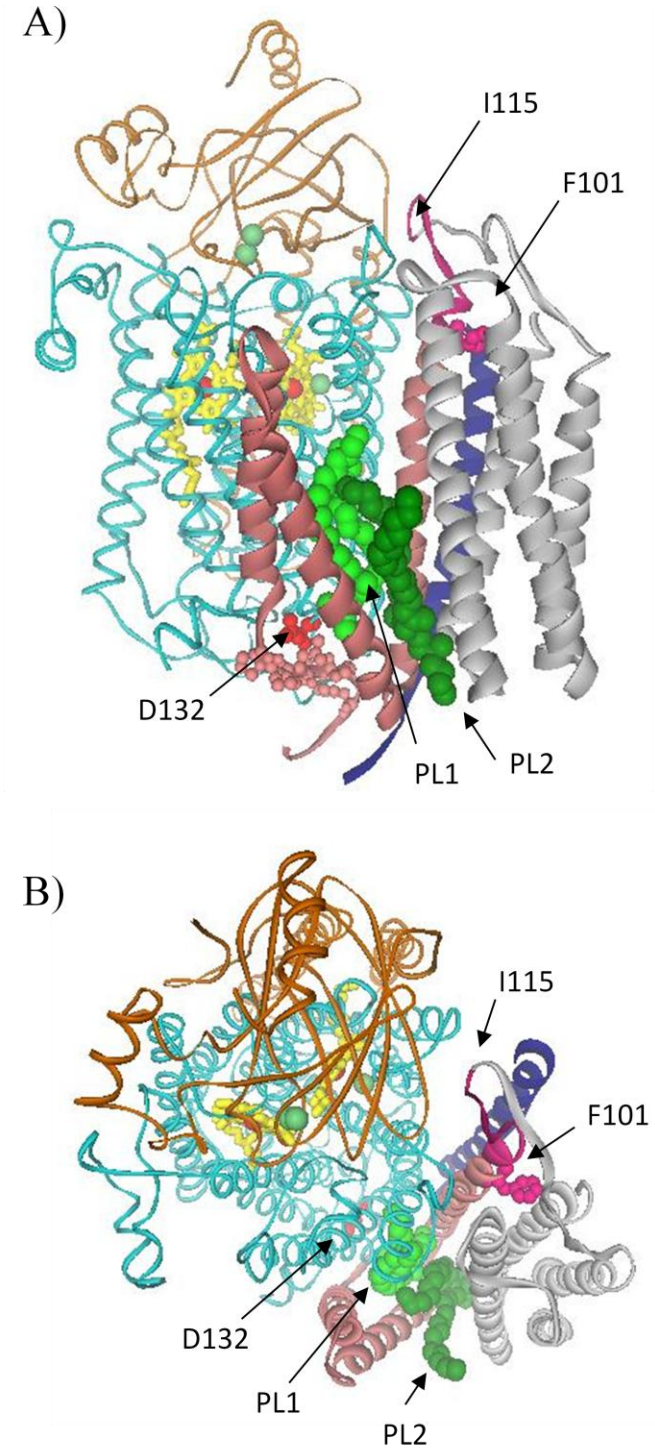
A)
I115
F101
D132
PL1
PL2
B)
I115
F101
D132
PL1
PL2

mutated plasmid pRK415, designed for COX overexpression, was introduced into *R.sph.* cells, and the protein was expressed and purified.

The bacterial growth rates and COX expression levels were compared between *R.sph*. cells containing overexpression vectors for wildtype COX, Δ114 COX or I-II_{GD} COX, in which subunit III has been genetically deleted. The strains of *R.sph*. cells overexpressing Δ114 or I-II_{GD} COX grew at similar rates to cells which overexpressed wildtype COX. After reaching an OD_{660} of 1.0, the cells were harvested and disrupted. The cytoplasmic membranes were collected, washed and analyzed for heme content via absorbance spectroscopy. The reduced *minus* oxidized spectrum of the purified membranes had peaks at 550 nm, 560 nm, and 605 nm corresponding to heme *c*, heme *b* and heme *a* content, respectively (Bratton et al., 2000). The ratio of the peak heights at 560 nm and 605 nm is proportional to the relative expression levels of *b*-type cytochromes and COX. There are a number of cytochromes containing heme *b* which are expressed in *R. sphaeroides*. In addition to the electron transport chain complex III (cytochrome bc_1) which contains cytochrome *b*, two of the alternate terminal oxidases expressed *R. sphaeroides* contain heme *b*, namely cytochrome cbb_3 and a quinol *bd*-type oxidase (Mackenzie et al., 2001). Cytochrome cbb_3 is expressed in high and low oxygen concentrations, and quinol *bd* oxidase is expressed when O_2 is limited or when electron flow to COX is interrupted (Mouncey et al., 2000). Table III shows the heme *b*:COX ratios for wildtype, Δ114 and I-II_{GD} cytoplasmic membranes. The elevated ratio for Δ114 and I-II_{GD} relative to wildtype indicated a lower proportion of COX in these membranes as compared to cytochromes containing heme *b*, suggesting either impairment in COX expression or higher expression of alternative oxidases containing heme *b*. A similar

Table III

Relative Expression Levels of Wildtype, Δ114 and I-II$_{GD}$ COX in *R.sph.* Purified Membranes

	$A_{(560nm)}/A_{(605nm)}$ [a]
R.sph. Wildtype	1.2 ± 0.2
R.sph. Δ114	2.4 ± 0.9
R.sph. I-II$_{GD}$ [b]	1.8

[a] Purified cytoplasmic membranes from *R.sph.* cells overexpressing either wildtype, Δ114 or I-II$_{GD}$ COX were analyzed for their heme content. The ratio of the reduced *minus* oxidized absorbance at 560 nm to that at 605 nm indicates the relative expression levels of heme *b* to heme *a* (COX). A lower ratio indicates higher relative COX expression.

[b] A similar value has been reported in the literature (Bratton et al., 2000).

result had been observed previously for *R.sph.* cells overexpressing I-II_{GD} COX (Bratton et al., 2000).

Ni^{2+}-NTA chromatography using a histidine tag engineered onto the c-terminus of subunit I (Mitchell and Gennis, 1995) was used to purify COX from the cytoplasmic membranes after they were solubilized with DM (Zhen et al., 1998). The Δ114 preparations consistently had reduced protein yields for nickel column purification (~25% yield versus ~75% yield for wildtype). The loss of enzyme occurred during the packing step of chromatography, suggesting impairment in the protein's ability to bind the nickel column. The packing flow through containing unbound Δ114 COX was analyzed by absorbance spectroscopy and had a reduced *minus* oxidized α-peak at 606 nm, indicating no significant disruption in the protein environment surrounding the heme centers. A repeated chromatography attempt was made with the unbound Δ114 protein in the packing flow, but it was almost completely unable to stick to the column (1% yield). A single preparation of I-II_{GD} COX had a ~40% yield for nickel column purification. The presence of a Δ114 truncation in COX subunit III therefore decreases both the expression level of the protein and its ability to bind to a nickel column (see Discussion).

Optical Absorbance Analysis of R.sph Δ114 COX

The spectral absorbance properties of purified Δ114 COX were compared to wildtype, I-II_{GD} and I-II_{BD} in order to assess the protein environment surrounding the subunit I heme centers, and the results are summarized in Table IV. In the reduced spectrum, the Soret and α peaks of Δ114 were respectively blue shifted by 2 and 1 nm relative to wildtype, which absorbs at 445 nm and 605 nm when reduced. There was a 2

Table IV

Optical Absorbance Parameters of Purified Wildtype, Δ114, I-II$_{GD}$ and I-II$_{BD}$ COX.

Reduced Spectrum[a]

	Soret$_{max}$[b]	α_{max}[c]	$A_{(soret)}/A_{(\alpha)}$[d]
R.sph. Wildtype	445 nm	605 nm	5.4 ± 0.1
R.sph. Δ114	443 nm	604 nm	4.6 ± 0.2
R.sph. I-II$_{GD}$[e]	443 nm	603 nm	4.5
R.sph. I-II$_{BD}$	445 nm	605 nm	5.3

Reduced *minus* Oxidized Spectrum[f]

	Soret$_{max}$	α_{max}
R.sph. Wildtype	446 nm	606 nm
R.sph. Δ114	446 nm	606 nm
R.sph. I-II$_{GD}$	446 nm	605 nm
R.sph. I-II$_{BD}$	446 nm	606 nm

[a] The dithionite-reduced spectra of Ni^{2+}-NTA-purified COX

[b] Maximal absorbance wavelength of the soret peak.

[c] Maximal absorbance wavelength of the α-peak.

[d] Ratio of the maximal absorbance of the soret to α-peak, indicating an increase in the ratio of heme *a* to heme a_3 content.

[e] Similar values are published (Bratton et al., 2000).

[f] The dithionite-reduced *minus* ferricyanide-oxidized spectra of Ni^{2+}-NTA-purified COX.

nm blue shift for both the Soret and α peak in the reduced spectrum of I-II_{GD}. The reduced spectral peaks of I-II_{BD} were not shifted compared to wildtype. The amplitude of the Soret to α peak for wildtype was 5.4 ± 0.1, and a similar value was observed for I-II_{BD} (5.3). The ratio of the two peaks was decreased in the reduced Δ114 spectrum to 4.6 ± 0.2, similar to the value observed for I-II_{GD} (4.5), which is in agreement with what has been observed in other labs (Bratton et al., 2000).

The spectral changes described have been shown to result from the presence of free subunit I*a* in the preparation (Bratton et al., 2000). This is a non-reduceable, inactive form of subunit I which does not contain heme a_3. Heme *a* and heme a_3 absorb at different intensities in the α-peak and Soret peaks such that the presence of subunit I*a*, which contains heme *a* but not heme a_3, decreases the ratio of the Soret to α-peak absorbance (Vanneste, 1966; Bratton et al., 2000). Bratton *et al*. have removed the free subunit I*a* from I-II_{GD} preparations and found that fully purified I-II_{GD} has wildtype spectral properties (Vanneste, 1966; Bratton et al., 2000). Therefore, the altered spectral properties of the heterogeneous preparations of I-II_{GD} and Δ114 are not indicative of misfolding in subunit I but rather to the presence of free subunit I*a*, which is inactive and does not disrupt activity.

Since the Fe^{3+} of heme *a* in free subunit I*a* does not reduce, its spectral effects should be minimized in a reduced *minus* oxidized (R-O) spectrum. Indeed, the R-O spectrum of Δ114 exhibited a Soret peak at 446 nm and an α–peak at 606 nm, the same values as were observed for wildtype and I-II_{BD} COX. The R-O spectral properties of I-II_{GD} were also closer to those of wildtype, displaying only a 1 nm blue shift in the α peak. Figure 16 compares the shape of the R-O α-peak for the different COX forms. Wildtype

Figure 16

Reduced *minus* oxidized α-peak of purified wildtype, Δ114, I-II$_{GD}$ and I-II$_{BD}$ COX. Samples were diluted to about 1 μM heme *aa*$_3$ in 50 mM potassium phosphate, pH 6.5. After the addition of ferricyanide, an oxidized spectrum was recorded on a Hewlett Packard diode array spectrometer. Dithionite was added and a reduced spectrum was recorded. The reduced *minus* oxidized spectra were normalized to 1 μM heme *aa*$_3$ for comparison of the different COX forms. Wildtype, Δ114 and I-II$_{BD}$ have a maximum at 606 nm, and the I-II$_{GD}$ peak is blue shifted 1 nm. Both Δ114 and I-II$_{GD}$ have a shoulder on the blue side of the peak.

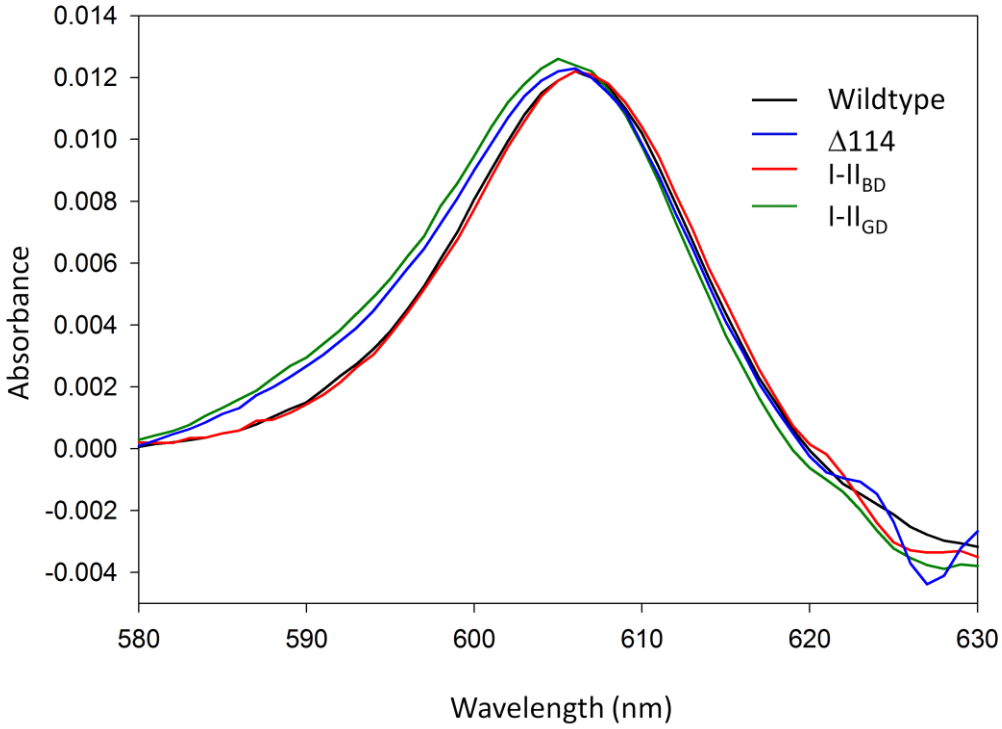
0.014
0.012
0.010
0.008
0.006
0.004
0.002
0.000
-0.002
-0.004
Absorbance
580
590
600
610
620
630
Wavelength (nm)
Wildtype
Δ114
I-II$_{BD}$
I-II$_{GD}$

(black) and I-II_{BD} (red) have similar peak shapes, but Δ114 (green) and I-II_{GD} (blue) both have a shoulder on the blue side of the peak. This R-O spectral feature is also indicative of the presence of free subunit I*a* (Bratton et al., 2000). Therefore, *R.sph.* cells expressing COX with either a genetic deletion or a Δ114 truncation of subunit III have increased levels of free subunit I*a*, which is purified in the preparations due to the presence of the histidine tag on subunit I. Implications of this result will be presented in the Discussion, although it is important to emphasize here that the presence of free subunit I*a* does not affect the functional properties of the enzyme because it is incapable of redox activity.

SDS-PAGE and Immunoblot Analysis of R.sph. Δ114 COX

The purity and subunit composition of Δ114 was analyzed by SDS-PAGE and immunoblotting. These experiments were conducted for a variety of reasons. Firstly, mutations of COX subunit III have in some cases resulted in a partial or nearly complete loss of subunit III from the COX complex, so confirmation of the presence of SIII-Δ114 was necessary (Tiranti et al., 2000; Varanasi et al., 2006; Geyer, 2007). In addition, a truncation mutation in which the seventh α-helix of subunit III was removed resulted in what appeared to be proteolytic degradation of the subunit, perhaps as a result of improper subunit III folding (Geyer, 2007). Δ114 COX needed to be assessed for a similar process. Finally, the spectral properties of Δ114 suggested the presence of free subunit I*a* in the preparation. The approximate quantity of free subunit I*a* could be estimated by the relative intensities of the subunit I bands in an SDS-PAGE gel of Δ114 and wildtype. Therefore, SDS-PAGE and protein immunoblotting were used to address these issues.

A representative Coomassie-stained SDS-PAGE gel comparing Δ114 and wildtype COX is shown in Figure 17A. Consistently, the Δ114 preparations had more intense staining in bands corresponding to impurities, a result which was further analyzed by two-dimensional PAGE as described below. The staining intensity of the subunit I band in Δ114 preparations was typically about 20-30% more intense than the subunit I band in wildtype COX, after normalizing these values by the intensities of their respective subunit II doublet bands. This suggests that for every 3-5 assembled, active COX molecules in the Δ114 preparations, there is about 1 molecule of free subunit I*a* which is not assembled with subunit II and is missing its active site. A similar enrichment in free subunit I*a* was observed for I-II_{GD} COX. Finally, in the Δ114 preparations there were two bands which ran with an apparent molecular weight of ~10-15 kD (indicated by arrows). These bands are likely candidates for the Δ114 truncation of subunit III (SIII-Δ114), a hypothesis which was further analyzed by both immunoblotting and MALDI-TOF mass spectrometry.

The putative SIII-Δ114 doublet band observed in SDS-PAGE gels was assessed by protein immunoblotting for its reactivity to a subunit III-specific polyclonal antibody. The primary antibody was raised against a peptide corresponding to residues 64-77 of subunit III, which are located in the short loop at the bottom of the subunit's v-shaped cleft. Figure 17B shows the protein immunoblot of wildtype and Δ114 COX. Due to the different migration rates of full length subunit III and the putative truncation bands, a sandwich of blotting membranes was used during the transfer. Shown are the blots selected from the sandwich which were most enriched in each of the three bands observed to have specific immunoreactivity. The bands at the top of the blots are due to

Figure 17

SDS-PAGE and immunoblot analysis of wildtype and Δ114 COX. A) An SDS-PAGE gel comparing wildtype and Δ114 COX. Seven μg of COX were denatured with 3% SDS in Laemmli buffer for 45 minutes at 37°C. Electrophoresis was conducted at 120 V for 2.5 hours on a 16% acrylamide gel containing 6 M urea and 0.1% SDS, pH 8.8. The gel was stained with Bio-Rad Coomassie G-250 and an image was taken on a Fuji analyzer. The Δ114 gels showed more impurities, had SI:SII band density ratios 1.2-1.3 times greater than wildtype, and had a doublet around 10-15 kD. B) Protein immunoblot of wildtype and Δ114 COX using a SIII-specfic antibody. Protein bands in SDS-PAGE gels were transferred using a Bio-Rad tank transfer apparatus onto a sandwich of 2-3 nitrocellulose membranes (200 mA for 1.5 hrs, 500 mA for 0.5 hrs). The sandwich was necessary due to differing transfer rates of full length and truncated subunit III. A polyclonal antibody raised against residues 64-77 of subunit III was used to probe for subunit III (Geyer, 2007). Wildtype had an immunoreactive band corresponding to full length subunit III. Δ114 had an immunoreactive doublet which migrated within the expected region for the truncation mutation.

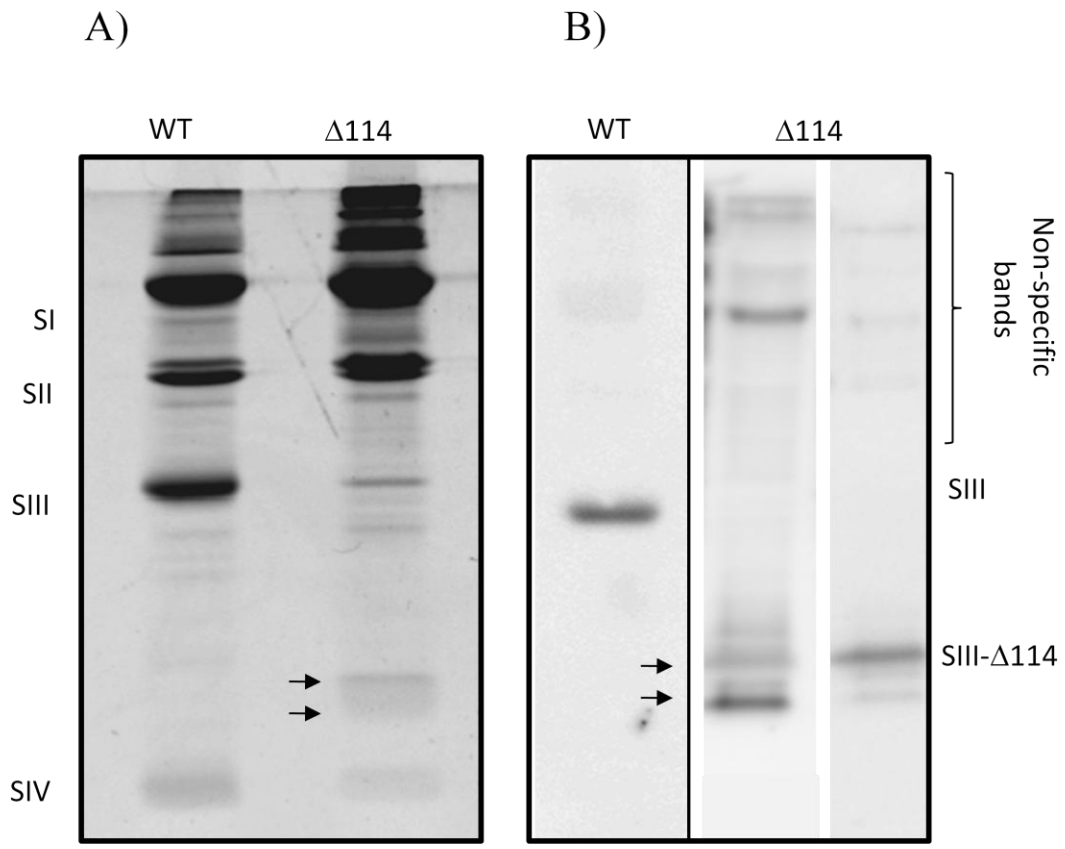
A)
B)
WT
Δ114
WT
Δ114
SI
SII
SIII
SIV
Non-specific bands
SIII
SIII-Δ114

nonspecific binding, as was previously shown by competitive immunoblotting using the purified peptide as a binding competitor (Geyer, 2007). A single band immunoreactive to the subunit III antibody was observed in wildtype COX at the expected migration distance of subunit III (22 kD). An immunoreactive band at this migration distance was not observed in Δ114 COX, confirming the absence of full length subunit III in this mutant. Notably, both bands in the putative Δ114 doublet were immunoreactive to the subunit III antibody. These bands are shown on two different blots of the membrane sandwich, as they had different transfer rates. These results confirm the presence of a truncated form of subunit III in Δ114 COX and suggest the possibility of limited proteolytic activity upon the truncated subunit.

MALDI-TOF Mass Spectral Analysis of R.sph. Δ114 COX

Immunoblot and SDS-PAGE analysis confirmed the presence of a truncated form of subunit III in Δ114 COX, which migrated in the gel at a rate corresponding to a molecular weight of ~10-15 kD. There was an additional immunoreactive band within this same region, which could have resulted from post-translational, proteolytic processing of subunit III-Δ114. MALDI-TOF mass spectrometry was employed to determine the exact molecular weights of these two forms of truncated subunit III in order to better understand the extent and nature of the putative proteolytic activity. In addition, the native processing of subunits II and IV in Δ114, wildtype and I-II_{GD} COX was analyzed.

The mass spectra in Figure 18 show peaks within the mass range expected for the subunit III truncation, comparing Δ114, I-II_{GD} and wildtype COX. Two peaks were

Figure 18

MALDI-TOF mass spectral analysis of *R.sph.* COX SIII-Δ114 content in *R.sph*. wildtype, Δ114 and I-II$_{GD}$ COX. Two μg of sample were diluted 1:1 in a CHCA matrix, spotted onto a Bruker stainless steel plate, and analyzed on a Bruker Autoflex III MALDI-TOF/TOF mass spectrometer. Δ114 COX samples consistently exhibited peaks at 11462 ± 8.9 *m/z* and 12919 ± 8.5 *m/z*, which were not observed in wildtype or I-II$_{GD}$. The expected mass of SIII-Δ114 is 12919 Da, and residues 2-101 of subunit III have a calculated mass of 11461 Da.

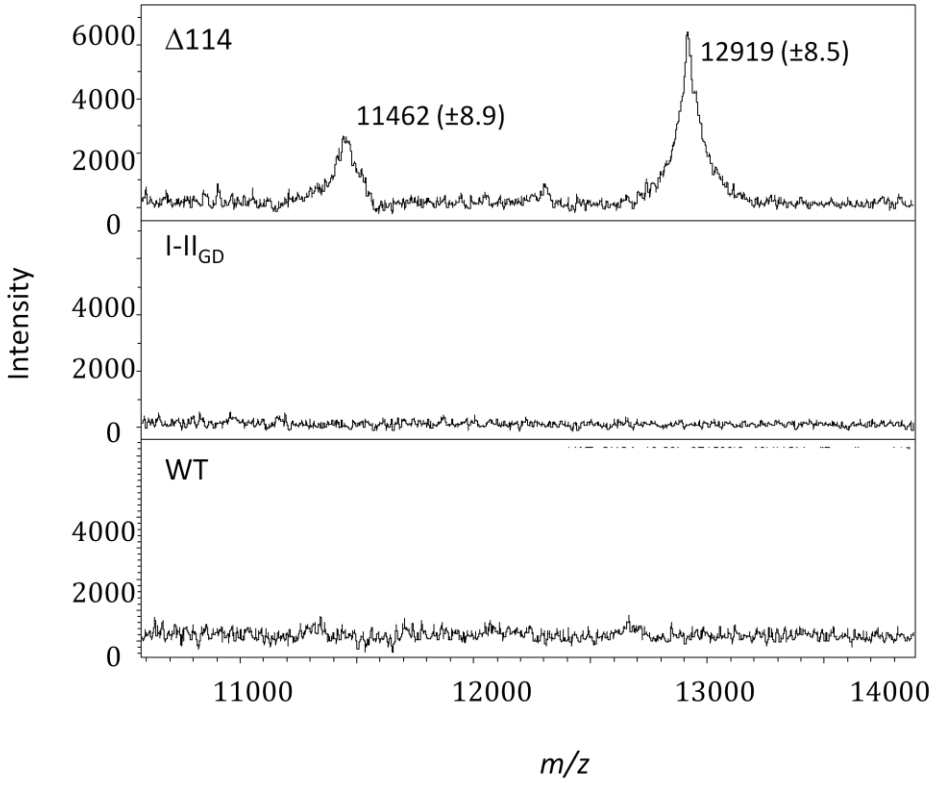
Δ114
11462 (±8.9)
12919 (±8.5)
I-II$_{GD}$
WT
Intensity
6000
4000
2000
0
11000
12000
13000
14000
m/z

Table V

Summary of Subunit Peaks Observed in MALDI-TOF Mass Spectra of *R.sph.* Wildtype, Δ114 and I-II$_{GD}$ COX.

Subunit	Expected Mass (Da)	Observed WT (*m/z*)	Observed Δ114 (*m/z*)	Observed I-II$_{GD}$ (*m/z*)
SIVA'[a]	5272	5271 ± 4.1	N.O.[b]	5279 ± 9.1
SIV'(-AE)[c]	6039	6032 ± 3.4	6033 ± 4.4	6031 ± 5.3
SIII [2-101][d]	11461	N.O.	11462 ± 8.9	N.O.
SIII [2-114][e]	12915	N.O.	12919 ± 8.5	N.O.
SIIA[f]	29122	29415 ± 61	29402 ± 64	29433 ± 88
SIIC[g]	30660	30628 ± 76	30612 ± 64	30608 ± 79
SII full[h] (?)	32930	31966 ± 30	31985 ± 51	32006 ± 65
SIII'[i]	30041	30029 ± 71	N.O.	N.O.

[a] Subunit IV which has been processed by removal of its 11 n-terminal amino acids.
[b] N.O. = Not observed.
[c] Subunit IV which has been process by removal of its 3 n-terminal amino acids.
[d] The portion of subunit III corresponding to residues 2-101.
[e] The portion of subunit III corresponding to residues 2-114.
[f] Subunit II which has been processed to remove its 25 n-terminal and 15 c-terminal amino acids.
[g] Subunit II which has been processed to remove its 25 n-terminal amino acids.
[h] Full length subunit II, notice the sizeable difference between observed and expected. This peak could alternatively be an impurity
[i] Subunit III with the n-terminal Met removed

consistently observed in Δ114, one at 12919 ± 8.5 *m/z* and one at 11462 ± 8.9 *m/z*. These peaks were absent from wildtype and I-II_{GD} COX spectra. The expected mass for a subunit III truncation after residue 114 is 12915 Da, given that the n-terminal methionine residue is cleaved from subunit III (Distler et al., 2004). The 12919 *m/z* peak, therefore, was assigned to the truncation in subunit III resulting from the genetic introduction of a stop codon at position 115 (SIII-Δ114). The peak observed 1457 *m/z* units smaller than SIII-Δ114 (at 11462 *m/z*) is consistent with the expected molecular weight of subunit III residues 2-101 (11461 *m/z*). This suggests that the 13 c-terminal amino acids of SIII-Δ114 can sometimes be cleaved from the truncated subunit, and the 11462 *m/z* peak was assigned to SIII-[2-101] accordingly (see Table V). The cleavage would occur after F101, which is located at the top of helix three at the phospholipid bilayer interface. The 13 amino acids putatively removed are the beginning of what would be in full length subunit III a large periplasmic loop extending 30 amino acids to the next helix (four) in the *R.sph*. COX structure (Svensson-Ek et al., 2002).

In *R.sph*. COX, subunit II undergoes native, post-translational proteolytic processing, resulting in the removal of its 25 n-terminal amino acids and its 15 c-terminal amino acids (Distler et al., 2004). The functional purpose of this processing is unknown, but it results in a heterogeneous preparation of enzyme upon purification. In particular, subunit II is present primarily in two forms. In subunit IIA, the processing has occurred at both termini resulting in a mass of 29122 Da, but for subunit IIC, processing has only occurred at the n-terminus to yield a mass of 30660 Da. Unprocessed subunit II can also be present in the preparation, having a mass of 32930 Da. These processing differences have not been observed to affect the activity of the protein (Hosler et al., 1992; Hiser et

al., 2001; Distler et al., 2004). All three processing forms of subunit II were observed in Δ114, wildtype and I-II_{GD} preparations, as depicted in Figure 19 (see Table V). Specifically, peaks near the expected mass of subunit IIA were observed in wildtype (29415 ± 61 *m/z*), Δ114 (29402 ± 64 *m/z*) and I-II_{GD} (29433 ± 88 *m/z*), and subunit IIC were also assigned for wildtype (30628 ± 76 *m/z*), Δ114 (30612 ± 64 *m/z*), and I-II_{GD} (30608 ± 79 *m/z*). A peak about 900-1000 *m/z* less than the expected mass of full length subunit II was observed in wildtype (31966 ± 30 *m/z*), Δ114 (31985 ± 51 *m/z*), and I-II_{GD} (32006 ± 65 *m/z*), but the sizeable difference from the expected value should be noted. As expected, a peak corresponding to the expected mass of subunit III (30041 Da) was observed only in wildtype COX (30029 ± 71 *m/z*).

An examination of the relative peak areas in Figure 19 of the subunit II forms revealed that in the Δ114 and I-II_{GD} preparations subunit IIA peak areas were ~3-4 fold less than the area of the subunit IIC peaks. On the other hand, in wildtype COX the peak areas corresponding to fully processed subunit IIA were ~5-7 fold *greater* than the peak areas for partially processed subunit IIC. This same pattern was observed in SDS-PAGE gels, as shown for Δ114 and wildtype COX in Figure 20. The relative band densities of subunit IIA and IIC were determined from these gels. For Δ114, the less processed subunit IIC band was ~3-5 times more intense than the fully processed subunit IIA band, similar to the result seen for I-II_{GD} COX. However, in wildtype COX, the fully processed subunit IIA band was ~7-9 fold more intense than the subunit IIC band, which was also the case for I-II_{BD} COX. Therefore, when subunit III is absent or truncated after its third helix, the native *in vivo* processing of subunit II appears to be altered. It should be

Figure 19

MALDI-TOF mass spectral analysis of subunit II and III content in *R.sph.* wildtype, Δ114 and I-II$_{GD}$ COX. Two μg of sample were diluted 1:1 in a SPA matrix, spotted onto a Bruker stainless steel plate, and analyzed on a Bruker Autoflex III MALDI-TOF/TOF mass spectrometer. Wildtype samples contained peaks assigned to subunit III and to three forms of subunit II (subunit II, IIA, IIC). Δ114 and I-II$_{GD}$ samples did not contain a subunit III peak but did contain three forms of subunit II. The peak areas for IIC were consistently greater than those of IIA in Δ114 and I-II$_{GD}$ COX preparations, contrary to the pattern observed in wildtype COX

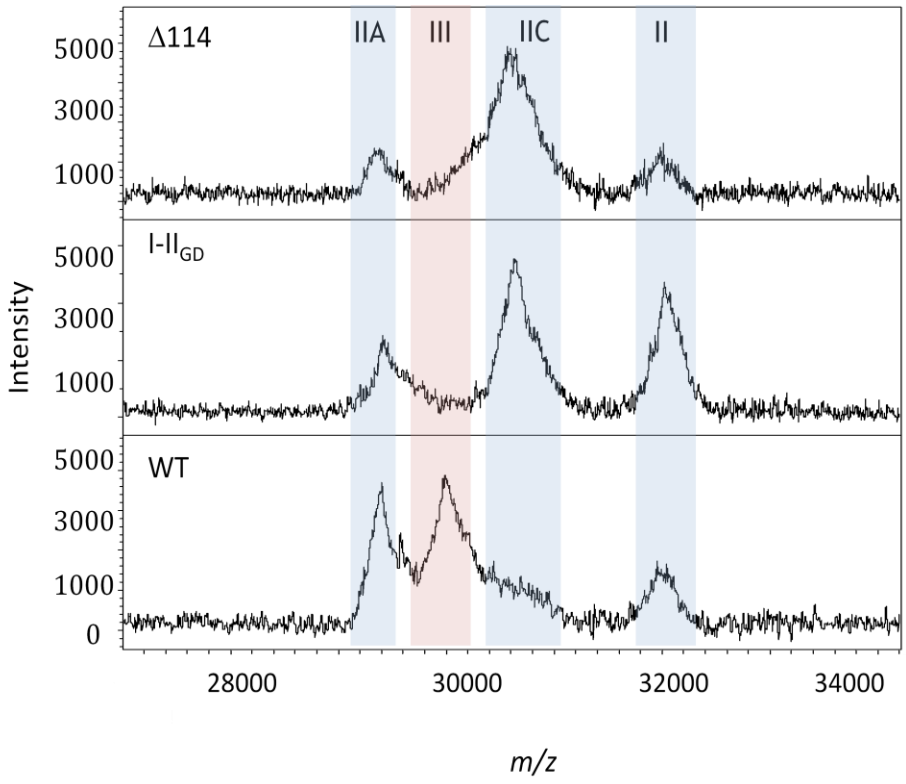
Δ114
IIA
III
IIC
II
I-II$_{GD}$
WT
Intensity
5000
3000
1000
0
28000
30000
32000
34000
m/z

Figure 20

SDS-PAGE analysis of subunit IIA and IIC in *R.sph.* wildtype and Δ114 COX. 1-10 μg COX samples were denatured with 3% SDS in Laemmli buffer for 45 minutes at 37°C. Electrophoresis was conducted at 120 V for 3.0 hours on a 16% acrylamide gel containing 6 M urea and 0.1% SDS, pH 8.8. The gel was stained with Bio-Rad Coomassie G-250 and an image was taken on a Fuji analyzer. The subunit II doublet in Δ114 had more intense staining in the slower migrating form (IIC) compared to the faster migrating form (IIA). In Δ114 COX, the IIC band was 3-5 more intense than the IIA band, as estimated using Accelrys Multigauge software. In wildtype, IIA was 7-9 more intense than IIC.

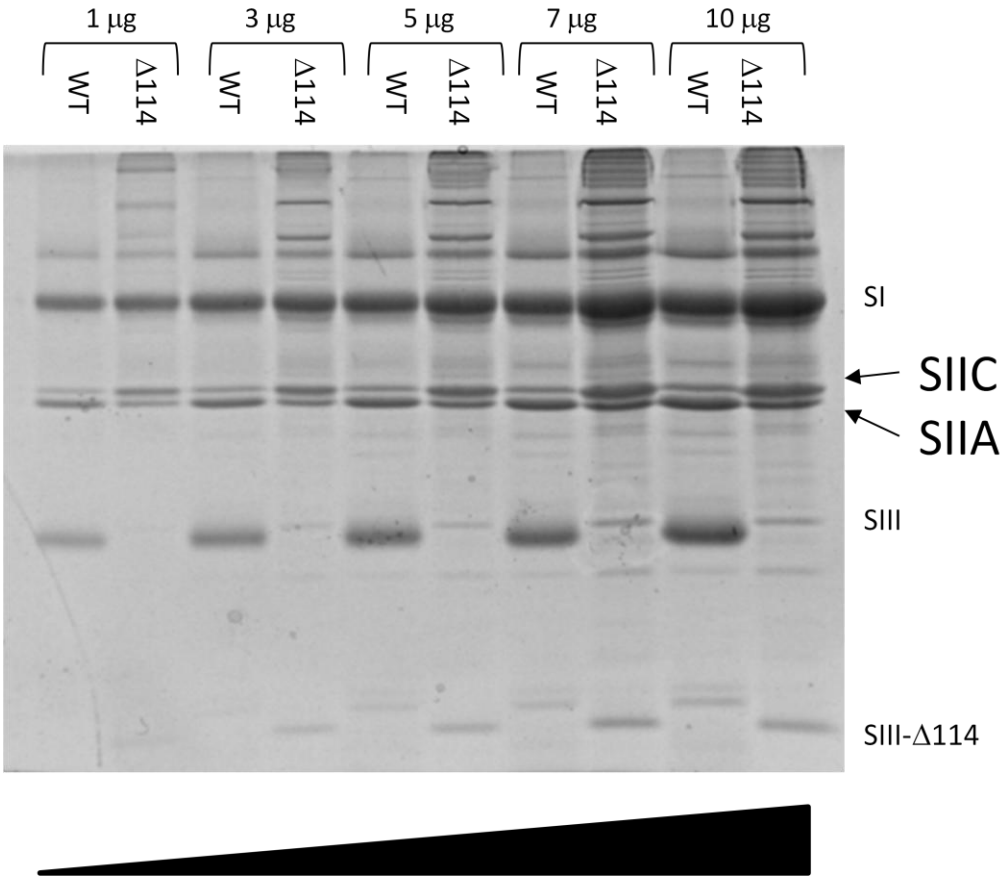
1 μg
3 μg
5 μg
7 μg
10 μg
WT
Δ114
SI
SIIC
SIIA
SIII
SIII-Δ114

Figure 21

MALDI-TOF mass spectral analysis of subunit IV content in *R.sph.* wildtype, Δ114 and I-II$_{GD}$ COX. Two μg of sample were diluted 1:1 in a CHCA matrix, spotted onto a Bruker stainless steel plate, and analyzed on a Bruker Autoflex III MALDI-TOF/TOF mass spectrometer. In wildtype and I-II$_{GD}$ COX, two forms of natively-processed subunit IV were observed consistently (IVA' and IV'(-AE)). In Δ114 preparations, the IV'(-AE) form was present, but the IVA' form was not observed.

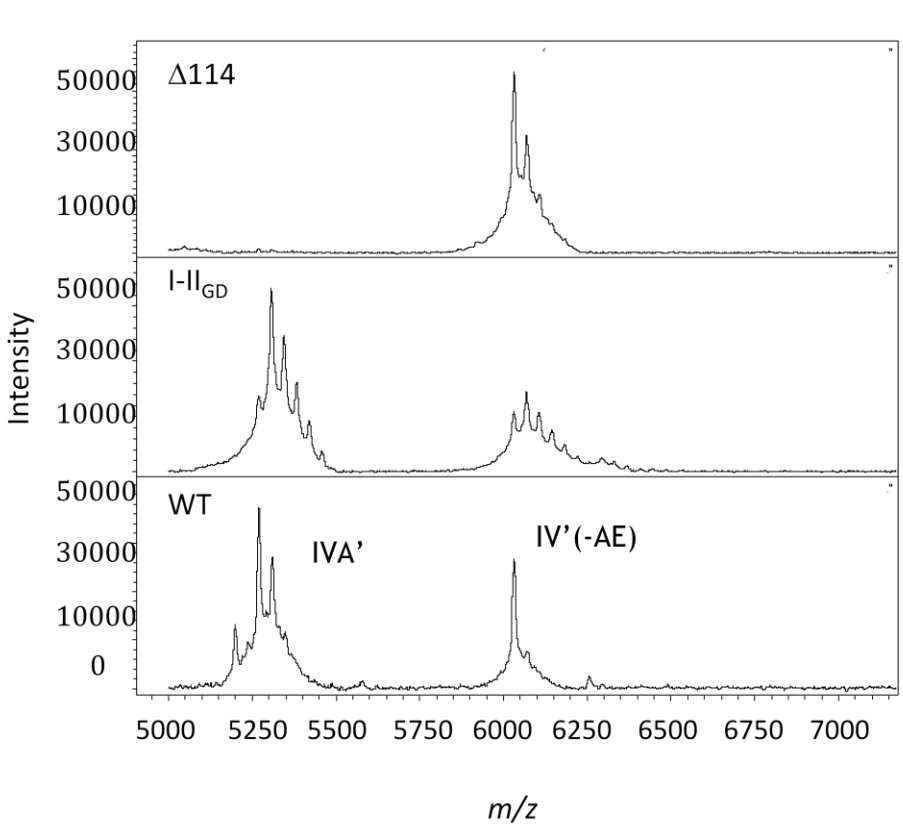
Δ114
I-II$_{GD}$
WT
IVA'
IV'(-AE)
Intensity
50000
30000
10000
0
5000
5250
5500
5750
6000
6250
6500
6750
7000
m/z

emphasized, however, that the differentially processed forms of subunit II do not have an observed affect on the steady state activity of COX.

Subunit IV has also been observed in a variety of different forms in wildtype COX (Distler et al., 2004). The expected mass range for subunit IV peaks is shown in Figure 21. Two forms of subunit IV were observed in the spectra (see Table VI). Subunit IVA' has its n-terminus cleaved after Met11, has an expected mass of 5272 Da, and is the form most abundant in wildtype COX (Distler et al., 2004). This form of the subunit could also result from using the Met11 codon as the translation start site rather than Met1. A subunit IVA' peak was observed in wildtype (5271 ± 4.1) and I-II_{GD} (5279 ± 9.1), but it was not observed in Δ114 COX. The subunit IV'(-AE) form has its first three n-terminal residues cleaved and has a mass of 6039 Da. A peak at this mass was observed in wildtype (6032 ± 3.4), Δ114 (6033 ± 4.4) and I-II_{GD} (6031 ± 5.3). These results indicate that the truncation of subunit III after its third helix alters the native processing of subunit IV as well as subunit II. Subunit IV has not been shown to have a functional role in COX activity.

Two Dimensional PAGE Analysis of R.sph. Δ114 COX

Certain subunit III mutations result in a disruption of the subunit III interaction with subunit I such that subunit III is partially depleted from the complex (Bratton et al., 2000). In particular, a truncation of subunit III after its sixth helix resulted in depletion of subunit III by up to 70% (Geyer, 2007). Since Δ114 COX could have different functional properties than I-II COX, it was important to determine the stoichiometry of SIII-Δ114 in the COX complex. Two dimensional PAGE was employed to this end.

Figure 22A shows a blue native PAGE gel of wildtype, Δ114 and I-II$_{GD}$ COX. The majority of wildtype COX migrates in two bands, which, as analyzed by a second SDS-denaturing dimension (Figure 22B), correspond to 4 subunit COX (*a*) and a small amount of COX containing only subunits I and II (*b*). Both Δ114 and I-II$_{GD}$ COX migrate in three bands on the native gel, with the I-II$_{GD}$ bands running faster than those of Δ114.

The Δ114 native bands, denoted *c*, *d* and *e*, were denatured in SDS and run on a second dimension in order to quantitate their purity and COX subunit content (Figure 22B). About 45% of the total Δ114 COX enzyme migrated in the native band *d* as determined by its denser subunit II band in the 2D gel relative to the subunit II densities of lanes *c* and *e*. The strikingly dark band corresponding to SIII-Δ114 in the second dimension of band *d* extends through 75% of the lane width. It was therefore assumed that this portion of the band had COX with full incorporation of SIII-Δ114. The Δ114 native band *d* also had a noticeable amount of impurities whose staining densities were a third of the total staining density of the second dimension lane. Native band *c*, the slower migrating band, contained an even greater amount of impurities; the 2D gel showed this band consisted of 70% impurities and about 30% COX, which contained SIII-Δ114. Native band *e* contained the least amount of impurities (20% of the total lane density), and some COX with SIII-Δ114. The stoichiometry of SIII-Δ114 incorporation for the COX contained in native bands *c* and *e* was determined by comparing the density of their subunit II bands in the 2D gel to density of their SIII-Δ114 bands, using lane *d* as calibration. Thus, bands *c* and *e* were found to incorporate SIII-Δ114 with 65%

Figure 22

Two-dimensional PAGE analysis of wildtype, Δ114 and I-II$_{GD}$ COX. A) Seven μg of COX were diluted in 16% glycerol and electrophoresis was conducted at 80 V for 4 hours at 4°C on a 4-15% gradient acrylamide gel, pH 8.8. A discontinuous buffer system was used which employed Serva Blue in the cathode buffer to induce a charge shift in the enzyme preparations (Schagger and von Jagow, 1991). Wildtype migrated primarily in two bands (*a, b*), and both Δ114 (*c*-*e*) and I-II$_{GD}$ (*f*-*h*) migrated in three bands. B) Bands from the native gel were excised and incubated in 2% SDS for 30 min at 37°C. The bands were fixed with 1% agarose to a 16% polyacrylamide gel containing 0.1% SDS and 6 M urea (pH 8.8), and electrophoresis was conducted at 120 V for 2.5 hours. The gels were silver stained and band intensity was analyzed. The composition of the native wildtype bands contained 4 subunit COX (*a*) and a small amount of I-II COX (*b*). The Δ114 lanes all contained COX with ~70% stoichiometry of SIII-Δ114 and varying degrees of impurities. The I-II$_{GD}$ lanes all contained I-II COX and varying degrees of impurities.

A)

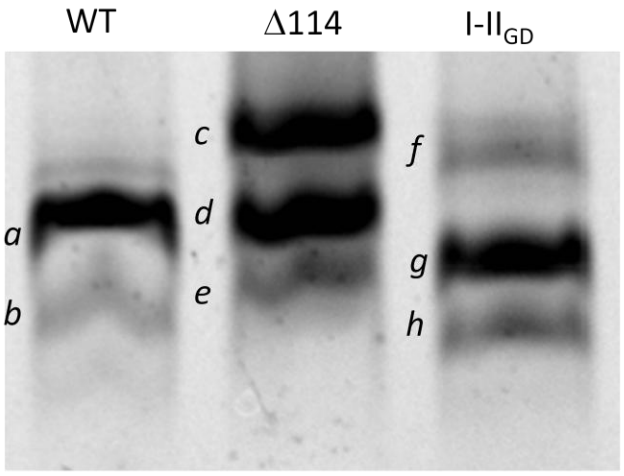
WT
Δ114
I-II$_{GD}$
a
b
c
d
e
f
g
h

B)

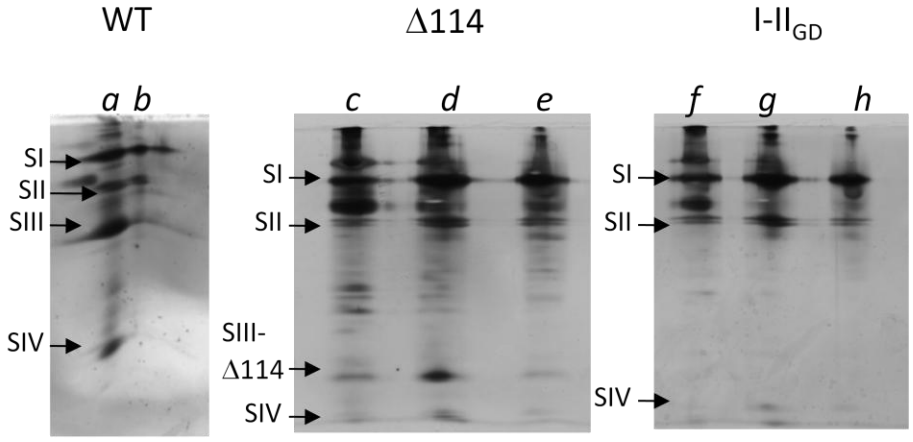
WT
Δ114
I-II$_{GD}$
a b
c d e
f g h
SI
SII
SIII
SIV
SIII-
Δ114

stoichiometry. The overall percentage of COX containing subunit III-Δ114 was estimated by a weighted average, given the percentage of COX migrating in the particular band and its estimated SIII-Δ114 incorporation. The results indicate that 65-75% of COX contains SIII-Δ114. This calculation is summarized in Table VI. It should be noted that possible saturation was not accounted for in the SIII-Δ114 2D band used for calibration, making these lower level estimates of SIII-Δ114 incorporation.

Figure 22B shows the 2D lanes corresponding to the native gel bands for I-II_{GD} COX. Similar to Δ114, these bands have decreasing amounts of impurity correlated to increasing migration rates on the native gel. The total amount of impurity appears to be less for I-II_{GD} than it is for Δ114. As expected, no subunit III band is present in I-II_{GD}.

These results indicate that the Δ114 preparations have a higher degree of impurity as compared to wildtype and I-II_{GD} COX. The enrichment of impurities relative to wildtype and I-II_{GD} was observed in SDS-PAGE gels for all three different purification preparations of Δ114, despite following the same purification protocol used for wildtype and I-II_{GD}. The molecular weights of these impurities were estimated by SDS-PAGE as shown in Figure 23. The left panel shows a Coomassie stained SDS-PAGE gel of *R.sph.* wildtype and Δ114 as well as bovine COX. The bovine COX subunits were used as calibration, as their migration rates relative to their apparent molecular weights are known (Kadenbach et al., 1983). The right panel is the silver stained second dimension SDS gel of lane *c* from Figure 22B, the Δ114 band most enriched in impurities. The four major impurities are labeled *1* through *4*. The apparent molecular weights of these impurities based on migration distances were calculated and the results are summarized

Table VI

Summary of Two-Dimensional PAGE Analysis of Δ114 COX

	Slow band[a]	Middle band[b]	Fast band[c]
Impurties:COX[d]	2.3	0.3	0.2
% of Total COX[e]	25%	45%	30%
Δ114 stoichiometry[f]	65%	75%	65%

[a] Slowest migrating band in the native PAGE gel (see Figure 22, band *c*).

[b] Middle band on the native PAGE gel (Figure 22, band *d*).

[c] Fastest migrating band in the native PAGE gel (Figure 22, band *e*).

[d] A second SDS dimension was employed to determine the subunit components of the three native gel bands observed for Δ114 COX. Silver staining density was determined using Accelrys Multiguage software. The staining intensity due to impurities was divided by the staining intensity of the sum of the COX subunits.

[e] The percentage of total COX which migrated within the specified native gel band, as determined from the second dimension SDS gel. The sum of the staining density due to COX subunits within the specified 2D lane divided by the total staining density of COX subunits in all 2D lanes.

[f] The percentage of COX which contained subunit III-Δ114, as determined from the second dimension SDS gel. The second dimension of the middle native gel band had an intense SIII-Δ114 band covering 75% of the lane width. This portion was assumed to have full incorporation of SIII-Δ114, and was used to calibrate the SIII-Δ114 stoichiometry of the other two bands.

Figure 23

SDS-PAGE analysis of impurities contained in Δ114 COX preparations. An SDS-PAGE Coomassie-stained gel with wildtype, Δ114 and bovine COX (A) is aligned with a second dimension SDS silver-stained gel of the slowest migrating Δ114 native gel band (B). This 2D band is the most enriched in impurities, which are enumerated *1-4* (see Figure 22, band *c*). The bovine subunit migration distances were used to as calibration in estimating the apparent molecular weight of impurity *1 (*39 kD), *2* (33 kD), *3* (22 kD) and *4* (19 kD).

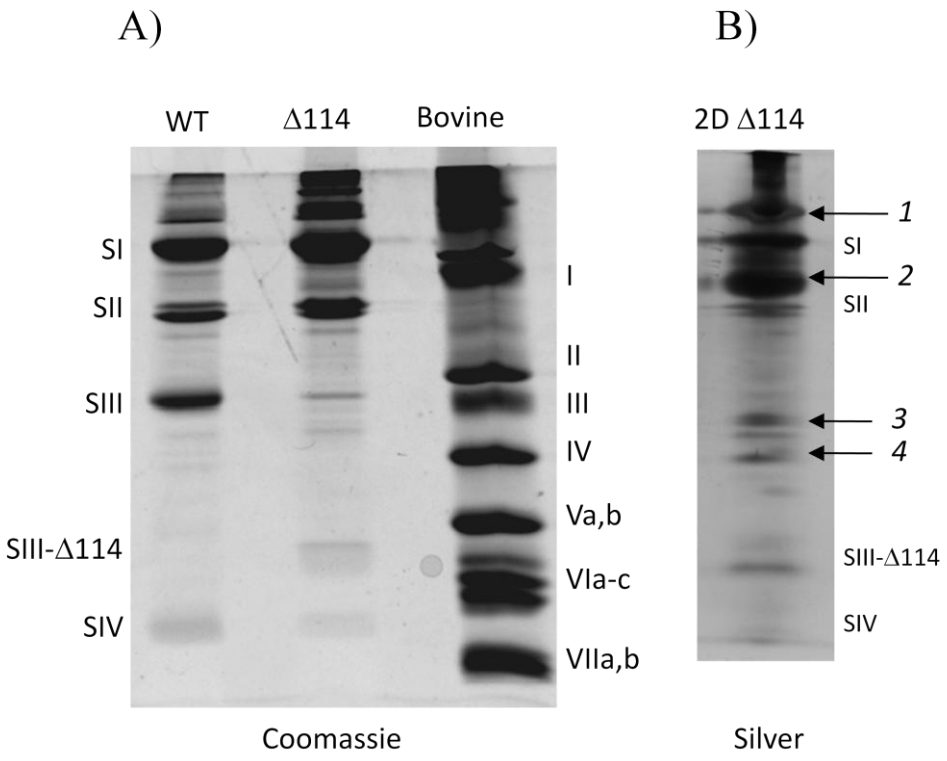
A)
B)
WT
Δ114
Bovine
2D Δ114
SI
SII
SIII
SIII-Δ114
SIV
I
II
III
IV
Va,b
VIa-c
VIIa,b
1
2
3
4
SI
SII
SIII-Δ114
SIV
Coomassie
Silver

Table VII

Summary of Masses of the Impurities Observed in Δ114 Preparations

Impurity[a]	Apparent MW[b]	MS peak[c]
1	38.7 kD	-
2	33.0 kD	~34.8 *m/z* or 32000 *m/z*[d]
3	22.0 kD	22931 *m/z*
4	18.9 kD	19496 *m/z*

[a] Four predominant impurities which are enriched in Δ114 preparations (see Figure 23).

[b] The apparent molecular weight calculated by migration distances on SDS-PAGE using bovine COX subunits as calibrating standards.

[c] Peaks routinely observed in MALDI-TOF mass spectra which correspond to the molecular weights estimated from SDS-PAGE.

[d] This peak was also tentatively assigned to full length subunit II, although it is nearly 1000 *m/z* less than the expected molecular weight of subunit II.

in Table VII. Also included in Table VII are comparable impurity peaks routinely observed in the MALDI-TOF spectra of wildtype and Δ114 COX. A mass corresponding to the ~38.7 kD impurity (*1*) was not observed in MALDI-TOF mass spectra. The ~ 33 kD impurity (*2*) could either be a protein of 34.8 *m/z* or an enrichment of full length subunit II in the preparation (~32000 *m/z*). A mass potentially corresponding to the ~22 kD impurity (*3*) was routinely observed around 22930 *m/z*. And the ~19 kD impurity (*4*) could be assigned to the 19490 *m/z* peak frequently observed. The identity of proteins with these masses is not obvious. Their enrichment in the Δ114 preparations will be discussed further.

Steady State Catalytic Activity of R.sph. Δ114 COX

When subunit III is removed from COX, the enzyme has a lower steady-state activity at physiological pH (Gilderson et al., 2003). A closer examination reveals that the pH dependence of steady-state activity is significantly altered in I-II COX. At low pH, the activity of I-II COX is close to that of wildtype, but the activity plummets sharply with increasing pH, displaying a pKa around 7.2 (Gilderson et al., 2003). For wildtype, high steady-state activity levels are maintained, having a pKa around 8.5. The impaired activity at physiological pH has been explained as a decreased ability of I-II COX to take up protons through the D-pathway (Gilderson et al., 2003). The steady-state activity at physiological pH and the pH dependence of activity were examined in Δ114 to determine the functional effects of removing the four c-terminal helices of subunit III.

The steady state catalytic activity of Δ114 at pH 7.4 was compared to wildype, I-II_{GD} and I-II_{BD} COX, and the results are depicted in Figure 24 and summarized in Table VIII. The assay was conducted under three different conditions: in 0.1% DM ("detergent," black bars), in 0.1% DM supplemented with 1 mg/mL asolectin ("lipid," light gray bars) and when COX was incorporated into phospholipid vesicles ("COV," medium gray bars). In detergent, wildtype COX displayed a steady state turnover of 1830 ± 160 sec^{-1} at pH 7.4. The activity at physiological pH for Δ114 (860 ± 110 sec^{-1}), I-II_{GD} (845 ± 100 sec^{-1}) and I-II_{BD} (1050 ± 205 sec^{-1}) were statistically equivalent to each other and about 50% that of wildtype. When the assay was conducted in lipid, the activity of wildtype increased 15% to 2190 ± 185 sec^{-1} (statistically significant increase). Inclusion of lipid in the assay did not statistically change the activity in Δ114 (890 ± 105 sec^{-1}), I-II_{GD} (900 ± 125 sec^{-1}) or I-II_{BD} (1140 ± 220 sec^{-1}). Reconstituting COX into phospholipid vesicles resulted in a decrease of steady state turnover for wildtype to 1160 ± 165 sec^{-1}, and a similar decrease was also observed for Δ114 (630 ± 30 sec^{-1}), I-II_{GD} (575 ± 35 sec^{-1}) and I-II_{BD} (760 ± 75 sec^{-1}). These results indicate that the catalytic activity of Δ114 is about half that of wildtype and is statistically equivalent to COX forms which do not contain subunit III.

Figure 25 depicts the pH dependence of catalytic activity for wildtype, Δ114 and I-II_{BD} COX. Wildtype (black) displays a decrease in activity with increasing pH. The data can be fitted to a sigmoidal curve with a single pKa of 8.7 ± 0.1, a value in agreement with published results (Gilderson et al., 2003). The pKa of I-II_{BD} COX steady-state activity was decreased to 7.1 ± 0.2 (red), as expected. Similarly, the pKa of Δ114 COX

Figure 24

Maximum steady state activity of *R.sph.* wildtype, Δ114, I-II$_{GD}$ and I-II$_{BD}$ COX. The maximum rate of electron transfer at pH 7.4 was measured polarographically by an oxygen electrode in saturating substrate conditions (50 μM cytochrome *c*, 18 mM ascorbate, 0.6 mM TMPD). The assay was conducted in 50 mM potassium phosphate, pH 7.4 which included 0.1% DM (black bars) or 0.1% DM and 1 mg/mL asolectin (light gray bars). The enzyme was reconstituted into phospholipid vesicles and the activity was determined in buffer without detergent and with 6 μM valinomycin and 6 μM CCCP included (medium gray bars). For each assay condition, Δ114, I-II$_{GD}$ and I-II$_{BD}$ COX activities were statistically equivalent to each other and about 50% of wildtype. The presence of lipid did not alter the activity (as shown by multiple paired t tests). Reconstitution into COVs uniformly reduced activity in all COX forms. N = 12.

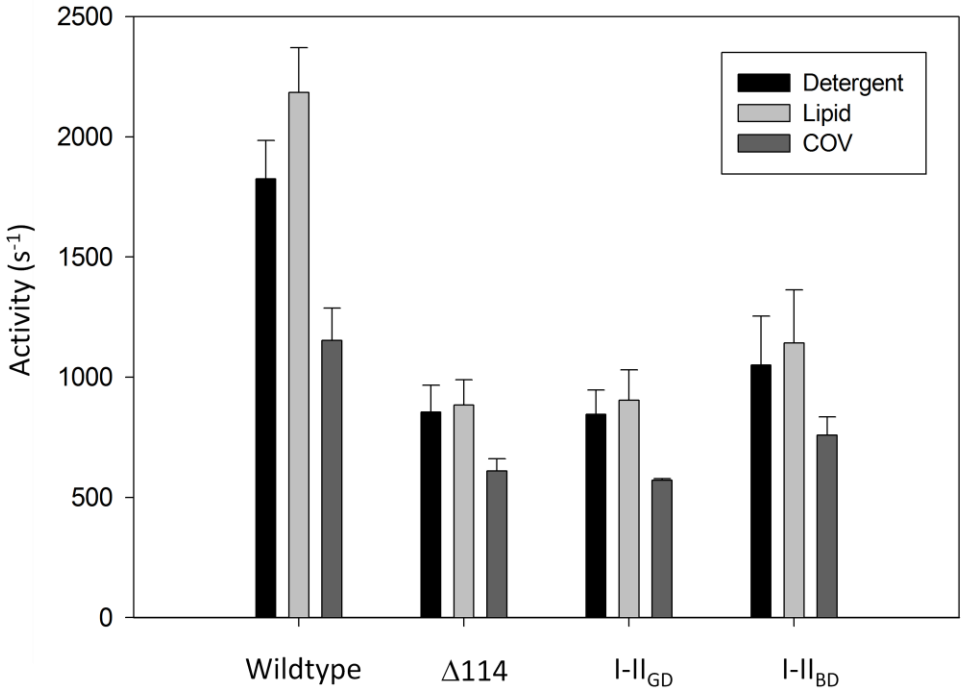
2500
2000
1500
1000
500
0
Activity (s^{-1})
Detergent
Lipid
COV
Wildtype
Δ114
I-II$_{GD}$
I-II$_{BD}$

Table VIII

Summary of Functional Properties of Wildtype, Δ114, I-II$_{BD}$ and I-II$_{GD}$ COX.

	Wildtype	Δ114	I-II$_{GD}$	I-II$_{BD}$
Activity (s^{-1}) [a]				
Detergent	1830±160	860±110	845±100	1050±205
Lipid	2190±185	890±105	900±125	1140±220
COV	1160±165	630±30	575±35	760±75
pKa [b]	8.7±0.1	7.4±0.1 [c]	-	7.1±0.2
TIA (#TN) [d]				
Detergent	~3×10^6 [e]	11470±1240	9340±440	10670±1070
Lipid	-	24270±3050	16090±2750	13160±220
COV	-	24110±2160	21000±2030	23160±1020
pKa [f]	-	6.5±0.2 [g]	-	6.1±0.5
H^+/e^- [h]	0.74±0.2	0.32±0.1	0.36±0.1	-

[a] Maximum steady state activity at pH 7.4

[b] pKa of the sigmoidal curve fit (single pKa fit) of steady state activity data taken from pH 6 to 10.

[c] pKa of Δ114 steady state activity in presence of lipid = 7.3±0.1

[d] Turnover induced inactivation CC_{50} values: the number of turnovers undergone before steady state activity reaches half maximum

[e] see (Varanasi et al., 2006)

[f] pKa of the sigmoidal curve fit to TIA data taken from pH 6 to 10.

[g] pKa of Δ114 TIA in presence of lipid = 6.5±0.1

[h] Proton pumping stoichiometry: the number of protons pumped per electron transfer to COX.

Figure 25

pH dependence of steady state activity in *R.sph.* wildtype, Δ114, and I-II$_{BD}$ COX. The steady state activity was measured polarographically by an oxygen electrode in saturating substrate conditions (50 μM cytochrome *c*, 18 mM ascorbate, 0.6 mM TMPD). Buffers suitable to the assay pH were selected (pH 6.0-6.5, 25 mM MES; pH 7.0-8.5, 25 mM HEPES; pH 9.0-10.0, 25 mM CHES). Each buffer contained 0.1% DM and the ionic strength of the buffers was adjusted to I=100 mM using KCl. The results are plotted as fraction of maximum activity with the fractional error indicated. A sigmoidal curve with a single pKa provided the best fit for the data. Wildtype (black) had a pKa of 8.7 ± 0.1, and Δ114 (royal blue, 7.4 ± 0.1) and I-II$_{BD}$ (red, 7.1 ± 0.2) both exhibited a decrease in pKa by 1.5 units. For Δ114, the assay was also conducted with 1 mg/mL asolectin included in the assay buffers (light blue, 7.3 ± 0.1). No shift in the pKa was observed relative to the detergent-only assay. N = 3.

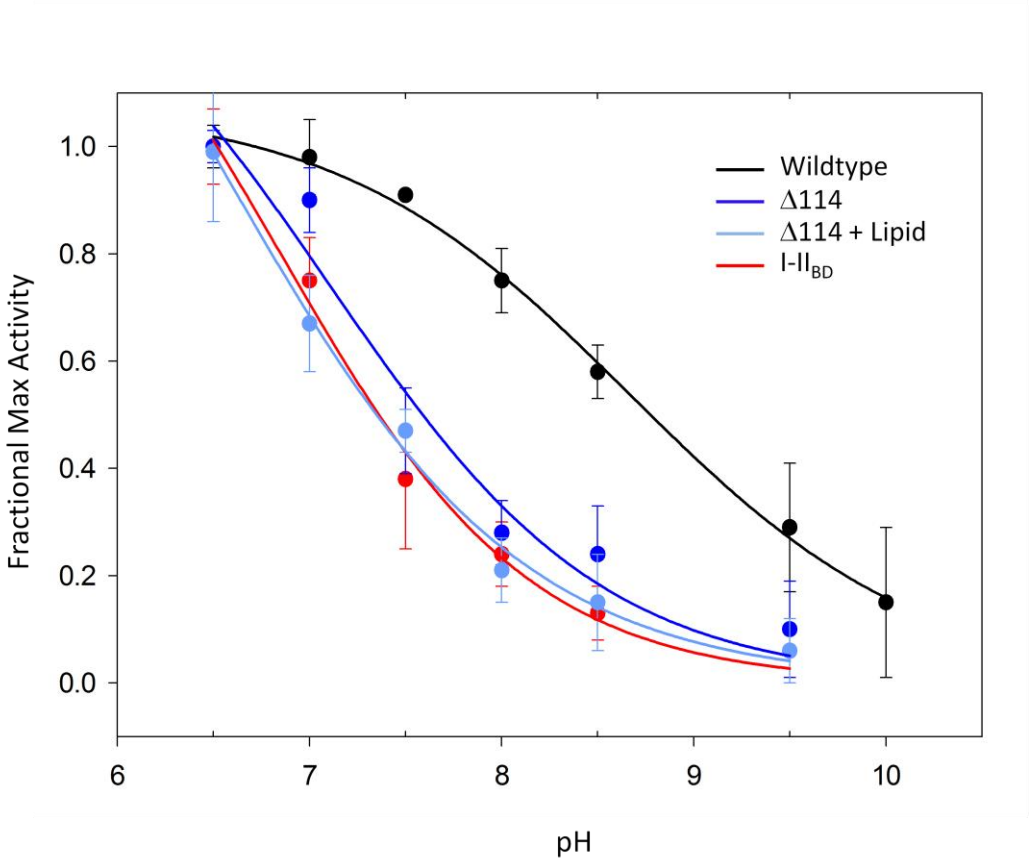
Fractional Max Activity
1.0
0.8
0.6
0.4
0.2
0.0
6
7
8
9
10
pH
Wildtype
Δ114
Δ114 + Lipid
I-II$_{BD}$

decreased to 7.4 ± 0.1 (royal blue), within statistical equivalence of the pKa of I-II_{BD} COX. Adding 1 mg/mL asolectin to the assay buffer did not significantly alter the pH dependence of activity for Δ114 COX (light blue). Therefore, Δ114 COX shows a similar pH dependence of steady-state activity to COX without subunit III. This profile is significantly altered compared to wildtype COX, and the inclusion of lipid does not ameliorate the deleterious effects on activity.

Turnover Induced Inactivation of R.sph. Δ114 COX

When subunit III is removed from COX, either through genetic or biochemical means, the enzyme undergoes turnover induced inactivation, which is an irreversible inactivation event occurring only during catalytic turnover (Bratton et al., 1999). The catalytic lifetime of the enzyme can be quantified as a CC_{50} value, the number of catalytic turnovers undergone before the activity reaches half maximum, assuming a first order decay process (see Methods). Other investigators have determined the CC_{50} values of wildtype (~3.0×10^6 turnovers) and found that the I-II COX catalytic lifetime dropped to about 10,000 turnovers, only 0.2-0.5% of wildytpe (Bratton et al., 1999; Gilderson et al., 2003; Mills et al., 2003; Mills and Hosler, 2005). Furthermore, turnover induced inactivation displays a pH dependence such that at low pH, the catalytic lifetime is increased. As pH increases, the catalytic lifetime drops off, displaying a pKa around 6-6.5 for I-II COX (Adelroth and Hosler, 2006). This suggests that turnover induced inactivation is related to the slowed proton uptake observed in the absence of subunit III (Gilderson et al., 2003; Mills et al., 2003; Mills and Hosler, 2005; Adelroth and Hosler, 2006). In addition to facilitating D-pathway proton uptake, subunit III has been proposed

to play a role in structurally stabilizing subunit I to protect it from inactivation (Mills and Hosler, 2005). The PL1 and PL2 lipids bound in the cleft region of subunit III (see Figure 15) have suggested involvement in this stabilization (Varanasi et al., 2006). Turnover induced inactivation in Δ114 was measured in the presence and absence of exogenous lipid and compared to I-II_{GD} and I-II_{BD} COX in order to assess the role that lipid and the three n-terminal helices of subunit III may play in protecting against inactivation.

The previously published value for turnover induced inactivation of I-II COX was reproduced for I-II_{GD} (9340 ± 440 turnovers) and I-II_{BD} (10670 ± 1070 turnovers) when the assay was conducted in 0.1% DM at pH 7.4 (Figure 26, black bars, also see Table VIII). The catalytic lifetime of Δ114 COX was statistically equivalent to I-II_{BD} and I-II_{GD} in the detergent assay (11470 ± 1240 turnovers). When the assay buffer was supplemented with 1 mg/mL asolectin, the catalytic lifetime of Δ114 increased 2.1 fold to 24270 ± 3050 turnovers. This result was statistically different ($p < 0.001$) than the more modest increases observed for I-II_{GD} (1.7 fold increase) and I-II_{BD} (1.2 fold increase), which had catalytic lifetimes in lipid micelles of 16090 ± 2750 turnovers and 13160 ± 220 turnovers, respectively (light gray bars). The catalytic lifetime of Δ114 was not further increased relative to the lipid micelle assay when the enzyme was reconstituted into phospholipid vesicles and measured in the presence of ionophores (24110 ± 2160 turnovers). However, reconstitution into lipid vesicles increased the catalytic lifetimes of both I-II_{BD} (23160 ± 1020 turnovers) and I-II_{GD} (21000 ± 2030 turnovers) to statistical equivalence with the catalytic lifetime of Δ114 achieved in lipid micelle (medium gray bars). These results indicate that the presence of subunit III-Δ114 provides a protective

Figure 26

Catalytic lifetimes of *R.sph.* Δ114, I-II$_{GD}$ and I-II$_{BD}$ COX. Turnover induced inactivation of COX can be quantitated by the CC_{50} value, which is the number of catalytic turnovers undergone by an enzyme population before reaching half maximal activity. The catalytic lifetimes were measured polarographically by an oxygen electrode in saturating substrate conditions (50 μM cytochrome *c*, 18 mM ascorbate, 0.6 mM TMPD). The assay buffer was 50 mM potassium phosphate, pH 7.4 and included 0.1% DM (black bars) or 0.1% DM and 1 mg/mL asolectin (light gray bars). The enzyme was reconstituted into phospholipid vesicles and assays were conducted in buffer without detergent and with the addition of 6 μM valinomycin and 6 μM CCCP (medium gray bars).

In the detergent assay (black bars), Δ114, I-II$_{GD}$ and I-II$_{BD}$ lifetimes were statistically equivalent to each other at about 10,000 turnovers. The presence of lipid (light gray bars) increased the catalytic lifetime of Δ114 to 24270±3050, more than 2 fold. There were more modest lipid-induced increases in the catalytic lifetimes of I-II$_{GD}$ (1.7 fold) and I-II$_{BD}$ (1.2 fold), but these changes were statistically smaller than the increase observed for Δ114 ($p < 0.001$). Reconstitution into COVs (medium gray bars) did not significantly alter the catalytic lifetime of Δ114 relative to its lipid-protected lifetime. The lifetimes of reconstituted I-II$_{GD}$ and I-II$_{BD}$ COX were increased to levels statistically equivalent to the lipid-protected Δ114 lifetime. These results indicate that the lipid micelle provides a protection against inactivation for Δ114 which can only be achieved for I-II$_{GD}$ and I-II$_{BD}$ COX in the lipid bilayer. N = 12.

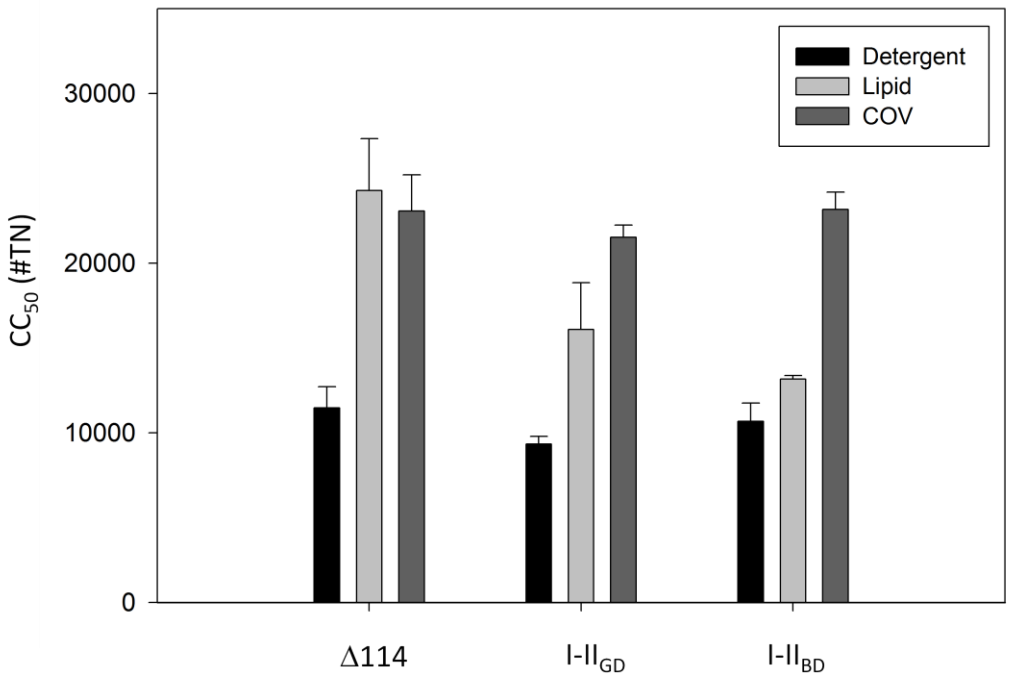
Detergent
Lipid
COV
30000
20000
10000
0
CC50 (#TN)
Δ114
I-II GD
I-II BD

effect against turnover induced inactivation in lipid micelles that can only be achieved for I-II COX when the enzyme is in the more constrained, lipid-saturated environment of a lipid vesicle. The implications of this significant result will be expounded further.

The pH dependence of turnover induced inactivation for Δ114 and I-II_{BD} COX is displayed in Figure 27 (see Table VIII). The data for I-II_{BD} COX (red) fit to a sigmoidal curve with a pKa of 6.1 ± 0.5, in agreement with literature values (Adelroth and Hosler, 2006). The pH dependence of inactivation of Δ114 was somewhat shifted to the alkaline (royal blue, 6.5 ± 0.2), although not to a statistically significant degree. Supplementing the assay buffer with 1 mg/mL asolectin did not modify the pH dependence of Δ114 inactivation (light blue, 6.5 ± 0.1). These results suggest that the protection effect provided by Δ114 COX in the presence of lipid is probably not due to improved D-pathway proton uptake but rather to structural stabilization of the enzyme (see Discussion).

Proton Pumping Activity of R.sph. Δ114 COX

Removing subunit III from COX decreases its proton pumping efficiency to one half that of wildtype COX (Mills et al., 2003). This effect could be due to the impaired proton uptake in the D-pathway and/or due to a minor structural change in the vicinity of E286 in subunit I, the point in the D-pathway at which the proton is transferred either to the active site or to the pump site (Gilderson et al., 2003; Brzezinski and Johansson, 2010). The proton pumping activity of Δ114 COX was compared to wildtype and I-II_{GD} COX in order to assess the importance of the three n-terminal helices for the proton pumping activity of COX.

Figure 27

pH dependence of the catalytic lifetimes in *R.sph.* Δ114, and I-II_{BD} COX. The catalytic lifetime (CC_{50}) was measured polarographically by an oxygen electrode in saturating substrate conditions (50 μM cytochrome *c*, 18 mM ascorbate, 0.6 mM TMPD). Buffers suitable to the assay pH were selected (pH 6.0-6.5, 25 mM MES; pH 7.0-8.5, 25 mM HEPES; pH 9.0-10.0, 25 mM CHES). Each buffer contained 0.1% DM and an ionic strength adjusted to I=100 mM using KCl. The results are plotted as fraction of maximum catalytic lifetime with the fractional error indicated. A sigmoidal curve with a single pKa provided the best fit for the data. The pKa values for Δ114 (royal blue, 6.5 ± 0.2) and I-II_{BD} (red, 6.1 ± 0.5) were statistically equivalent. For Δ114, the assay was also conducted with 1 mg/mL asolectin and 0.1% DM in the assay buffers (light blue, 6.5 ± 0.1). No shift in the pKa was observed relative to the detergent-only assay. N = 3.

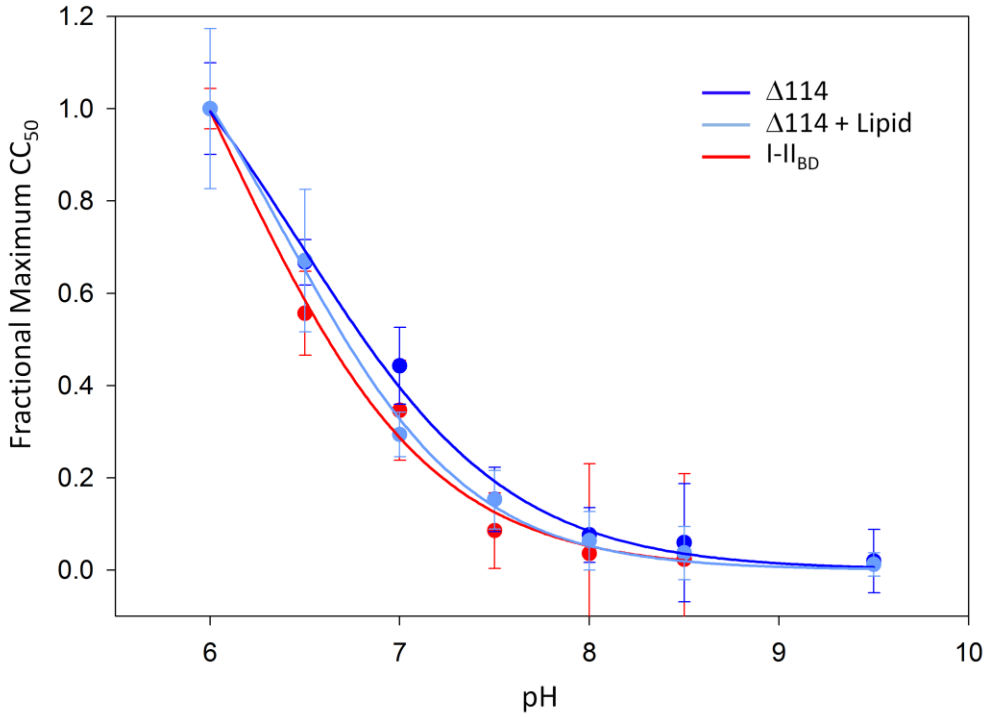
1.2
1.0
0.8
0.6
0.4
0.2
0.0
Fractional Maximum CC50
6
7
8
9
10
pH
Δ114
Δ114 + Lipid
I-IIBD

Figure 28

Proton pumping activity of *R.sph.* wildtype, Δ114 and I-II$_{GD}$ COVs. Proton pumping activity was measured by stopped-flow absorbance spectroscopy on an Applied Photophysics SV.20 Reaction Analyzer. Phenol red was used as a pH indicator to monitor acidification-induced absorbance changes caused by the proton pumping activity of reconstituted COX in the presence of valinomycin (lower traces). The alkalinization phase (upper traces) results from the consumption of protons for O_2 reduction observed when reconstituted COX undergoes turnover in the presence of CCCP and valinomycin. This absorbance change is proportional to the number of electrons transferred to COX. The H^+/e^- ratio is calculated from the extents of the lower and upper traces. Displayed are averaged traces for a 5 turnover experiment (0.05 μM COX, 1 μM ferrocytochrome *c*, 5 μM CCCP, and/or 5 μM valinomycin, pH 7.2). The COVs had RCR values of 6-10 and RCR_{val} values of 2-2.5.

Wildtype COVs (black) had an H^+/e^- ratio of 0.74 ± 0.2. The H^+/e^- ratios of Δ114 COVs (blue, 0.32 ± 0.1) and I-II$_{GD}$ COVs (green, 0.36 ± 0.1) were statistically equivalent and about 50% less than wildtype.

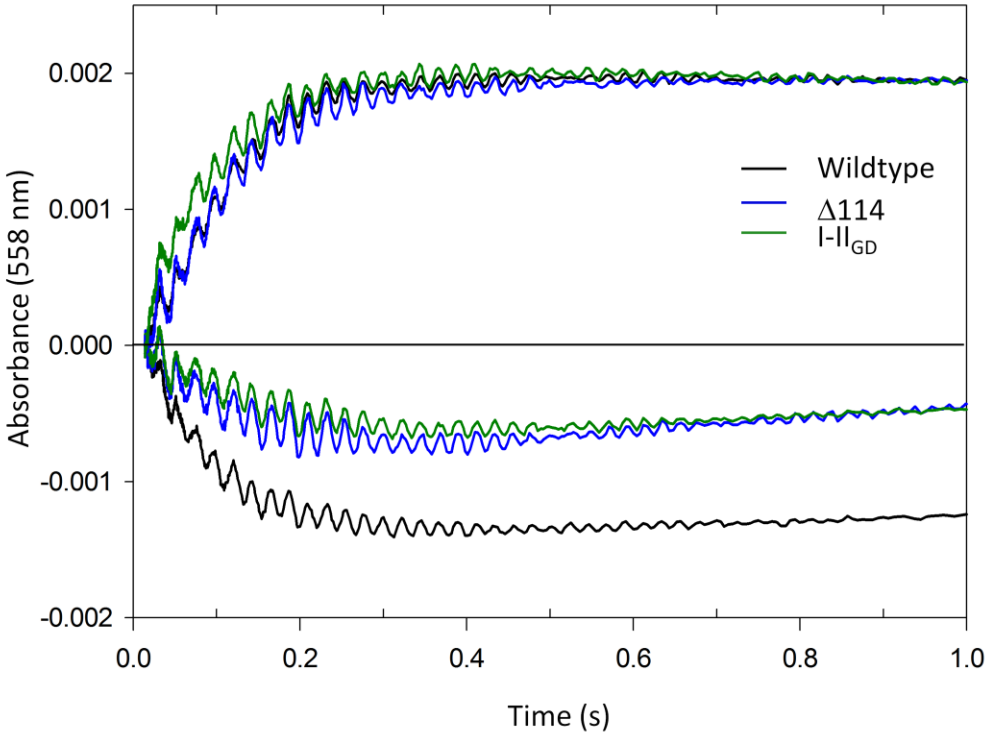
0.002
0.001
0.000
-0.001
-0.002
Absorbance (558 nm)
0.0
0.2
0.4
0.6
0.8
1.0
Time (s)
Wildtype
Δ114
I-II$_{GD}$

The proton pumping activities of wildtype, Δ114 and I-II$_{GD}$ COVs were measured by stopped flow absorbance spectroscopy, and the traces are shown in Figure 28. The upper traces have been normalized, allowing a comparison of the pumping efficiencies of wildtype (black), I-II$_{GD}$ (green) and Δ114 (blue). The proton pumping efficiency of Δ114 (0.32 ± 0.1 H^+/e^-) is equivalent to I-II$_{GD}$ (0.36 ± 0.2 H^+/e^-) and is about half the efficiency of wildtype, which had an H^+/e^- of 0.74 ± 0.2 (see Table VIII). These results indicate that the n-terminal region of subunit III is not sufficient to prevent the deleterious effects on proton pumping that are seen in the absence of subunit III, a result which will be further discussed.

IV. Discussion

Biophysical and Biochemical Characterization of *R.sph.* pCOV Sheds Insight into the Oligomeric Structure of *R.sph.* Cytochrome *c* Oxidase

Discontinuous sucrose gradient ultracentrifugation was used to separate proteoliposomes containing *R.sph*. COX from liposomes devoid of enzyme. The purified fraction containing COX (pCOV) was analyzed for its functional and biophysical properties and compared to unpurified COVs. It was found that the purification technique reduced the excess lipid concentration resulting in a decrease in the net buffering capacity of the solution. Light scattering was also reduced, making pCOV better suited for low buffer spectroscopic studies. The oxygen reduction and proton pumping activities of pCOVs were maintained to a high degree relative to COVs, indicating that the technique does not significantly damage the liposomes. Finally, the number of COX molecules per vesicle was estimated by the lipid and protein concentration of the pCOV fraction and the known size of the vesicles. It was found that there is only one *R.sph*. COX molecule per liposome. A similar study conducted on bovine pCOV estimated the number of bovine COX per vesicles was two or three. Taken together, these results indicate that maximally functional *R.sph*. COX exists in the monomeric state when in the lipid bilayer, contrary to the bovine enzyme which is dimeric.

Discontinuous Sucrose Gradient Ultracentrifugation and Biophysical and Biochemical Characterization of pCOV

Previous work on reconstituted bovine COX showed that discontinuous sucrose gradient ultracentrifugation is a technique by which liposomes containing enzyme can be purified away from liposomes devoid of enzyme (Nguyen et al., 2002). Unpurified liposomal preparations (COV) typically contain about 6–7 liposomes devoid of enzyme to every COX-containing liposome, so the need for such a purification method is critical due to increased net buffering capacity from the phospholipid headgroups, deleterious binding interactions between cytochrome *c* and the excess lipids (Choi and Dimitriais, 2004; Gorbenko et al., 2006), and due to light scattering which can complicate spectroscopic measurements in the unpurified COV preparation. Since mutagenesis studies in the bovine form of the enzyme are not easily performed and are inefficient (Hosler et al., 2006), the structural and functional models for mutagenesis studies of COX are bacterial oxidases, such as *Rhodobacter sphaeroides* and *Paracoccus denitrificans* COX (Cao et al., 1992; Hosler et al., 1992; Hosler et al., 2006; Lee et al., 2009; Brzezinski and Johansson, 2010). It was therefore important to ensure that the sucrose ultracentrifugation technique would yield similar results for the *R.sph.* enzyme.

The results showed that *R.sph.* COX behaved somewhat differently in the gradient than did bovine COX. *R.sph.* pCOV yields were somewhat lower (40% versus 60%) and the bands were more diffuse than those seen for bovine COVs. This could be due to increased protein–protein or protein–lipid interactions during the sedimentation process. An attempt to disrupt ionic interactions revealed, however, that the sedimentation pattern did not change in salt concentrations as high as 100 mM KCl. In any case, the bands were tight enough and the yields were high enough for satisfactory purification of pCOVs.

It was found that the purification procedure reduced the lipid concentration 6-8 fold in the pCOV fraction. The net buffering capacity of the solution was decreased as evidenced by 30% greater extents of pH-induced absorbance changes, as monitored by phenol red absorbance in proton pumping assays. Also, the light scatter of the pCOV solutions was reduced by about half compared to unpurified COVs. The reduction in buffer capacity and light scattering makes pCOVs more suited for low buffer spectroscopic studies such as proton pumping assays.

Following ultracentrifugation, there was a decrease in maximum steady-state turnover, in RCR values and in the H^+/e^- ratios of the pCOVs relative to unpurified COVs. These decreases mirror the results seen in the bovine pCOVs (Nguyen et al., 2002). A factor potentially contributing to the reduction in the functional activities could be the high hydrostatic pressure (1500 atm) experienced by the COVs during centrifugation. This pressure could cause physical damage to the enzyme, leakage of intravesicular buffer, or cause the vesicles to break and reseal with complete exchange of intravesicular buffer. Previous work presents evidence which suggests that vesicular breakage is not a major cause for concern (Nguyen et al., 2002). Following ultracentrifugation, the orientation of the cytochrome *c* binding face was assayed, and it was found that proper orientation was equivalent in bovine COVs and pCOVs (85-90% facing external). Furthermore, bovine pCOV were made with rhodamine labeled phospholipids and found to migrate to the same position when recentrifuged on a fresh gradient without significant loss of labeled phospholipid. Together, these tests suggest that the vesicles are not breaking and resealing; no loss of lipid, no change in protein density, and no alteration of the orientation of the COX molecules were observed.

The effects of high hydrostatic pressure on detergent-solubilized bovine COX have been examined elsewhere. At hydrostatic pressures above 2000 atm, the monomeric form of bovine COX experienced dissociation of subunits VIa, VIb, III and VIIa and a loss of electron transport activity (Stanicova et al., 2004; Stanicova et al., 2007). The dimeric form of the enzyme was significantly more resistant to these high pressures and did not undergo subunit dissociation. For bovine pCOV, SDS–PAGE analysis with Coomassie staining of the lysed pCOV enzyme showed no such loss in subunit content following discontinuous sucrose gradient ultracentrifugation (Nguyen and Prochaska, unpublished results). Since the *R.sph.* enzyme lacks the nuclear subunits, the most likely candidate for subunit dissociation under elevated hydrostatic pressures would be subunit III, as the binding interaction between subunits I and II is more substantial (Thompson and Ferguson-Miller, 1983; Qin et al., 2006). The fact that *R.sph.* COX undergoes turnover induced inactivation in the absence of subunit III can be used as to test for subunit III dissociation (Bratton et al., 1999; Gilderson et al., 2003; Mills et al., 2003; Mills and Hosler, 2005). No evidence of turnover induced inactivation was observed in the electron transfer activity assays of *R.sph.* pCOV, indicating that the enzyme is still intact.

Elevated hydrostatic pressures have been shown to induce transient shape changes in lipid vesicles which can cause intravesicular water leakage by an undefined mechanism (Beney et al., 1997; Perrier-Cornet et al., 2005). It is possible that the mechanism could involve transient pore formation, which could allow intravesicular buffer to leak as well (Perrier-Cornet et al., 2005). In other words, the hydrostatic pressures experienced by the pCOV during ultracentrifugation could potentially result in

the loss of some intravesicular buffering capacity, although the use of zwitterionic HEPES reduces this likelihood. To test this possibility, the intravesicular buffering capacity was measured for bovine pCOVs and compared to unpurified COVs. The pCOV fraction maintained about 70% of the buffering capacity of unpurified COVs (data not shown). This minimal intravesicular buffer leakage could explain why proton pumping experiments utilizing 10 enzymatic turnovers have decreased H^+/e^- pumping stoichiometries relative to experiments using 5 catalytic turnovers (see Table I). The decrease in the H^+/e^- ratio is not likely due to a decrease in the proton pumping capability of the enzyme, but rather to the diminished intravesicular source of protons for pumping. Taken together, these results indicate that our purification technique results in a pCOV preparation suitable for low turnover studies; enzymatic activity, vesicle proton impermeability and proton pumping capabilities are sufficiently retained.

The number of *R.sph.* COX molecules per lipid vesicle was found to be one, contrary to the results for bovine COX which had 2-3 COX molecules per vesicle. The manner in which this value was estimated assumes a uniform distribution of protein molecules in the vesicles of the pCOV band. To test the validity of this assumption, COVs were purified in sucrose concentrations as high as 17%. If the distribution of the protein in the liposomes were not uniform, the liposomes containing more protein molecules would have a greater density and therefore migrate farther through the gradient, forming additional bands. A single band was still observed in the higher sucrose concentrations, indicating that the *R.sph.* COX molecules are distributed uniformly in the liposomes. Therefore, each pCOV typically contains only one COX molecule, which

sheds insight into the oligomeric structure of *R.sph*. COX as will be further discussed below.

Alternative procedures have been used to purify COX-containing liposomes from those devoid of enzyme. These procedures include cytochrome *c* affinity chromatography for the beef heart enzyme (Madden and Cullis, 1985) and nickel affinity chromatography using the *R.sph.* enzyme with a poly-histidine tag located on the outward facing c-terminus of subunit II (Hiser et al., 2001). Anion exchange chromatography of bovine COVs resulted in a preparation of COX-containing liposomes with the proper orientation of the cytochrome *c* binding face. However, the resulting preparations were very dilute, of very low yield (less than 20% recovery), and were found unsuitable for proton pumping experiments. *R.sph.* COX with a poly-histidine tag on subunit II was engineered by Hiser et al. (Hiser et al., 2001). Nickel affinity chromatography of these COVs yielded a purified preparation with complete retention of respiratory control and both electron transfer and proton pumping activity (Hiser et al., 2001), results qualitatively similar to those we observed with our technique, although the yield of the pCOV from the starting COV was not discussed. They also estimated that 5–20 molecules of *R.sph.* COX were incorporated per liposome based upon previously published electron microscopy estimations of the number of bovine COX molecules in 300 Å diameter unpurified liposomes (Tihova et al., 1993). Our results, based on direct measurement, indicate that there is only one *R.sph.* COX molecule per liposome. In addressing this potential contradiction it should be noted that our estimation was based on direct measurements of the lipid and protein concentration. Hiser *et al.* estimated the number of COX molecules based on electron microscopy of bovine liposomes and then assumed a similar number

for *R.sph*. It is physically unlikely for 5–20 molecules of COX (dimensions of 44 by 76 Å in the plane of the bilayer) to fit into a liposome only 300 Å in diameter, especially due to the high radius of curvature of the bilayer. In addition, our direct measurements of vesicle lipid and protein content have at most 20% error, not 5 to 20 fold error. Thus, the electron microscopy result is most likely an overestimate of the number of COX molecules per pCOV.

To summarize, discontinuous sucrose gradient ultracentrifugation was found to be a useful method for separating *R.sph*. COX-containing vesicles from liposomes devoid of enzyme. Decreased external buffering capacity of solution and reduced light scattering were two positive effects of this purification procedure. The decreases in activities following ultracentrifugation were minimal and could be explained by slight damage caused by hydrostatic pressure to the enzyme and to the vesicles. The intravesicular buffering capacity of the pCOV was maintained to a degree adequate for low turnover proton pumping studies. It was found that the proteoliposomes contained one molecule of *R.sph*. COX per vesicle.

The Oligomeric Structure of R.sph. COX in the Lipid Membrane

The oligomeric structure of bovine COX has been the subject of investigation for some years. Early on, ultracentrifugal sedimentation velocity and gel filtration studies indicated the enzyme was monomeric in DM detergent and had maximal electron transfer and proton pumping activity as a monomer (Suarez et al., 1984; Thompson et al., 1985). However, it was later shown that the bovine enzyme dimerizes when it is introduced into the membrane environment, and it was proposed that dimerization was necessary for full

proton pumping efficiency (Finel and Wikstrom, 1986). Chemical cross-linking experiments were used to further validate that bovine COX exists in the dimeric state when reconstituted into lipid vesicles (Estey and Prochaska, 1993). When the three-dimensional x-ray crystal structure was obtained, bovine COX crystallized in the dimeric state (Tsukihara et al., 1996). In the crystal structure, the monomer–monomer contacts are largely via subunits VIa and VIb, which are lacking in the bacterial forms of the enzyme (Lee et al., 2001). Musatov and Robinson confirmed that the presence of subunits VIa and VIb were necessary for dimerization of the bovine enzyme and provided further evidence that the bovine enzyme has a strong, intrinsic propensity to dimerize in the phospholipid bilayer (Musatov and Robinson, 2002). It was also shown that when bovine COX was converted to the monomeric form by exposure to Triton X-100 or alkaline pH, the rate of the F to O step in the catalytic cycle was altered (Sadoski et al., 2001). Since this reaction step is coupled to proton uptake and translocation, it was proposed that the oligomeric structure of the enzyme plays some role in these functions. Taken together, these results indicate that bovine COX dimerizes in the membrane and that the dimer might be necessary for maximal proton pumping efficiency.

The oligomeric states of the bacterial COX forms have not been intensely studied, so the oligomeric structure of *R.sph.* COX was unknown. Since *R.sph.* COX lacks subunits VIa and VIb, it has been suggested to be monomeric, as it also crystallizes essentially as a head to tail dimer, which is structurally impossible in the bilayer (Lee et al., 2001; Svensson-Ek et al., 2002; Qin et al., 2006). Furthermore, it was shown that cytochrome bo_3 from *E. coli* was monomeric when in detergent micelle (Musatov et al., 1999). Cytochrome bo_3 is an ubiquinol oxidase belonging to the same heme-copper

oxidase family as cytochrome *c* oxidase, catalyzing oxygen reduction coupled to proton translocation. The four subunit *E. coli* ubiquinol oxidase has substantial structural similarities to bacterial cytochrome aa_3 oxidases (Chepuri et al., 1990; Abramson et al., 2000). By analogy, it is therefore likely that *R.sph*. COX is also monomeric in detergent micelle. However, given the evidence that the lipid membrane environment induces bovine COX to dimerize, it is important to address whether a similar process could be dimerizing *R.sph*. COX upon reconstitution into lipid vesicles. If *R.sph*. COX retains its monomeric state in the lipid bilayer, this result could shed insight into whether or not dimerization is critical to the proton pumping function of COX.

The results of this dissertation indicate that there is only one *R.sph.* COX molecule per liposome. For the bovine enzyme, 2–3 COX molecules per liposome were observed, consistent with the proposal that bovine COX experiences a driving force for dimerization upon reconstitution into lipid vesicles (Musatov and Robinson, 2002; Nguyen et al., 2002). No such driving force is apparent for *R.sph.* COX. The enzyme appears to be in the monomeric state when reconstituted into lipid vesicles, suggesting that the functional form of *R.sph.* COX is monomeric *in vivo* as well. This result further highlights the role that the nuclear subunits play in facilitating dimerization, as their absence in *R.sph*. COX is the predominant structural difference between the bacterial and mitochondrial forms of the enzyme (Tsukihara et al., 1996; Iwata et al., 2002; Svensson-Ek et al., 2002). Furthermore, the results indicate that the monomeric form of *R.sph.* COX is capable of maximal electron transfer and proton pumping activity. This is a novel result in that COX has not been definitively shown to be capable of maximal proton pumping activity when in the monomeric state. Dimerization is therefore unlikely to be

required for maximal proton pumping activity of mitochondrial COX, and the dimerization behavior observed for bovine COX must play an alternate role such as regulation or added stability, as has been previously proposed (Sadoski et al., 2001; Stanicova et al., 2007; Fornuskova et al., 2010).

Structural and Functional Characterization of *R.sph.* Δ114 COX Sheds Insight into the Role of Subunit III in the Proper Assembly and Function of COX

Cytochrome *c* oxidase subunit III is a member of the three subunit functional core of the enzyme, although the explicit role of this subunit has not been fully elucidated. A human mitochondrial disease has been shown to be due to a genetic truncation of subunit III after only three of its seven helices. This mutation was modeled in *R.sph.* COX in order to gain insight into the structural and functional significance of subunit III. The Δ114 mutation is ideally suited for studying any specific roles of the n-terminus, the v-shaped cleft and the c-terminal bundle of the subunit (see Figure 15). When expressed in *R.sph.* cells, the Δ114 COX mutant had lower levels of expression and seemed to impede the rate of COX assembly. The enzyme incorporated the truncated subunit III with at least 70% stoichiometry, and the subunit was subject to only minor proteolytic processing at one specific cleavage site. Additionally, the native processing of subunits II and IV was altered in the Δ114 and I-II COX forms. The proton pumping and oxygen electrode activities were about half that of wildtype at physiological pH and were about equivalent to I-II COX forms. Finally, Δ114 COX underwent turnover induced inactivation at a similar rate as I-II COX. However, when the assay buffer was supplemented with asolectin, the catalytic lifetime was statistically greater than that of I-II COX forms.

Taken together, these results indicate that the c-terminal bundle of subunit III plays a role in maximizing the assembly efficiency of COX and optimizing the native processing of subunit II. Furthermore, the importance of the structural lipids within the v-shaped cleft is highlighted as being important in providing protection against turnover-induced inactivation.

The Role of Subunit III in the Assembly of R.sph. COX

Subunit III has been proposed to play a role in the proper assembly of COX. Bratton *et al.* conducted a study in which the genes for subunit III and/or subunit II were deleted from an overexpression vector which also contained the gene for subunit I with a poly histidine tag (Bratton et al., 2000). In the absence of subunits II and III, a form of subunit I was purified which contained heme *a* but not the heme a_3-Cu_B active site (subunit I*a*). This suggested that subunit II is required for proper metal insertion of the heme a_3 active center. Indeed, when the genes for subunits I and II but not III were present, a heterogeneous preparation resulted which had I-II COX with proper metal center insertion and also a noticeable amount of free subunit I*a*. This indicated that subunit III was not required for the proper assembly of subunit I and II, but it did participate in the process, as evidenced by the pooling of the subunit I*a* assembly intermediate in the absence of subunit III (Bratton et al., 2000). Free subunit I*a* has been shown to be an early assembly intermediate in COX assembly, both in prokaryotic and mitochondrial forms of the enzyme (Bratton et al., 2000; Fontanesi et al., 2008; Fernandez-Vizarra et al., 2009).

The data presented here support the conclusion that subunit III is involved in assembly and extend the argument by highlighting the necessity of the c-terminal domain in this process. In both I-II_{GD} and Δ114 COX preparations, there was an enrichment of free subunit I*a* as compared to the wildtype preparations, and lower levels of COX were noted in the membranes, suggesting assembly was hindered. A similar result was also observed for a truncation mutation in subunit III which removed the seventh c-terminal helix to form Δ238 COX (Geyer, 2007). It is not entirely clear what role the c-terminal domain of subunit III could be playing in the proper assembly of COX. Since I-II COX can form in the absence of subunit III, it is not a required component of the assembly process, but its absence or truncation seems to present a bottleneck in the process such that the assembly intermediate upstream accumulates. Therefore, it is likely to provide stabilization which increases the rate of an assembly step (Bratton et al., 2000). Along these lines, subunit III could be stabilizing an interaction between subunit I and surf1. Surf1 is a COX assembly protein conserved from mammals to prokaryotes and is involved in the insertion of heme a_3 into subunit I (Smith et al., 2005; Stiburek and Zeman, 2010). Heme a_3 insertion seems to enhance the binding of subunit I to subunit II (Stiburek and Zeman, 2010), so an impedance in the rate of heme a_3 insertion would result in a pooling of subunit I which would be devoid of heme a_3 and unable to interact with subunit II – in other words, free subunit I*a*. Surf1 is a ~30 kD protein composed of two transmembrane domains and a large globular domain extending into the periplasm or inner membrane space (Stiburek and Zeman, 2010). The c-terminal domain of subunit III could enhance a binding interaction between Surf1 and COX subunit I. If Surf1 bound to helix 6 or 7 of subunit I – helices surrounding the subunit I heme a_3 center – the c-

terminal domain of subunit III would be ideally situated to foster the Surf 1 – subunit I interaction. Subunit III would not be required for the interaction, but would stabilize it and enhance the rate of heme a_3 insertion and subsequent binding of subunit II. In *R.sph.*, putative COX assembly intermediates have also been isolated consisting of only subunits I and III, so this type of interaction could be possible (Hiser and Hosler, 2001). There is still much to be elucidated concerning the assembly process of COX, so there are many other possible ways in which subunit III could be involved in the process. This example highlights the type of role subunit III could putatively play.

The Role of Subunit III in the Native Processing of Subunit II

Early in the development of COX bacterial model systems, COX from *P.dent.* and *R.sph*. were observed to undergo native processing in subunit II at the n- and c-termini (Steinrucke et al., 1987; Cao et al., 1991). The reason for this processing is unknown, although it could be to remove a targeting peptide (Cao et al., 1991). *R.sph*. COX which has been purified by Ni^{2+}-NTA chromatography contains three forms of subunit II – a 32930 Da form which is unprocessed, a 30660 Da form (IIC) which is only processed at its n-terminus, and a 29122 Da form (IIA) which is fully processed at both termini (Hosler et al., 1992; Zhen et al., 1998; Hiser et al., 2001; Distler et al., 2004). Hosler *et al*. used DEAE-5PW chromatography to separate these three forms of COX and found that they had equivalent rates of electron transfer (Hosler et al., 1992). Further analysis by Hiser *et al.* confirmed equivalent steady state activity between a preparation with a mixture of subunit II forms and a preparation of the purified fully-processed form (IIA). Upon closer examination, however, evidence was revealed that the presence of the

unprocessed form of subunit II might slightly elevate the K_M of cytochrome *c* binding, although the increase was close to the error in the measurements (Hiser et al., 2001). In this dissertation, it was observed that I-II_{GD} and Δ114 COX had noticeably elevated levels of the partially processed form of subunit II (form IIC) as compared to wildtype preparations. This suggests that subunit III might participate in maintaining optimal rates of proteolytic processing in subunit II, a step that could be required for optimal COX activity in a limited substrate environment. This putative role for subunit III involves the entire c-terminal domain, as Δ114 COX showed the same proteolytic processing patterns in subunit II as I-II_{GD} COX. Steady-state levels of activity were not affected in I-II_{GD} and Δ114 COX as compared to I-II_{BD} COX. I-II_{BD} has the same ratios between the subunit II forms as wildtype COX, due to the fact that for I-II_{BD}, subunit III is removed biochemically from wildtype COX. Therefore, this demonstrates that the reduction in steady-state activity of I-II_{GD} and Δ114 COX compared to wildtype COX was due to a mechanism other than elevated levels of unprocessed subunit II.

At limiting levels of cytochrome *c*, the relative enrichment of the unprocessed form of subunit II in the Δ114 and I-II_{GD} preparations might have a greater effect on COX activity, providing a selective pressure for subunit II processing. However, it should be noted that although both *P. denitrificans* and *R. sphaeroides* undergo subunit II processing, the cleavage site at the n-terminus is not identical, suggesting that the processing mechanism is not highly conserved (Hiser et al., 2001). Evidence for a similar process in mitochondrial COX has not been observed, as subunit II from bovine COX routinely runs as a single band on SDS-PAGE gels (Kadenbach et al., 1983; Ogunjimi et al., 2000). Indeed, the protein coding sequence of bovine COX at the c-terminus

terminates 20 amino acids shorter than *R.sph.*, immediately after its last surface-exposed helix, so the subunit appears to be translated devoid of the sequence that is usually subsequently removed from the prokaryotic forms of COX (Tsukihara et al., 1996; Hiser et al., 2001). This observation raises interesting evolutionary questions regarding the different strategies of mammalian and prokaryotic COX assembly and native proteolytic processing.

The Role of Subunit III in D-pathway Proton Uptake

In the absence of subunit III, steady-state activity, proton pumping efficiency and the catalytic lifetime of COX decrease. It has been proposed that these effects are due to decreased proton uptake through the D-pathway and due to a loss of structural support of subunit I provided by subunit III (Gilderson et al., 2003; Mills and Hosler, 2005; Adelroth and Hosler, 2006). In the Δ114 COX mutation, the four c-terminal helices of subunit III have been removed, but the three n-terminal helices are retained, a region which contains a putative proton antenna and the v-shaped cleft which binds lipids of proposed functional importance. A functional analysis of this mutant is of value for further elucidating the structural features of subunit III which allow it to confer its protective effect to COX during catalytic turnover.

It has been proposed that subunit III helps maintain proton uptake through the D-pathway by acting as a proton antenna and/or by fine turning the pKa of subunit I residue D132 to a value optimal for its role as the primary proton acceptor in the D-pathway (Gilderson et al., 2003; Adelroth and Hosler, 2006). The subunit III residues thought to be responsible for these proposed roles are located on its n-terminus. Specifically, the

conserved histidines at positions 7 and 10 could act as a proton reservoir by virtue of the fact that their pKa values are likely to be in the physiological range. Their presence could serve to increase the local concentration of protons in order to maximize the rate of proton uptake (Gilderson et al., 2003; Hosler, 2004). In addition, there are four hydrophobic residues on the n-terminus of subunit III – Ile 11, Leu 12, Pro 13 and Pro 14. These residues form part of a ring around the shallow well in which D132 is located. It has been proposed that they could be acting to raise the pKa of D132 by partially shielding it from the aqueous phase (Gilderson et al., 2003; Hosler, 2004). All of these residues are retained in Δ114 COX but missing in I-II COX, so the Δ114 COX mutant provides an opportunity to test these proposed roles for the n-terminus of subunit III.

Despite the presence of the n-terminal region of subunit III in the Δ114 mutant, the rate of proton uptake through the D-pathway and the apparent pKa of D132 in Δ114 COX are similar to that of I-II COX. Firstly, the catalytic lifetimes were observed to be equivalent in the I-II COX forms and Δ114 COX at physiological pH in DM (see Table VIII). The catalytic lifetime as measured by the CC_{50} value has been shown to be a qualitative measure of the rate of proton uptake through the D-pathway (Adelroth and Hosler, 2006). The equivalent CC_{50} values of Δ114 and I-II COX indicates that the rate of proton uptake through the D-pathway is similar in the two enzyme forms. There was an elevated catalytic lifetime seen for Δ114 in lipid micelle compared to I-II COX, but the fact that this was not observed in detergent implies that this lipid-mediated effect results from a mechanism other than the action of the putative proton antenna region, as will be discussed below. Secondly, the apparent pKa of the D-pathway is equivalent in Δ114 and I-II COX, as monitored by steady-state electron transfer activity (Figure 25, Table VIII).

When D-pathway proton uptake is impaired, the rate limiting step in the reaction cycle is proton uptake through the D-pathway during the F → O transition (Adelroth and Hosler, 2006). The pKa of steady-state activity under impaired uptake conditions is therefore closely related to the apparent pKa of a critical D-pathway residue, putatively D132 (Gilderson et al., 2003; Mills and Hosler, 2005; Adelroth and Hosler, 2006). In the case of wildtype, proton uptake through the D-pathway is not rate limiting, so the pH profile of wildtype steady-state activity also reflects a large contribution from E286 (Adelroth and Hosler, 2006). The equivalent pH profiles of I-II COX and Δ114 suggests that the subunit III n-terminal residues are not altering the apparent pKa of the D-pathway as had been previously proposed.

The results do not entirely dismiss the proton antenna and/or hydrophobic tuning roles for subunit III, however. As already articulated, the lipid-mediated link between the c-terminal bundle and the n-terminal bundle seems to be of functional significance. It is possible that the c-terminal bundle serves to properly position the n-terminus of subunit III so as to maximize its function as a proton antenna or as a shield from aqueous solution. In other words, it could be that the reason no evidence was seen for n-terminal proton collection or elevation in the pKa of D132 was because the n-terminus cannot properly align for such functions without the c-terminal bundle.

The yield and purity of Ni^{2+}-NTA purified Δ114 COX provides some evidence for improper folding of subunit III-Δ114. Protein yields for Ni^{2+}-NTA purification were only about 25% for Δ114 COX, compared to 75% yields typically obtained for wildtype COX. The Δ114 COX protein that did not bind to the nickel column had normal spectral properties indicating that subunit I was properly folded, however it never bound to the

column despite repetitive recycling attempts. It could be that the truncated subunit III was misfolded and facilitated aggregation that masked the histidine tag and prevented binding and subsequent purification. It should be noted that if this is the case, then the majority of the misfolded subunit III would not be purified, and perhaps the portion that was purified had a properly folded subunit III-Δ114.

It was also the case that the Δ114 preparations had greater enrichment in the impurities often noticed in *R.sph.* COX preparations. The molecular weights of these impurities were measured (see Table VII), but no obvious protein candidates could be identified from known assembly factors or proteases which might be specifically interacting with subunit III if it were misfolded. These impurities could be present due to non-specific interactions with partially misfolded subunit III-Δ114.

Although subunit III-Δ114 might be somewhat misfolded, there are a few reasons why this structural disruption is probably not severe. Firstly, the specific protection provided by the lipids against turnover induced inactivation for Δ114 COX would require binding to a three-dimensional protein structure that is not significantly perturbed. Secondly, subunit III-Δ114 binds well to subunit I. It was estimated by two dimensional PAGE that at least 70% of COX had subunit III-Δ114 incorporated (see Figure 22B, Table VI). This was a much higher stoichiometry of subunit III incorporation than was observed for another truncation in subunit III which removed only the last c-terminal helix, Δ238 COX. The Δ238 mutant was suspected of extensive folding problems as it seemed to be undergoing significant proteolytic degradation *in vivo* (Geyer, 2007). The high level of subunit III-Δ114 binding to subunit I, therefore, suggests that this interaction is not significantly perturbed by improper folding. Related to this point is the

fact that Δ114 did not seem to be undergoing extensive proteolytic degradation of the truncated subunit III. Only one proteolytic product of SIII-Δ114 was observed (see Figures 17 and 18, Table V), and this product resulted from the removal of the 13 n-terminal amino acids of SIII-Δ114 which would form part of a periplasmic loop in wildtype COX (Svensson-Ek et al., 2002). Disorder in this small stretch of SIII-Δ114 would be expected, so its proteolytic removal is not indicative of systemic misfolding of SIII-Δ114.

Although severe misfolding of subunit III is not likely to be the case, it is possible that minor structural alterations of the n-terminus of subunit III could prevent it from performing its proposed roles in proton collection and in shielding of D132 from the aqueous environment thereby raising its pKa. This hypothesis could be tested by a series of mutational experiments in the n-terminal region of subunit III. Firstly, the conserved histidines His7 and His10 could be mutated to non-protonatable residues. If these residues are critical to maintaining rapid D-pathway proton uptake, mutating them should decrease the catalytic lifetime of the protein. Secondly, the conserved hydrophobic patch – Ile11 and Leu12 – could be mutated to more polar residues to examine their contribution to rapid proton uptake. If a shift in the pKa of steady-state turnover is observed, it is likely that the residues are important for elevating the pKa of D132. Finally, the conserved proline residues at positions 13 and 14 could be mutated to glycine residues. The two adjacent prolines introduce a sharp turn in the structure and may orient the n-terminus in an optimal position for proton collection and hydrophobic tuning of D132's pKa. These proline mutations would shed insight into the conformational sensitivity of the n-terminal region. If deleterious effects were noted for the histidine

and/or hydrophobic mutants, the putative roles of proton collection and pKa fine tuning would be more firmly established. Then, if deleterious effects were also noted for the proline mutations, it could help to explain why the proton antenna and hydrophobic tuner functions were not observed in Δ114 COX and could highlight the importance of the c-terminal domain in aligning the n-terminus of subunit III.

The Role of Subunit III and Its Cleft Lipids in Stabilizing the D-pathway and Active Site

Subunit III has been proposed to stabilize the proper structure of the ordered water molecules that compose the D-pathway, thereby facilitating maximum proton uptake through the D-pathway and preventing turnover induced inactivation (Hosler, 2004). A comparison of the x-ray crystal structures for wildtype and I-II COX revealed a difference in the water arrangement of the D-pathway when subunit III was absent (Qin et al., 2006). Proton transfer through the D-pathway is accomplished by the Grotthuss mechanism, which requires a reorientation of the water molecules after each proton transfer event (Nagle and Tristram-Nagle, 1983; Hosler, 2004). An optimal flexibility in the proton pathway would allow the water molecules to reorient but not to diffuse to different locations. Subunit III, in combination with its putative structural lipids has been proposed to play such a role in providing the optimal structural support for the D-pathway (Hosler, 2004; Varanasi et al., 2006).

The results of this dissertation are consistent with the hypothesis that subunit III and its cleft lipids aid in stabilizing the D-pathway to prevent turnover induced inactivation. The catalytic lifetime of Δ114 COX was statistically equivalent to both forms of I-II COX when the assay was conducted in DM detergent (see Table VIII).

However, upon supplementing the assay buffer with 1 mg/mL asolectin, the catalytic lifetime of Δ114 increased 2.1 fold, a value statistically greater than the more modest increases observed for the two different I-II COX forms. The catalytic lifetime of Δ114 was not further increased relative to the lipid micelle assay when the enzyme was reconstituted into phospholipid vesicles and assayed in the presence of ionophores. However, reconstitution into lipid vesicles increased the catalytic lifetimes of both forms of I-II COX to statistical equivalence with the catalytic lifetime of Δ114 achieved in lipid micelle. The presence of subunit III-Δ114 and excess lipid, therefore, seems to provide a protective effect against turnover induced inactivation that can only be achieved for I-II COX when the enzyme is in the more constrained environment of a lipid vesicle.

The elevated protection against turnover induced inactivation provided by SIII-Δ114 and lipid suggests a specific binding effect of the lipid to subunit III-Δ114. The Δ114 truncation of subunit III retains all but one of the conserved amino acids which bind the lipids (see Figure 6). Specifically, all the residues associated with PL1 are present (amino acids R137, L145, L196 and L203 of subunit I; amino acids W58, W59, M55, F86 and F93 of subunit III), and all of the residues in van der Waals contact with the fatty acid tails of PL2 are also present (amino acids W59, M55 and F86). The only subunit III lipid-associated residue which is missing in Δ114 COX is R226, which coordinates the head group of PL2 by an ionic and h-bond interaction between its guanidinium nitrogens and the negatively charged phosphate head group (Svensson-Ek et al., 2002; Varanasi et al., 2006). R226 is located on helix 6 of subunit III and therefore fosters a lipid-mediated connection between the c-terminal and n-terminal domains of subunit III. The interaction with R226 is the strongest single protein interaction for PL2 (Varanasi et al., 2006), so its

absence might cause PL2 to be partially depleted from the enzyme. In the *R.sph.* crystal structure, the bound cleft lipids are phosphatidyl ethanolamines with oleic acid tails (18:1) (Svensson-Ek et al., 2002; Varanasi et al., 2006), a lipid which is present in asolectin (Varanasi et al., 2006). Therefore, in the assay in which asolectin is present in the buffer, the high lipid concentrations could be increasing the likelihood that a lipid will bind in the potentially vacated PL2 site.

It is therefore proposed that the elevated catalytic lifetime seen in the presence of excess lipid results from a lipid binding in the PL2 position and conferring added structural support to help maintain the proper orientation of the D-pathway waters. Several of the conserved residues in subunit III interact with both lipids. For instance, Trp 59 on helix 2 intercalates between the fatty acid tails of PL1 and PL2, and F86 on helix 3 makes contact with both lipids as well. The presence of PL2 would therefore confer greater stability to the entire protein-lipid-protein structure which bridges the v-shaped cleft of subunit III. PL1 binds on the opposite face of subunit I helices 3 and 4, which contain most of the conserved residues coordinating the water molecules of the D-pathway (N139, S197, S200, S201, N207). On these same subunit I helices are residues which interact with portions of the fatty acid tail of PL1 (L196, L203). Also, the subunit I residue which coordinates the PL1 headgroup (R137) is only two amino acids removed from the conserved D-pathway residue N139 (Svensson-Ek et al., 2002; Hosler, 2004; Varanasi et al., 2006). As such, there is a strong potential for a structural link between the lipids in the v-shaped cleft and the coordination of the water molecules in the D-pathway.

When the two different I-II COX forms were reconstituted into phospholipid vesicles, they had protection against turnover induced inactivation at levels similar to

what Δ114 COX achieved in lipid micelle. In an attempt to decipher whether the increased lifetime was due to a biophysical property of the phospholipid bilayer or due to a lipid binding interaction with I-II COX, the asolectin concentration was increased 10 fold in the solubilized assay. The catalytic lifetime of I-II$_{GD}$ COX was not increased when asolectin concentrations were as high as 10 mg/mL in solution, suggesting that the molecular mechanism for the protection effect observed in Δ114 COX in lipid micelle is impaired or absent in forms of COX that have subunit III removed (I-II COX). Since Δ114 COX has the three n-terminal helices of subunit III containing most of the conserved lipid-associated amino acids, this observation strengthens the proposal that the cleft lipids are bound in conserved locations in order to provide structural support which protects COX from inactivation. The increased lifetime observed upon reconstitution of I-II COX is likely caused by a biophysical property of the phospholipid bilayer, rather than by a lipid binding in a specific location within the three-dimensional structure of the protein, as is proposed for Δ114 COX. Phospholipid bilayers have been shown to laterally compress and decrease the conformational dynamics of transmembrane proteins (Dan and Safran, 1998; Kusnetzow et al., 2006). As such, the bilayer could serve to reduce deleterious structural oscillations in I-II COX by a lateral compression mechanism, thereby reducing the likelihood of turnover induced inactivation to levels similar to those achieved by Δ114 COX through the proposed binding in the v-shaped cleft of a phospholipid molecule from the lipid micelle.

Some phospholipids have been shown to increase the rate of proton uptake through the D-pathway by serving as proton donors via ionizable phospholipid headgroups (Adelroth and Hosler, 2006). The pH profiles of steady-state activity and

turnover induced inactivation are not altered for Δ114 COX when they are conducted in the presence or absence of lipid. This suggests that the partial lipid protection against inactivation is not due to the introduction of an additional proton donor to the D-pathway. Rather, the protection seems to be structural in nature.

Given this proposed role, it is of particular interest that subunit III labeling with DCCD perturbs the tails of the lipids within the v-shaped cleft (Shinzawa-Itoh et al., 2007). Prochaska *et al.* showed that subunit III can be specifically labeled at position E90 with DCCD, a modification which decreases proton pumping efficiency as well as steady-state activity (Prochaska et al., 1981). E90 is flanked by F86 and F93, two of the amino acids which are in van der Waals contact with the fatty acid tails of PL1 (Svensson-Ek et al., 2002; Varanasi et al., 2006). The x-ray crystal structure of bovine COX labeled at E90 with DCCD shows that the tails of the cleft lipids are perturbed by the bulky cyclohexyl groups (Shinzawa-Itoh et al., 2007). The positions of the lipids in bovine and *R.sph*. COX are conserved, so it is of relevance that one of the tails of PL1 which is perturbed by DCCD has a conserved structural connection extending 16 Å to H284, which is a ligand of Cu_B – the active site copper which is depleted from enzyme that has undergone turnover induced inactivation (Svensson-Ek et al., 2002; Tsukihara et al., 2003; Varanasi et al., 2006). To add further weight, our lab has recently shown that turnover induced inactivation occurs in bovine and *R.sph*. COX when they are labeled with DCCD (unpublished results). Perhaps the deleterious effects of DCCD labeling on COX pumping, steady-state activity and catalytic lifetime are in part due to structural perturbation of the subunit III cleft lipid tails.

The structural support putatively offered by the cleft lipids of subunit III is not sufficient to maintain adequate rates of proton uptake for maximal function in the absence of the c-terminal bundle. Upon truncation of the four c-terminal helices, activity levels and proton pumping are diminished to I-II COX levels, even in the presence of lipid. Additionally, the more than two fold increase in the catalytic lifetime of Δ114 COX afforded by excess lipid still increases the lifetime to only about 1% of the lifetime of wildtype COX, highlighting the importance of the c-terminal bundle. Mutations in full length subunit III which disrupt the binding interactions of the lipids have been shown to result in turnover induced inactivation as well (Varanasi et al., 2006). This suggests that both full length subunit III and the cleft lipids are necessary for maximal protection from turnover induced inactivation.

The importance of the c-terminal bundle for maintenance of native proton pumping stoichiometries may also be partially mediated by the subunit III cleft lipids. In this work, it was found that Δ114 COX pumped with the same stoichiometry as I-II_{GD} COX, which was about half the efficiency of wildtype (see Figure 28, Table VIII). As stated previously, the only conserved lipid-binding residue which is truncated in Δ114 is R226 on helix 6 of subunit III. A point mutation has been made in subunit III which converts R226 to an alanine, thereby abolishing the interaction it forms with the head group of PL2 (Varanasi et al., 2006). Remarkably, the R226A mutant pumps with only about 50% the efficiency of wildtype COX, similar to the efficiency seen when the bulk of the c-terminal domain is removed entirely (this work; Varanasi et al., 2006). These results point to the importance of the lipid-mediated interaction between the n- and c-terminal bundles of subunit III for maintaining maximal proton pumping efficiency.

In short, structural and functional studies on *R.sph*. Δ114 COX have provided further evidence for the importance of the subunit III cleft lipids and for the criticalness of the lipid-mediated interactions within subunit III. *R.sph*. Δ114 COX was observed to have an increased catalytic lifetime when in lipid micelle, an effect which seems to result from the specific binding of lipid. It was proposed that a lipid binds in the PL2 position and serves to increase the protein-lipid interactions within the cleft. An examination of the crystal structure reveals that this could have a fairly direct stabilizing effect on the coordination of D-pathway water molecules and on the stability of the subunit I active site via a Cu_B ligand. The limitedness of the stabilizing effect, however, points to the importance of the c-terminal bundle and to the importance of intra-subunit interactions between the n- and c-terminal bundles.

R.sph. Δ114 COX and Human Mitochondrial Disease

The *R.sph*. Δ114 COX mutation was modeled after a mutation in human mitochondrial cytochrome *c* oxidase subunit III which results in a disease state typified by severe lactic acidosis episodes and neuromuscular impairments (Tiranti et al., 2000). When the corresponding mutation was made in the simpler *R.sph.* form of the enzyme, the protein was found to have electron transfer and proton pumping activities that were reduced to about half that of wildtype COX. The Δ114 COX protein was also subject to turnover induced inactivation, suggesting that proton uptake through the D-pathway was impaired. Furthermore, evidence of early assembly intermediate pooling suggested that the rate of COX assembly was not optimal, and that there were lower levels of COX protein in the membranes as compared to alternative terminal oxidases. These results can

be gleaned for insight into the molecular mechanisms of the diseased state and into some of the differences between mitochondrial and bacterial COX forms.

The pathological condition that resulted from the truncation in subunit III COX was reported by Tiranti *et al.* (Tiranti et al., 2000). A stable cell line homoplasmic for the mutation was created using the fibroblasts from a patient. Western blot analysis of Blue Native PAGE gels of the mitochondrial fraction of digitonin-treated cells indicated that fully assembled COX was absent and that COX assembly intermediates were accumulated. The investigators did not find evidence of a subunit III peptide resulting from the confirmed presence of the mutated mRNA transcript for subunit III, although they were limited by a lack of a specific antibody for subunit III. From pulse-chase experiments with [^{35}S] methionine, they concluded that truncated subunit III was not being translated. This however, is likely to be a premature and faulty conclusion; an examination of the polyacrylamide gel of the translation products showed multiple bands in the region where truncated subunit III runs in our SDS-PAGE gels of purified *R.sph.* Δ114 COX. The band is likely to be faint, given that 3 of the 10 methionines are removed when subunit III is truncated and that the band for full length subunit III was already faint in the control cell lines as compared to other COX subunits (Tiranti et al., 2000). It is likely that the faint band corresponding to truncated subunit III is occluded by the multiple translation products of similar molecular weight. To add to this argument, the BN-PAGE gels of the mutant mitochondrial cells displayed a shift in the band position of one of the assembly intermediates. The authors attributed this to a "qualitative abnormality of COX assembly," but given that truncated subunit III-Δ114 incorporated in the bacterial COX with high stoichiometry, the shift observed in the BN-PAGE of the

mitochondrial COX assembly intermediates is likely to be due to incorporation of the truncated form of subunit III.

The assembly of mitochondrial COX is more complicated than it is for bacterial COX, as there are 10 nuclear-encoded subunits incorporated into the complex (Tsukihara et al., 1996; Fontanesi et al., 2008; Fornuskova et al., 2010; Stiburek and Zeman, 2010). The initial assembly intermediate is subunit I*a*, similar to the case for the *R.sph.* system (Bratton et al., 2000; Fontanesi et al., 2008). Next, the nuclear subunits IV and Va bind to subunit I to form intermediate 2 (Fernandez-Vizarra et al., 2009). Subunit II binds to intermediate 2, followed by subunit III. The binding of subunit III initiates a cascade of nuclear subunit binding (Fontanesi et al., 2006; Fernandez-Vizarra et al., 2009). Tiranti *et al*. postulated that downstream assembly of the nuclear encoded subunits was impaired due to the absence of subunit III (Tiranti et al., 2000). As already noted, it is debatable that truncated subunit III was missing from the mitochondrial COX complex, as the authors did acknowledge in their discussion. The results described in this dissertation highlight the necessity of a more thorough investigation of the presence of truncated subunit III in the mitochondrial COX mutant cell lines. Furthermore, they provide evidence that the truncation of subunit III can also affect what is thought to be upstream assembly of COX. Whether or not this is also the case in the mitochondrial enzyme remains to be tested, as assembly is likely to be more stringent and regulated for mitochondrial COX (Hiser and Hosler, 2001; Fontanesi et al., 2006; Fontanesi et al., 2008; Fornuskova et al., 2010).

Functional assays of the human mitochondrial COX mutant with truncated subunit III were limited due to the fact that the protein was not purified. The rate of

oxygen reduction in the mutant cell lines was reduced to about 15% of the control cell lines when the assay was conducted in whole mitochondria (Tiranti et al., 2000). These assays were normalized to the activity of citrate synthase, which is a marker enzyme for the relative number of mitochondria. Since they were not normalized to the concentration of COX, it is difficult to interpret the meaning of this result. The authors assumed the decreased activity was due to presumed lower levels of COX protein rather than to a decrease in the activity of mutated COX. The functional studies of the *R.sph.* Δ114 COX mutant provide a better glimpse into the deleterious functional effects of the subunit III mutation. It is likely that the mitochondrial subunit III truncation resulted in a similar loss of electron transfer and proton pumping activity. Furthermore, our lab has recently shown that bovine COX also undergoes turnover induced inactivation in the absence of subunit III (A. Kaliappan, unpublished results). Since the *R.sph*. Δ114 COX mutant demonstrated that the full length of subunit III is required for prevention of inactivation, it is possible that turnover-induced inactivation of COX is occurring in the diseased mitochondria.

In summary, modeling the human mitochondrial disease by the *R.sph.* Δ114 COX mutation has served to provide a more full view of what could be occurring in the mutated mitochondrial COX. This work points to the necessity of a more robust assay for the presence of truncated subunit III in the mutated mitochondrial COX complex. It also raises the possibility of upstream impairment in COX assembly. Finally, it provides evidence that the mutated mitochondrial COX is likely to be hindered in its electron transfer and proton pumping capacities and to be subject to turnover induced inactivation. Continued investigation of the mitochondrial and bacterial COX mutation has the potential to shed further insight into the structural features of subunit III which enable it

to play roles in COX assembly and maximal function and into the differences between the mitochondrial and bacterial systems.

V. Conclusions

Discontinuous sucrose gradient ultracentrifugation was found to be a suitable technique for removing liposomes lacking protein from those containing *R.sph.* COX. The reduced lipid concentrations resulted in lower net buffering capacity and decreased light scattering, making the technique useful for low buffer spectroscopic studies. It was found that there is only one *R.sph*. COX molecule per liposome. The enzyme therefore appears to be in the monomeric state when reconstituted into lipid vesicles, suggesting that the functional form of *R.sph.* COX is monomeric *in vivo* as well. The results show that monomeric *R.sph.* COX is capable of maximal turnover and proton pumping activity. This is a novel result in that COX has not been definitively shown to be capable of maximal proton pumping activity when in the monomeric state.

Structural and functional characterization of a c-terminal subunit III truncation mutation have provided further evidence that subunit III and its cleft lipids aid in stabilizing the D-pathway to prevent turnover induced inactivation. This mutant removes the four c-terminal helices of subunit III, leaving the three n-terminal helices which form a v-shaped cleft containing a conserved binding region for two lipids. The mutant with truncated subunit III provided greater protective effects against turnover-induced inactivation when assayed in lipid micelle as compared to COX with subunit III removed either by biochemical or genetic means. The exogenous lipid used in the assay is proposed to bind in the potentially vacated lipid site contained in truncated subunit III.

An examination of the crystal structure reveals that the bound lipid could have a fairly direct stabilizing effect on the coordination of D-pathway water molecules and on the stability of the subunit I active site. The stabilizing effect is limited in that the mutant does not support wildtype activities, which points to the importance of the c-terminal bundle and to the importance of intra-subunit interactions between the n- and c-terminal bundles. The c-terminal bundle of subunit III was also found to play roles in maximizing the assembly of COX and in optimizing the native processing of subunit II. Since the truncation mutation is modeled from a human mitochondrial disease mutation, these findings can be used to further understand the molecular mechanisms of that disease state and to shed insight into the differences between mitochondrial and bacterial COX forms.

Appendix

Probing the Dynamic Conformation of *R.sph.* COX Subunit III with Thiol-Reactive Fluorophores

The role of subunit III in the structure and function of cytochrome *c* oxidase is a matter of continued investigation. In this dissertation, a role for subunit III in stabilizing the D-pathway and subunit I active site was investigated. It is possible that this stabilization role could be affected through redox-linked conformational changes. These conformational changes could also serve to regulate the catalytic activity of the enzyme. Site-directed antibodies bound to subunit III of bovine COX have been shown to increase the rate of electron transfer, perhaps by locking the enzyme into a more active conformation (Lincoln et al., 2003). In addition, specific peptides within the three-dimensional structure of COX subunit III have been identified which have altered solvent accessibility in the various catalytic intermediate states, indicating that structural conformational changes in subunit III could be occurring during the catalytic cycle of COX (Busenlehner et al., 2006). These putative conformational changes have not been completely described, and the possibility of a link between the conformation of subunit III and activity at the subunit I active site is still being investigated. The experiments described in this appendix are aimed at testing the hypothesis that redox-linked conformational changes occur in COX subunit III. These putative conformational changes could play a regulatory or stabilization role for COX.

Site-specific fluorescence spectroscopy is a method by which protein conformational dynamics can be studied. Thiol-reactive fluorophores can be conjugated to the cysteine residues in proteins (Haughland, 2002). The local environment of the protein surrounding the probe will influence the fluorescent properties of the probe (Haughland, 2002; Lakowicz, 2006). For example, changes in the hydrophobicity or flexibility of the environment will alter the emission wavelength/intensity or the anisotropy of the probe's emission (Hudson and Weber, 1973; Haughland, 2002). Therefore, if a conformational change in the protein alters the location of the fluorophore such that it is in an environment with altered hydrophobicity or flexibility, the conformational change will influence the measureable fluorescence properties of the probe (Hibbs et al., 2005; Bell et al., 2006). The long term goal of these studies is to direct fluorescent probes to specific locations in the three dimensional structure of COX subunit III by preparing single cysteine mutants. Conformational changes in these specific locations can then be assessed through a variety of fluorescence experiments. This appendix described the progress made toward creating and characterizing single cysteine mutants and toward developing protocols for assaying conformational dynamics.

Methods

Mutagenesis of R.sph. COX Subunit III to Create Single Cysteine Mutants

A pRK415-CA1CS3 plasmid was received from Robert Gennis at the University of Illinois, Champaign-Urbana. This plasmid is a broad host range overexpression vector used for expressing COX in *R.sph.* The plasmid contained a subunit I gene in which the two native cysteines (C64, C88) were mutated to alanines and which had a polyhistidine

tag engineered onto the c-terminus. In addition, the subunit III gene in the plasmid had its three native cysteines mutated to serines (C143, C146, C223). Also contained in the plasmid were a subunit II gene and two accessory proteins for COX assembly. The CA1CS3 COX protein expressed from this plasmid has no cysteine residues available for bioconjugation.

The subunit III gene from the pRK415-CA1CS3 plasmid was engineered into the pMB301 vector and used as the template DNA for introducing single cysteines into subunit III by replacing non-conserved amino acids. Two single cysteine mutants were created using the protocols described (see Methods). The mutants were sequenced by Davis Sequencing to verify correct mutagenesis. The A4C mutant was created to analyze the conformational dynamics at the n-terminus of subunit III (mutagenesis primer sequence: 5'-GGG AAC CAT GGC CCA CTG CAA-3'). The S187C mutant was created to study the conformation dynamics of the periplasmic loop which extends from helix 5 to helix 6 in subunit III (mutagenesis primer sequence: 5'-CAG GCC TAC GAA TAC TGC CAC GCG GCT TTC-3'). The conformation of this loop is suspected of playing a regulatory role for COX activity; a site-directed antibody bound on this loop in bovine COX increased the catalytic activity of the enzyme (Lincoln et al., 2003). These mutants were expressed and purified and their functional properties were assessed according to protocols described in the Methods section.

Bioconjugation of R.sph. Wildtype COX with Thiol-Reactive Fluorophores

R.sph. COX contains three native cysteines in subunit III which can be conjugated to thiol-reactive flourophores. For labeling with 5-((((2-iodoacetyl)amino)ethyl)amino)

naphthalene-1-sulfonic acid (IAEDANS), a stock solution of 1-2 mM IAEDANS was prepared in 20 mM HEPES, pH 8.0, and its concentration was verified spectroscopically using an extinction coefficient of 5,700 $M^{-1}cm^{-1}$ at 336 nm (Haughland, 2002). COX samples were diluted to 1-5 μM in 20 mM HEPES, pH 8.0. IAEDANS was added at COX:IAEDANS stoichiometry of 1:10, and the reaction was incubated in the dark at room temperature for 1 hour. A 100 molar excess of DTT was used to quench unreacted IAEDANS, which was then removed by successive washes in Millipore YM-100 Microcon filter devices. In the second wash step, 20 mM ferricyanide was added to oxidize the enzyme. Wash steps were repeated approximately four times until the flow through buffer was free of DTT, ferricyanide and IAEDANS as analyzed by UV and fluorescence spectroscopy.

For labeling with MIANS (2-(4'-maleimidylanilino)naphthalene-6-sulfonic acid), 1-2 mM stock solutions were made in methanol and the concentration was verified spectroscopically using an extinction coefficient of 27,000 $M^{-1}cm^{-1}$ at 322 nm (Haughland, 2002). COX samples were diluted to 1-5 μM in 20 mM HEPES, 0.1% DM, pH 7.5. MIANS was added at COX:MIANS stoichiometry of 1:5. Total methanol concentrations did not exceed 0.5%. The reaction was incubated in the dark at room temperature for 1 hour. A 100 molar excess of DTT was used to quench unreacted MIANS, which was then removed by successive washes as described above.

Labeling Stoichiometry and Subunit Localization of R.sph. COX-AEDANS

The subunit localization of the AEDANS and MIANS probes in conjugated COX was determined via SDS-PAGE. Labeled COX was denatured in 3% SDS, Laemmli

sample buffer (Bio-Rad) and run on a 16% polyacrylamide (37.5:1 acrylamide:bis) gel containing 6 M urea and 0.1% SDS (Fuller et al., 1981). The fluorescence signal of the gel was captured using a Fuji LAS-4000 Imager with a UV box for excitation, a 515 nm cutoff filter and an exposure time of 5-15 seconds. The gels were stained with Coomassie G-250 and an image of the protein bands was recorded on a Fuji LAS-4000 imager.

To determine the stoichiometry of probe labeling, the extinction coefficients of oxidized *R.sph.* COX at 336 nm (43,000 $M^{-1}cm^{-1}$) and 322 nm (37,000 $M^{-1}cm^{-1}$) were determined using the known extinction coefficient for the reduced *minus* oxidized peak at 606 nm (24,000 $mM^{-1}cm^{-1}$, see (van Gelder, 1966)). The extinction coefficient of IAEDANS at 336 nm is 5,700 $M^{-1}cm^{-1}$, and MIANS has an extinction coefficient of 27,000 $M^{-1}cm^{-1}$ at 322 nm (Haughland, 2002). COX concentration was determined from the reduced *minus* oxidized spectrum (van Gelder, 1966), and the absorbance of the oxidized COX spectrum at 336 nm or 322 nm was used to determine the concentration of AEDANS or MIANS after correcting for the absorbance contribution from oxidized COX at this wavelength. The labeling stoichiometry was calculated by dividing the probe concentration by the COX concentration. To verify the spectroscopic result, MALDI-TOF mass spectrometry was conducted on COX-AEDANS and the mass peaks of the subunits were compared to wildtype.

Trapping R.sph. COX in the P_M State

The P_M state was prepared by exposing oxidized COX to a mixture of carbon monoxide (CO) and air at a pH of 8.0 (Junemann et al., 2000; Rich et al., 2002). Conjugated, oxidized COX (1 μM COX in 20 mM HEPES, 0.1% DM, pH 8.0) was

sealed in a quartz cuvette and connected to a vacuum/gas line inserted through the septum cap. Oxidized COX was exposed to 3 cycles of vacuum (10 seconds) and CO (5 seconds). CO was of ultra high purity (Weiler Gases and Welding Supplies). After CO exposure, the septum was briefly punctured with a needle to allow exposure to air. The kinetics of P_M formation were followed via absorbance spectroscopy on Hewlett Packard 8453 UV/Visible diode array spectrophotometer. The P_M *minus* O spectrum has characteristic absorbance features at 441 nm and 607 nm (peaks) and 417 nm (trough). The amount of P_M formation was calculated using an extinction coefficient of 10,400 $M^{-1}cm^{-1}$ at 607-630 nm in the P_M *minus* O spectrum (Rich et al., 2002). The P_M state was formed with 90-95% yield and within 2-3 minutes (τ = 1.3 min), as shown in Figure A-1.

Fluorescence Characterization of R.sph. COX-AEDANS in the O and P_M States

The fluorescence properties of COX-AEDANS in the O and P_M states were measured on a Varian Cary Eclipse fluorescence spectrometer. The emission spectrum of oxidized 1 μM COX-AEDANS in 20 mM HEPES, 0.1% DM, pH 8.0 was obtained using a PMT setting of 850 V and excitation and emission slit widths of 5 nm each (excitation λ = 336 nm). An average of five spectra was taken per sample. The anisotropy of O state COX-AEDANS was measured using a Varian manual polarizer accessory. An average of five anisotropy readings were taken using an excitation wavelength of 336 nm, an emission wavelength of 471 nm, and the same PMT and slit width settings as for the emission spectral measurements. Anisotropy values were corrected for the G factor of the instrument which was determined using Aldrich Ludox TM-50 colloidal silica suspension as a light scattering agent.

Figure A-1

Formation of the P_M state of *R.sph*. COX. The P_M state was prepared by exposing oxidized COX to a mixture of carbon monoxide (CO) and air at a pH of 8.0 (Junemann et al., 2000; Rich et al., 2002). Conjugated, oxidized COX (1 mM COX in 20 mM HEPES, 0.1% DM, pH 8.0) was sealed in a quartz cuvette and connected to a vacuum/gas line inserted through the septum cap. Oxidized COX was exposed to 3 cycles of vacuum (10 seconds) and CO (5 seconds). CO was of ultra high purity (Weiler Gases and Welding Supplies). After CO exposure, the septum was briefly punctured with a needle to allow exposure to air. The kinetics of P_M formation were followed via absorbance spectroscopy on a Hewlett Packard 8453 UV/Visible diode array spectrophotometer. A) P_M *minus* O spectra with respect to time. The arrows indicate direction of absorbance changes. The P_M *minus* O spectrum has characteristic absorbance features at 441 nm, 607 nm and 417 nm. B) Kinetics of P_M formation (P_M *minus* O absorbance at 607 – 630 nm). The P_M state was formed with 90-95% yield. A time constant was derived from a single exponential fit of the data (τ = 1.3 min).

A)

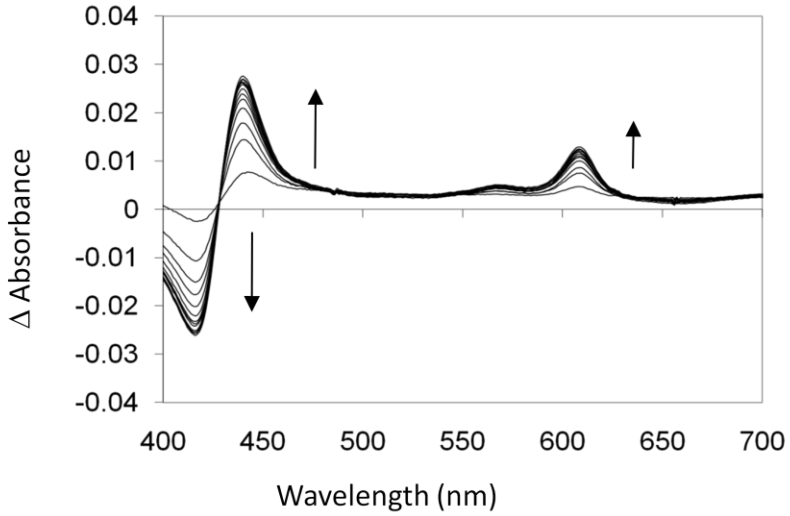
0.04
0.03
0.02
0.01
0
-0.01
-0.02
-0.03
-0.04
Δ Absorbance
400
450
500
550
600
650
700
Wavelength (nm)

B)

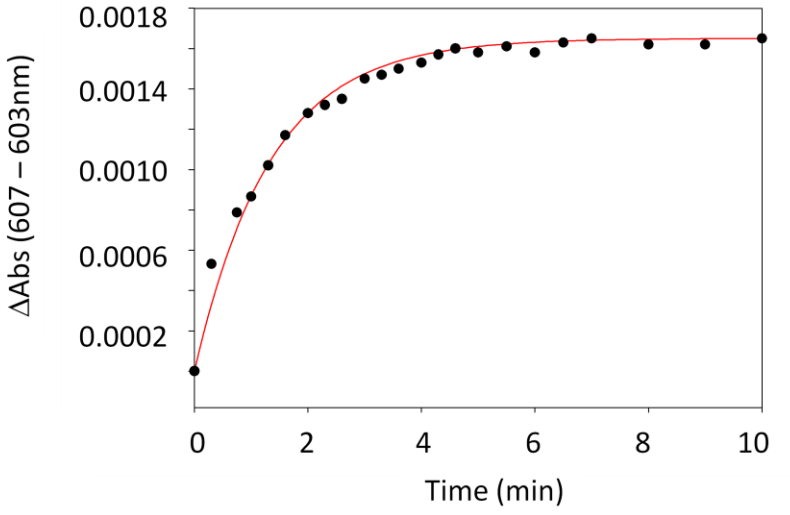
0.0018
0.0014
0.0010
0.0006
0.0002
ΔAbs (607 – 603nm)
0
2
4
6
8
10
Time (min)

After exposing the sample to CO and air, as described above, the changes in emission intensity at 471 nm were monitored with respect to time using the Varian kinetics software provided with the instrument and the same instrumental parameters used for the emission spectrum. After complete formation of the P_M intermediate (15 minutes), five emission spectra were recorded and averaged. The anisotropy readings were then recorded for the P_M state as described above.

Results and Discussion

The long term goal of this project is to study the conformational dynamics of COX subunit III by site-directed fluorescence spectroscopy. Single cysteine mutants of subunit III will be used to study conformational dynamics within specific regions of the subunit. After labeling the mutants with thiol-reactive fluorophores, the fluorescence properties of the probes will be characterized during assays in which COX is undergoing putative conformational changes. Toward this end, two single cysteine mutants were created and their functional properties were assessed and found to be similar to wildtype COX. In addition, wildtype COX was used to develop protocols for labeling the enzyme with flourophores and for developing conformational dynamics assays. It was found that the native cysteines in subunit III could be specifically and efficiently labeled with MIANS or IAEDANS fluorophores. Developing assays for conformational dynamics proved difficult due to inner filter effects caused by COX and substrates and due to instrumental limitations. The approach which best minimized the inner filter effect was to trap the labeled enzyme in the O and P_M intermediate states and to comparatively characterize the fluorescent properties of these states. The fluorescence properties of

wildtype COX-AEDANS were found to be equivalent in the O and P_M states; the maximal emission wavelength and anisotropy were statistically equal. The shapes of the emission spectra were also similar. The only statistically significant difference between the two states was that the P_M state had a lower maximal intensity than the O state. However, due to the large bandwidth that was required for the fluorescence experiments, this difference cannot be distinguished from an inner filter effect. Since the native cysteines in subunit III are located on helices 4 and 6 of COX subunit III, results indicate that these regions of the subunit do not move when the enzyme proceeds from the O state to the P_M state. A positive control and heightened instrumental sensitivity are necessary in order to draw definitive conclusions and to pursue these studies further.

Functional Properties of R.sph. COX Subunit III Cysteine Mutants

The functional properties of three cysteine mutants were tested in order to assess their suitability for use in site-directed fluorescence studies of COX. A cysteine-free mutant was created by mutating the cysteines in subunit I to alanines and the cysteines in subunit III to serines (CA1CS3). The plasmid for this mutant was given to us by Robert Gennis and was used to create two single cysteine mutants in subunit III, namely CA1CS3-A4C and CA1CS3-S187C. The cells expressing these mutants grew similar to wildtype and the purified proteins had spectral properties identical to wildtype (not shown), indicating that the mutations did not alter the protein environment surrounding the heme centers. SDS-PAGE analysis revealed that all the subunits of the mutants were present in approximately stoichiometric amounts. The electron transfer activities of all mutants were statistically equivalent to wildtype (Table A-I). Furthermore, the proton

Table A-I

***R.sph.* Wildtype and Cysteine Mutant COX Maximal Catalytic Activities**

	Activity (s^{-1})[a]
Wildtype	1370 ± 130
CA1CS3[b]	1390 ± 140
CA1CS3-A4C	1320 ± 150
CA1CS3-S187C	1260 ± 120

[a] Maximum catalytic activity measured via oxygen electrode (50 mM potassium phosphate, pH 7.4; 0.1% DM; 50 μM cytochrome *c*, 18 mM ascorbate, 0.6 mM TMPD).
[b] Cysteine-free mutant. The cysteines in subunit I and III were replaced with alanines and serines, respectively.

Figure A-2

Proton Pumping Traces for *R.sph.* Wildtype and Cysteine-Free COX. Proton pumping activity was measured by stopped-flow absorbance spectroscopy on an Applied Photophysics SV.20 Reaction Analyzer. The reaction commenced upon mixing reconstituted COX with reduced cytochrome *c*. Phenol red was included as a pH indicator to monitor pH-induced changes in absorbance at 556 nm, an isosbestic point for cytochrome *c* reduction. Acidification induced by the proton pumping activity of reconstituted COX in the presence of valinomycin is shown in the lower traces. The alkalinization phase (upper traces) results from the consumption of protons when reconstituted COX undergoes turnover in the presence of CCCP and valinomycin. This trace is proportional to the number of electrons transferred to COX. The H^+/e^- ratio is calculated from the extents of the lower and upper traces. Displayed are representative traces for a 5 turnover experiment (0.05 μM COX, 1 μM ferrocytochrome *c*, 5 μM CCCP and/or 5 μM valinomycin, pH 7.2). A) Wildtype COX vesicles had H^+/e^- ratios of 0.9 ± 0.2 (5 turnovers). B) Cysteine-free (CA1CS3) COX vesicles had H^+/e^- ratios of 0.9 ± 0.1 (5 turnovers).

A)

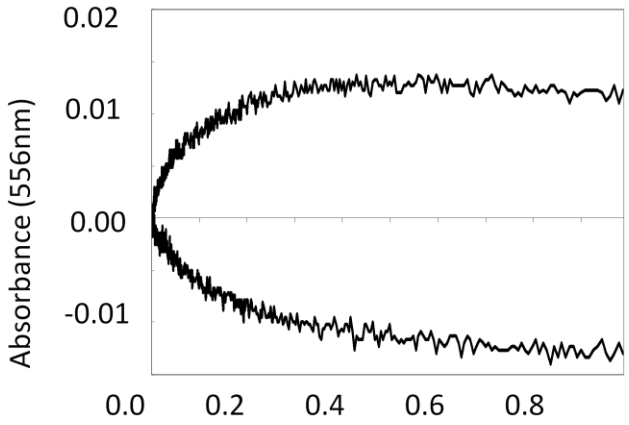
0.02
0.01
0.00
-0.01
Absorbance (556nm)
0.0
0.2
0.4
0.6
0.8

B)

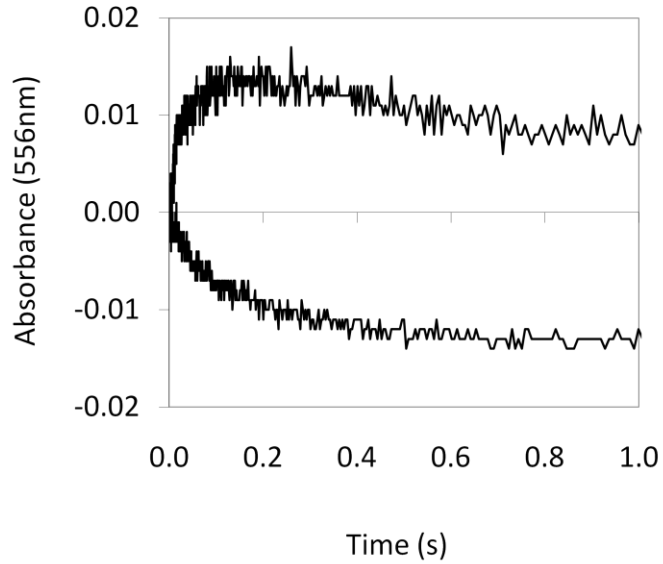
0.02
0.01
0.00
-0.01
-0.02
Absorbance (556nm)
0.0
0.2
0.4
0.6
0.8
1.0
Time (s)

pumping H^+/e^- ratio of CA1CS3 (0.9 ± 0.1) was equivalent to wildtype (0.9 ± 0.2) as shown in Figure A-2. These preliminary results indicate that these mutants are likely to be suitable for site-directed fluorescence studies, having functional properties similar to wildtype. These mutants are of value for directing thiol-reactive probes to the n-terminus of subunit III (CA1CS3-A4C), and for studying the conformation of the subunit III periplasmic loop which may be linked to the redox activity of the enzyme (CA1CS3-S187C).

Labeling Wildtype COX Subunit III with Thiol-Reactive Fluorophores

Wildtype *R.sph.* COX was used to develop fluorophore labeling protocols by virtue of the fact that subunit III contains three native cysteines and the native cysteines in the other subunits are substantially less reactive, being involved in disulfide bonds or metal ligation. COX contains internal chromophores, so the fluorophores used for site-directed labeling must have spectroscopic properties that do not overlap with those of COX (Yonetani, 1961; Vanneste, 1966; Lambeth et al., 1973). Other factors to consider when selecting fluorophores are as follows: 1) smaller probes are less likely to be excluded from the reaction site due to stearic interference and will be more confined to a discrete, localized area, 2) probes with faster and more specific thiol-reactivity will have reduced cross-reactivity with amine groups, and 3) the hydrophobicity of a probe determines whether it will react with buried or solvent-accessible residues. Due to their conformity to the above criterion and their use in other protein conformation studies, two fluorescent probes were identified as candidates for these experiments. IAEDANS is a hydrophilic probe which undergoes spectral shifts and changes in emission intensity in

response to alterations in aqueous solvation (Hudson and Weber, 1973; Haughland, 2002). It also has a relatively long fluorescence lifetime making it suitable for anisotropy experiments (Haughland, 2002). MIANS is a hydrophobic probe with emission properties highly sensitive to changes in ionic strength and hydrophobicity (Abbott et al., 2000; Haughland, 2002).

Both IAEDANS and MIANS were found to react efficiently and specifically with the native cysteines contained in COX subunit III. When labeled COX-AEDANS and COX-MIANS were denatured and run out on an SDS-PAGE gel, the fluorescence signal was localized to the subunit III band (Figure A-3). Absorbance spectroscopy revealed that COX-MIANS contained 2-3 MIANS molecules per COX molecule and that COX-AEDANS contained two AEDANS molecules per COX (Table A-II). The subunit III peak in the MALDI-TOF mass spectrum of COX-AEDANS was shifted by a mass equivalent to two AEDANS molecules (615 Da). Given that the subunit contains three native cysteine residues, these results indicate specific and efficient labeling of COX subunit III.

Two of the subunit III cysteines (C143 and C146) are located on helix 4 about half way through the bilayer. The other cysteine (C223) is located on helix 6, about a quarter of the way into the bilayer on the cytoplasmic side. The environment surrounding C223 is more hydrophobic than helix 4, and so it is possible that the hydrophilic IAEDANS probe labels the two cysteines on helix 4, and that the more hydrophobic MIANS probe labels both helix 4 and 6.

Figure A-3

Bioconjugation of *R.sph.*wildtype COX with IAEDANS and MIANS fluorophores. A) Wildtype COX labeled with IAEADANS. COX samples were diluted to 1-5 μM in 20 mM HEPES, pH 8.0. IAEDANS was added at COX:IAEDANS stoichiometry of 1:10, and the reaction was incubated in the dark at room temperature for 1 hour. A 100 molar excess of DTT was used to quench unreacted IAEDANS, which was then removed by successive washes in Millipore YM-100 Microcon filter devices. Seven μg of COX-AEDANS were denatured with 3% SDS in Laemmli buffer for 45 minutes at 37°C. Electrophoresis was conducted at 120 V for 2.5 hours on a 16% acrylamide gel containing 6 M urea and 0.1% SDS, pH 8.8. An image of the fluorescence emission was recorded on a Fuji LAS-4000 imager (left panel). The gel was then stained with Coomassie G-250 and an image was recorded (right panel). B) Wildtype COX labeled with MIANS. Labeling protocol was the same as for IAEDANS, except the buffer was 20 mM HEPES, pH 7.5, 0.1% DM, and a COX:MIANS stoichiometry of 1:5 was used.

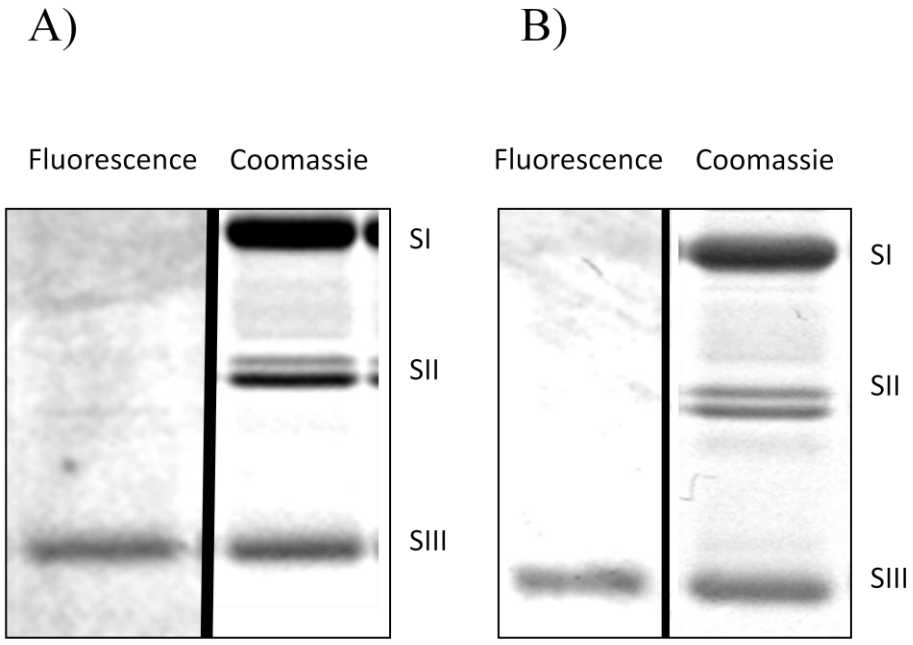
A)
B)
Fluorescence
Coomassie
Fluorescence
Coomassie
SI
SII
SIII
SI
SII
SIII

Table A-II

Stoichiometry of Flourophore Labeling in *R.sph.* Wildtype COX

	PROBE:COX UV-Vis[a]	PROBE:SIII Mass Spec[b]
COX-AEDANS	2.1 ± 0.3	2
COX-MIANS	2.5 ± 0.4	-

[a] Number of probe molecules per COX determined by UV-Vis spectroscopy using extinction coefficients for oxidized COX and for the probe at 336 nm (IAEDANS) or 322 nm (MIANS), as described in the text.

[b] MALDI-TOF mass spectrometry was conducted on COX-AEDANS and the subunit peaks were compared to those of wildtype. The subunit III peak was shifted by the mass of two AEDANS molecules.

Characterizing the Fluorescent Properties of COX-AEDANS in the O and P_M States

The fluorescence properties of COX-AEDANS were compared in the O and the P_M states in order to assess any putative conformational changes taking place during the transition between these catalytic states during the redox cycle of COX. The emission of AEDANS is highly sensitive to the degree of aqueous solvation; spectral shifts and intensity changes are observed corresponding to the hydrophobicity of the probe's environment (Hudson and Weber, 1973). The maximal emission wavelength of COX-AEDANS in the O state (471 ± 2 nm) did not change when the enzyme was converted to the P_M state (Table A-III). The shapes of the emission spectra in the O and the P_M states were also similar (Figure A-4A). First derivative plots of the emission spectra did not elucidate any differences (Figure A-4B), indicating that there were no spectral shifts in AEDANS fluorescence when COX was in the O versus the P_M state. This indicates that the hydrophobicity of the environment surrounding the probes was not different in the O and P_M states.

Fluorescence anisotropy is a measure of the degree of rotational freedom allowed to a fluorophore (Haughland, 2002; Lakowicz, 2006). When a probe is conjugated to a protein, the anisotropy of the probe is influenced by the flexibility of that region of the protein. The anisotropy of COX-AEDANS in the O and P_M states was assessed in order to probe for changes in protein flexibility. The anisotropy of AEDANS did not change when COX was in the O state (0.21 ± 0.01) versus the P_M state (Table A-III), which indicates that the protein environment surrounding the probe had about the same degree of flexibility in the two states.

Table A-III

Emission and Anisotropy Properties of COX-AEDANS in the O and P_M States.

	O State[a]	P_M State[b]
λ_{MAX}[c]	471 ± 2	471 ± 1
I_{MAX}[d]	286 ± 6	262 ± 16
ρ[e]	0.21 ± 0.01	0.21 ± 0.02

[a] The O state was formed by exposing COX-AEDANS to potassium ferricyanide and then washing in 20 mM HEPES, pH 8.0 to remove excess reagent.

[b] The P_M state was formed by exposing oxidized COX-AEDANS to carbon monoxide and air at pH 8.0.

[c] The wavelength of maximal emission intensity.

[d] Fluorescence emission intensity at the maximal emission wavelength.

[e] The anisotropy of the sample at λ_{MAX}

Figure A-4

Fluorescence Properties of COX-AEDANS in the O and P_M State. A) Emission spectra of the O (black) and P_M (red) states. Oxidized COX-AEDANS was diluted to 1 μM in 20 mM HEPES, 0.1% DM, pH 8.0. The emission spectrum was recorded using an excitation wavelength of 336 nm, a PMT setting of 850 V and slit widths of 5 nm for both excitation and emission. The sample was then exposed to CO and air and allowed to sit for 15 minutes to form the P_M state. The emission spectrum were then recorded for the P_M state. B) A first derivative plot of the emission spectra of the O (black) and P_M (red) states of COX-AEDANS. C) Emission intensity at 471 nm during the transition from the O to the P_M state. This is an example trace of the emission intensity following exposure of oxidized COX-AEDANS to CO and air. The decrease in fluorescence observed was biphasic. The first phase was not always observed and had a time constant of $\tau = 0.6$ min. The second phase had a time constant of $\tau = 526$ min. Total decreases in fluorescence intensity ranged from 2-16%, which could be correlated to an inner filter effect, i.e. changes in absorbance of the sample at the excitation and emission wavelengths resulted in a decrease in emission intensity.

A)

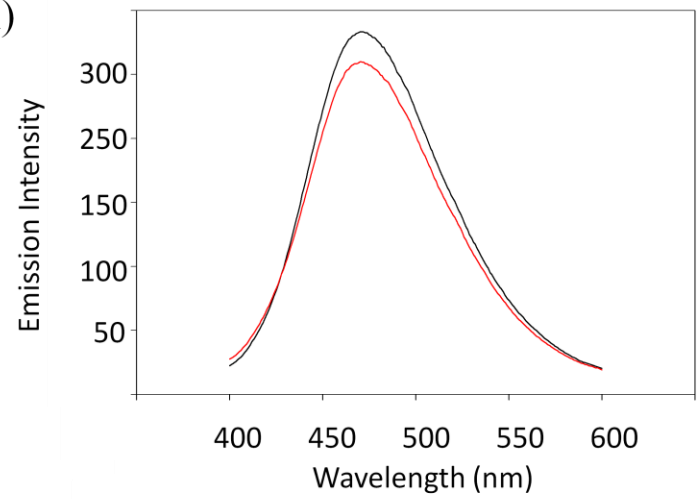
Emission Intensity
300
250
150
100
50
400
450
500
550
600
Wavelength (nm)

B)

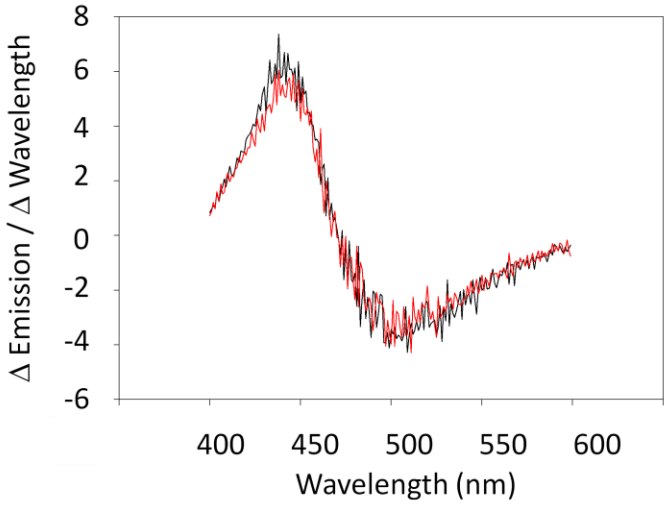
Δ Emission / Δ Wavelength
8
6
4
2
0
-2
-4
-6
400
450
500
550
600
Wavelength (nm)

C)

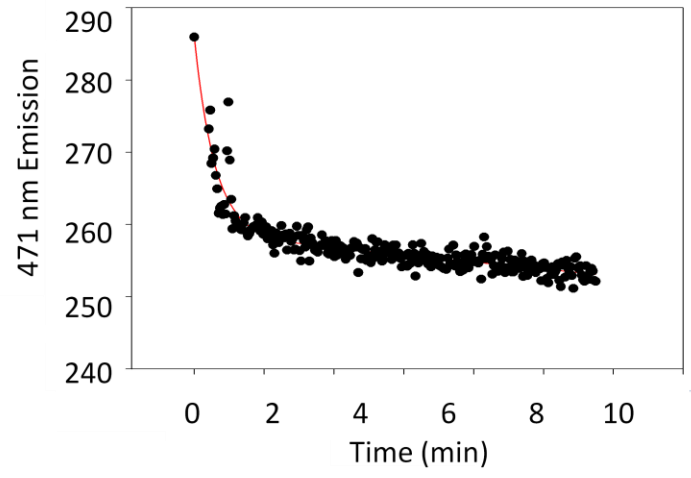
471 nm Emission
290
280
270
260
250
240
0
2
4
6
8
10
Time (min)

There was a statistically significant decrease in AEDANS emission intensity when COX was in the P_M versus the O state (Table A-III, Figure A-4A). The kinetics of the fluorescence emission decrease were monitored during the O to the P_M state following exposure to CO and air (Figure A-4C). The decrease was biphasic, although the initial fast phase was not reproducible. Neither of the time constants (τ_1 = 0.6 min, τ_2 = 526 min) matched the kinetics of the O → PM transition as measured by absorbance spectroscopy, which was a monophasic process (of τ = 1.3 min). Since there were no corresponding spectral shifts, this decrease in emission cannot be attributed to a change in the hydrophobicity surrounding the probe. It could be due to either the introduction of a quenching species or due to an inner filter effect. An inner filter effect is a change in the sample absorbance at the excitation and/or emission wavelength (Yappert and Ingle, 1989; Puchalski et al., 1991; Kubista et al., 1994). If the absorbance at 336 and/or 471 nm of COX-AEDANS is increased in the P_M versus the O state, this will filter the excitation and emission light and decrease the fluorescence emission. This would not be reflective of a change in fluorescence properties of the probe. The changes in emission intensity expected from the inner filter effect were calculated from the absorbance changes at 336 and 471 nm of the COX-AEDANS sample in the O and the P_M states, taking into account that the bandwidth used for fluorescence measurements was five times larger than the bandwidth used for measuring the absorbance at these wavelengths (Yappert and Ingle, 1989; Puchalski et al., 1991; Kubista et al., 1994). The expected changes due to the inner filter effect were such that the emission changes observed between the O and the P_M states could be attributed to the inner filter effect.

Taken together, these results indicate that there are no differences in the hydrophobicity or flexibility of COX subunit III in the regions surrounding the probes on helix four and possibly six. It may be that there are conformational changes occurring that the experimental technique cannot measure. For instance, the helices could be moving vertical to the plane of the membrane, which would not necessarily result in altered hydrophobicity or flexibility. To test for this kind of motion, a single cysteine should be introduced at the top or bottom of the transmembrane helix. If a vertical motion is occurring in the helix, the probe may move in or out of the membrane, which would alter its fluorescence properties. The CA1CS3-S187C mutant introduces a single cysteine into subunit III on the periplasmic side of helix five at the bilayer interface. Conducting these experiments on that mutant could be of benefit.

The sensitivity of these experiments is limited by the broad bandwidth that is required to receive an adequate signal. The 10 nm bandwidth used makes the technique less sensitive to spectral shifts and it augments the inner filter effect. One way of circumventing this problem would be to use a probe with a higher extinction coefficient at the excitation wavelength. This proves to be difficult given that COX has internal chromophores and that the probes must have spectroscopic properties which do not overlap with COX absorbance. Another option for reducing the bandwidth is to use a more sensitive instrument. The feasibility of conducting these experiments on an ISS PC1 photon counting spectrophotometer is being assessed.

Conclusions

Definitive evidence for conformational movement in COX subunit III was not observed when the native cysteines of subunit III were labeled with AEDANS and the fluorescence properties of the O and P_M state were compared. The probes are most likely localized within the bilayer on helix four and possibly six. Vertical motion within the plane of the bilayer would not be easily assessed by probe in these locations, so conformational changes in this vicinity cannot be ruled out. The techniques developed should be useful for examining potential motion in other areas of subunit III which are more likely to undergo conformational change. Toward that end, the single cysteine mutants A4C and S187C were constructed and their functional properties were found to be similar to wildtype, making them suitable candidates for these studies. The minor absorbance changes in COX at the excitation and emission wavelengths of the probe are magnified by the broad bandwidth required for these experiments. In order to detect potentially small fluorescence changes, an instrument with higher sensitivity is required.

LIST OF ABBREVIATIONS

A_{560}	Absorbance measured at 560 nm
A_{605}	Absorbance measured at 605 nm
aa_3	Hemes *a* and a_3 of cytochrome *c* oxidase
ATP	Adenosine 5'-triphosphate
BN-PAGE	Blue native polyacrylamide gel electrophoresis
bp	Basepair
CAPS	N-cyclohexyl-3-aminopropanesulfonic acid
CCCP	Carbonyl cyanide m-chlorophenylhydrazone
CHCA	α-cyano-4-hydroxysuccinnamic acid
CHES	N-cyclohexyl-2-aminoethanesulfonic acid
CO	Carbon monoxide
COV	Phospholipid vesicles containing cytochrome *c* oxidase
COX	Cytochrome *c* oxidase
Da	Dalton
DCCD	N, N'-dicyclohexylcarbodiimide
DM	Dodecyl-β-D-maltoside
DNA	Deoxyribonucleic acid
DNAse	Deoxyribonuclease
dNTP	Deoxy nucleotide triphosphate
EAM	Energy absorbing matrix

EDTA	Ethlenediaminetetraacetic acid
F State	An oxyferryl intermediate of cytochrome *c* oxidase
FAD^+	Flavin adenine dinucleotide
$FADH_2$	Reduced flavin adenine dinucleotide
H^+/e^-	Ratio of protons translocated to electrons transferred
H-bond	Hydrogen bond
HEPES	N-(2-hydroxyethyl) piperazine-N'-2-ethanesulfonic acid
IAEDANS	5-((((2-iodoacetyl)amino)ethyl)amino) naphthalene-1-sulfonic acid
I-II COX	Cytochrome *c* oxidase in which subunit III is removed either biochemically or genetically
$I\text{-}II_{BD}$ COX	Cytochrome *c* oxidase in which subunit III is biochemically depleted
$I\text{-}II_{GD}$ COX	Cytochrome *c* oxidase in which subunit III is genetically deleted
kb	Kilobase
kD	Kilodalton
LB	Luria-Bertani
m/z	Mass to charge ratio
mA	Milliamps
MALDI-TOF	matrix assisted laser desorption time of flight
MIANS	2-(4'-maleimidylanilino)naphthalene-6-sulfonic acid
NAD^+	Nicotinamide adenine dinucleotide
NADH	Reduced nicotinamide adenine dinucleotide
O State	The oxidized state of cytochrome *c* oxidase
OD_{660}	Optical density measured at 660 nm
P.dent.	*Paracoccus denitrificans*

pCOV	Cytochrome *c* oxidase vesicles purified by discontinuous sucrose gradient ultracentrifugation
PDB	Protein databank
pH	-log [H^+]
PL1	The phospholipid bound in the v-shaped cleft of subunit III at position 1
PL2	The phospholipid bound in the v-shaped cleft of subunit III at position 2
P_M State	An oxyferryl intermediate of cytochrome *c* oxidase
PMSF	Phenylmethylsulfonylfluoride
R State	The reduced state of cytochrome *c* oxidase
R.sph.	*Rhodobacter sphaeroides*
RCR	Respiratory control ratio
RCR_{val}	Respiratory control ratio relative to the valinomycin rate
R-O	Reduced *minus* oxidized
SDS	Sodium dodecyl sulfate
SDS-PAGE	Sodium dodecyl sulfate-polyacrylamide gel electrophoresis
SI	Subunit I
SII	Subunit II
SIII	Subunit III
SIII-Δ114	Subunit III genetically truncated after residue 114
SIV	Subunit IV
SPA	Sinapinic acid
TBS-B	Tris buffered saline containing 5% powdered milk
TFA	Trifluoroacetic acid

TMPD	N, N, N', N', -tetramethyl-p-phenylenediamine
TN	Turnover number (number of electrons transferred per second per mole of cytochrome *c* oxidase
Tris	Tris (hydroxymethyl) aminoethane
Val	Valinomycin
WT	Wild-type *Rhodobacter sphaeroides* cytochrome *c* oxidase
Δ114 COX	Cytochrome *c* oxidase in which subunit III is genetically truncated after residue 114

LIST OF REFERENCES

Abbott, M. B., Gaponenko, V., Abusamhadneh, E., Finley, N., Li, G., Dvoretsky, A., Rance, M., Solaro, R. J. and Rosevear, P. R. (2000) Regulatory domain conformational exchange and linker region flexibility in cardiac troponin C bound to cardiac troponin I. *J. Biol. Chem.* **275,** 20610-20617.

Abramson, J., Riistama, S., Larsson, G., Jasaitis, A., Svensson-Ek, M., Laakkonen, L., Puustinen, A., Iwata, S. and Wikstrom, M. (2000) The structure of the ubiquinol oxidase from Escherichia coli and its ubiquinone binding site. *Nat Struct Biol* **7,** 910-7.

Adelroth, P. and Hosler, J. (2006) Surface proton donors for the D-pathway of cytochrome c oxidase in the absence of subunit III. *Biochemistry* **45,** 8308-18.

Adelroth, P., Mitchell, D. M., Gennis, R. B. and Brzezinski, P. (1997) Factors determining electron-transfer rates in cytochrome c oxidase: studies of the FQ(I-391) mutant of the Rhodobacter sphaeroides enzyme. *Biochemistry* **36,** 11787-96.

Andrews, R. M., Kubacka, I., Chinnery, P. F., Lightowlers, R. N., Turnbull, D. M. and Howell, N. (1999) Reanalysis and revision of the Cambridge reference sequence for human mitochondrial DNA. *Nat. Genet.* **23,** 147.

Bay, D. C. and Court, D. A. (2002) Origami in the outer membrane: the transmembrane arrangement of mitochondrial porins. *Biochem. Cell Biol.* **80,** 551-562.

Bell, S. P., Curran, P. K., Choi, S. and Mindell, J. A. (2006) Site-directed fluorescence studies of a prokaryotic ClC antiporter. *Biochemistry* **45,** 6773-6782.

Beney, L., Perrier-Cornet, J. M., Hayert, M. and Gervais, P. (1997) Shape modification of phospholipid vesicles induced by high pressure: influence of bilayer compressibility. *Biophys. J.* **72,** 1258-1263.

Branden, G., Branden, M., Schmidt, B., Mills, D. A., Ferguson-Miller, S. and Brzezinski, P. (2005) The protonation state of a heme propionate controls electron transfer in cytochrome c oxidase. *Biochemistry* **44,** 10466-74.

Bratton, M., Mills, D., Castleden, C. K., Hosler, J. and Meunier, B. (2003) Disease-related mutations in cytochrome c oxidase studied in yeast and bacterial models. *Eur J Biochem* **270,** 1222-30.

Bratton, M. R., Hiser, L., Antholine, W. E., Hoganson, C. and Hosler, J. P. (2000) Identification of the structural subunits required for formation of the metal centers in subunit I of cytochrome c oxidase of Rhodobacter sphaeroides. *Biochemistry* **39,** 12989-95.

Bratton, M. R., Pressler, M. A. and Hosler, J. P. (1999) Suicide inactivation of cytochrome *c* oxidase: catalytic turnover in the absence of subunit III alters the active site. *Biochemistry* **38,** 16236-45.

Brega, A., Narula, J. and Arbustini, E. (2001) Functional, structural and genetic mitochondrial abnormalities in myocardial diseases. *J Nucl Cardiol* **8,** 89-97.

Brzezinski, P. and Gennis, R. B. (2008) Cytochrome c oxidase: exciting progress and remaining mysteries. *J. Bioenerg. Biomembr.* **40,** 521-531.

Brzezinski, P. and Johansson, A. L. (2010) Variable proton-pumping stoichiometry in structural variants of cytochrome c oxidase. *Biochim. Biophys. Acta* doi:10.1016/j.bbabio.2010.02.020

Brzezinski, P., Reimann, J. and Adelroth, P. (2008) Molecular architecture of the proton diode of cytochrome c oxidase. *Biochem. Soc. Trans.* **36,** 1169-1174.

Busenlehner, L. S., Salomonsson, L., Brzezinski, P. and Armstrong, R. N. (2006) Mapping protein dynamics in catalytic intermediates of the redox-driven proton pump cytochrome c oxidase. *Proc Natl Acad Sci U S A* **103,** 15398-15403.

Cao, J., Hosler, J., Shapleigh, J., Revzin, A. and Ferguson-Miller, S. (1992) Cytochrome aa_3 of *Rhodobacter sphaeroides* as a model for mitochondrial cytochrome *c* oxidase. The coxII/coxIII operon codes for structural and assembly proteins homologous to those in yeast. *J. Biol. Chem.* **267,** 24273-8.

Cao, J., Shapleigh, J., Gennis, R., Revzin, A. and Ferguson-Miller, S. (1991) The gene encoding cytochrome c oxidase subunit II from Rhodobacter sphaeroides; comparison of the deduced amino acid sequence with sequences of corresponding peptides from other species. *Gene* **101,** 133-7.

Cecchini, G. (2003) Function and structure of complex II of the respiratory chain. *Annu. Rev. Biochem.* **72,** 77-109.

Chepuri, V., Lemieux, L., Au, D. C. and Gennis, R. B. (1990) The sequence of the cyo operon indicates substantial structural similarities between the cytochrome o ubiquinol oxidase of Escherichia coli and the aa3-type family of cytochrome c oxidases. *J Biol Chem* **265,** 11185-92.

Choi, E. J. and Dimitriais, E. K. (2004) Cytochrome *c* adsorption to supported, anionic lipid bilayers studied via atomic force microscopy. *Biophys. J.* **87,** 3234-3241.

Crofts, A. R. (2004) The cytochrome bc1 complex: function in the context of structure. *Annu. Rev. Physiol.* **66,** 689-733.

Crofts, A. R., Holland, J. T., Victoria, D., Kolling, D. R., Dikanov, S. A., Gilbreth, R., Lhee, S., Kuras, R. and Kuras, M. G. (2008) The Q-cycle reviewed: How well does a monomeric mechanism of the bc(1) complex account for the function of a dimeric complex? *Biochim. Biophys. Acta* **1777,** 1001-1019.

Cvetkov, T. L. and Prochaska, L. J. (2007) Biophysical and biochemical characterization of reconstituted and purified Rhodobacter sphaeroides cytochrome c oxidase in phospholipid vesicles sheds insight into its functional oligomeric structure. *Protein Expr Purif* **56,** 189-196.

Dan, N. and Safran, S. A. (1998) Effect of lipid characteristics on the structure of transmembrane proteins. *Biophys. J.* **75,** 1410-1414.

DiBiase, V. A. and Prochaska, L. J. (1985) Characterization of electron transfer and proton translocation activities in trypsin-treated bovine heart mitochondrial cytochrome c oxidase. *Arch. Biochem. Biophys.* **243,** 668-677.

DiMauro, S., Hirano, M. and Schon, E. A. (2006) Approaches to the treatment of mitochondrial diseases. *Muscle Nerve* **34,** 265-283.

DiMauro, S. and Schon, E. A. (2003) Mitochondrial respiratory-chain diseases. *New England Journal of Medicine* **348,** 2656-2668.

Distler, A. M., Allison, J., Hiser, C., Qin, L., Hilmi, Y. and Ferguson-Miller, S. (2004) Mass spectrometric detection of protein, lipid and heme components of cytochrome c oxidase from R. sphaeroides and the stabilization of non-covalent complexes from the enzyme. *Eur J Mass Spectrom (Chichester, Eng)* **10,** 295-308.

Egawa, T., Lin, M. T., Hosler, J. P., Gennis, R. B., Yeh, S. R. and Rousseau, D. L. (2009) Communication between R481 and Cu(B) in cytochrome bo(3) ubiquinol oxidase from Escherichia coli. *Biochemistry* **48,** 12113-12124.

Estey, L. A. and Prochaska, L. J. (1993) Detection of bovine heart mitochondrial cytochrome *c* oxidase dimers in Triton X-100 and phospholipid vesicles by chemical cross-linking. *Biochemistry* **32,** 13270-6.

Ferguson-Miller, S., Brautigan, D. L. and Margoliash, E. (1978) Definition of cytochrome c binding domains by chemical modification. III. Kinetics of reaction of carboxydinitrophenyl cytochromes c with cytochrome c oxidase. *J Biol Chem* **253,** 149-59.

Fernandez-Vizarra, E., Tiranti, V. and Zeviani, M. (2009) Assembly of the oxidative phosphorylation system in humans: what we have learned by studying its defects. *Biochim. Biophys. Acta* **1793,** 200-211.

Figurski, D. H. and Helinski, D. R. (1979) Replication of an origin-containing derivative of plasmid RK2 dependent on a plasmid function provided in trans. *Proc. Natl. Acad. Sci. U. S. A.* **76,** 1648-1652.

Finel, M. and Wikstrom, M. (1986) Studies on the role of the oligomeric state and subunit III of cytochrome oxidase in proton translocation. *Biochim Biophys Acta* **851,** 99-108.

Fontanesi, F., Soto, I. C. and Barrientos, A. (2008) Cytochrome c oxidase biogenesis: new levels of regulation. *IUBMB Life* **60,** 557-568.

Fontanesi, F., Soto, I. C., Horn, D. and Barrientos, A. (2006) Assembly of mitochondrial cytochrome c-oxidase, a complicated and highly regulated cellular process. *Am. J. Physiol. Cell. Physiol.* **291,** C1129-47.

Fornuskova, D., Stiburek, L., Wenchich, L., Vinsova, K., Hansikova, H. and Zeman, J. (2010) Novel insights into the assembly and function of human nuclear-encoded cytochrome c oxidase subunits 4, 5a, 6a, 7a and 7b. *Biochem. J.* **428**, 363-374.

Frey, T. G. and Mannella, C. A. (2000) The internal structure of mitochondria. *Trends Biochem. Sci.* **25,** 319-324.

Fuller, S. D., Darley-Usmar, V. M. and Capaldi, R. A. (1981) Covalent complex between yeast cytochrome c and beef heart cytochrome c oxidase which is active in electron transfer. *Biochemistry* **20,** 7046-7053.

Galati, D., Srinivasan, S., Raza, H., Prabu, S. K., Hardy, M., Chandran, K., Lopez, M., Kalyanaraman, B. and Avadhani, N. G. (2009) Role of nuclear-encoded subunit Vb in the assembly and stability of cytochrome c oxidase complex: implications in mitochondrial dysfunction and ROS production. *Biochem. J.* **420,** 439-449.

Ganesan, K. and Gennis, R. B. (2010) Blocking the K-pathway still allows rapid one-electron reduction of the binuclear center during the anaerobic reduction of the aa(3)-type cytochrome c oxidase from Rhodobacter sphaeroides. *Biochim. Biophys. Acta*, in press, doi:10.1016/j.bbabio.2010.03.012

Geyer, R. R. (2007) Investigating the Role of Subunit III in the Structure and Function of *Rhodobacter sphaeroides* Cytochrome *c* Oxidase.

Gilderson, G., Salomonsson, L., Aagaard, A., Gray, J., Brzezinski, P. and Hosler, J. (2003) Subunit III of cytochrome *c* oxidase of *Rhodobacter sphaeroides* is required to

maintain rapid proton uptake through the D pathway at physiologic pH. *Biochemistry* **42,** 7400-9.

Gorbenko, G. P., Molotkovsy, J. G. and Kinnunen, P. K. J. (2006) Cytochrome *c* interaction with cardiolipin/phosphatidylcholine model membranes: effect of cardiolipid protonation. *Biophys. J.* **90,** 4093-4103.

Gorbikova, E. A., Belevich, I., Wikstrom, M. and Verkhovsky, M. I. (2008) The proton donor for O-O bond scission by cytochrome c oxidase. *Proc. Natl. Acad. Sci. U. S. A.* **105,** 10733-10737.

Gorbikova, E. A., Wikstrom, M. and Verkhovsky, M. I. (2008) The protonation state of the cross-linked tyrosine during the catalytic cycle of cytochrome c oxidase. *J. Biol. Chem.* **283,** 34907-34912.

Gray, M. W., Burger, G. and Lang, B. F. (1999) Mitochondrial evolution. *Science* **283,** 1476-1481.

Han, D., Morgan, J. E. and Gennis, R. B. (2005) G204D, a mutation that blocks the proton-conducting D-channel of the aa3-type cytochrome c oxidase from Rhodobacter sphaeroides. *Biochemistry* **44,** 12767-74.

Haughland, R. P. (2002) *Handbook of fluorescent probes and research chemicals,* Molecular Probes Inc., Eugene, OR.

Hibbs, R. E., Johnson, D. A., Shi, J., Hansen, S. B. and Taylor, P. (2005) Structural dynamics of the alpha-neurotoxin-acetylcholine-binding protein complex: hydrodynamic and fluorescence anisotropy decay analyses. *Biochemistry* **44,** 16602-16611.

Hirst, J. (2009) Towards the molecular mechanism of respiratory complex I. *Biochem. J.* **425,** 327-339.

Hiser, C., Mills, D. A., Schall, M. and Ferguson-Miller, S. (2001) C-terminal truncation and histidine-tagging of cytochrome c oxidase subunit II reveals the native processing site, shows involvement of the C-terminus in cytochrome c binding, and improves the assay for proton pumping. *Biochemistry* **40,** 1606-15.

Hiser, L. and Hosler, J. P. (2001) Heme A is not essential for assembly of the subunits of cytochrome c oxidase of Rhodobacter sphaeroides. *J Biol Chem* **276,** 45403-7.

Holt, I. J., He, J., Mao, C. C., Boyd-Kirkup, J. D., Martinsson, P., Sembongi, H., Reyes, A. and Spelbrink, J. N. (2007) Mammalian mitochondrial nucleoids: organizing an independently minded genome. *Mitochondrion* **7,** 311-321.

Horsefield, R., Yankovskaya, V., Sexton, G., Whittingham, W., Shiomi, K., Omura, S., Byrne, B., Cecchini, G. and Iwata, S. (2006) Structural and computational analysis of the

quinone-binding site of complex II (succinate-ubiquinone oxidoreductase): a mechanism of electron transfer and proton conduction during ubiquinone reduction. *J. Biol. Chem.* **281,** 7309-7316.

Horvath, R., Scharfe, C., Hoeltzenbein, M., Do, B. H., Schroder, C., Warzok, R., Vogelgesang, S., Lochmuller, H., Muller-Hocker, J., Gerbitz, K. D., P.J., O. and Jaksch, M. (2002) Childhood onset mitochondrial myopathy and lactic acidosis caused by a stop mutation in the mitochondrial cytochrome c oxidase subunit III gene. *Journal of Medical Genetics* **39,** 812-816.

Horvath, R., Schonser, B. G., Muller-Hocker, J., Volpel, M., Jaksch, M. and Lochmuller, H. (2005) Mutations in mtDNA-encoded cytochrome c oxidase subunit genes causing isolated myopather or severe encephalomyopathy. *Neuromuscular Disorders* **15,** 851-857.

Hosler, J. P. (2004) The influence of subunit III of cytochrome c oxidase on the D pathway, the proton exit pathway and mechanism-based inactivation in subunit I. *Biochim Biophys Acta* **1655,** 332-9.

Hosler, J. P., Ferguson-Miller, S. and Mills, D. A. (2006) Energy transduction: proton transfer through the respiratory complexes. *Annu. Rev. Biochem.* **75,** 165-87.

Hosler, J. P., Fetter, J., Tecklenburg, M. M., Espe, M., Lerma, C. and Ferguson-Miller, S. (1992) Cytochrome aa_3 of *Rhodobacter sphaeroides* as a model for mitochondrial cytochrome *c* oxidase. Purification, kinetics, proton pumping, and spectral analysis. *J. Biol. Chem.* **267,** 24264-72.

Huang, C. and Mason, J. T. (1978) Geometric packing constraints in egg phosphatidylcholine vesicles. *Proc. Natl. Acad. Sci. U.S.A.* **75,** 308-310.

Hudson, E. N. and Weber, G. (1973) Synthesis and characterization of two fluorescent sulfhydryl reagents. *Biochemistry* **12,** 4154-4161.

Iwata, S., Lee, J. W., Okada, K., Lee, J. K., Iwata, M., Rasmussen, B., Link, T. A., Ramaswamy, S. and Jap, B. K. (1998) Complete structure of the 11-subunit bovine mitochondrial cytochrome bc1 complex. *Science* **281,** 64-71.

Iwata, S., Ostermeier, C., Ludwig, B. and Michel, H. (2002) Structure at 2.8 Å resolution of cytochrome *c* oxidase from *Paracoccus denitrificans*. *Nature* **376,** 660-669.

Jancura, D., Antalik, M., Berka, V., Palmer, G. and Fabian, M. (2006) Filling the catalytic site of cytochrome *c* oxidase with electrons: reduced Cu_B facilitates internal electron transfer to heme a_3. *J. Biol. Chem.* **281,** 20003-20010.

Jasaitis, A., Verkhovsky, M. I., Morgan, J. E., Verkhovskaya, M. L. and Wikstrom, M. (1999) Assignment and charge translocation stoichiometries of the major electrogenic

phases in the reaction of cytochrome *c* oxidase with dioxygen. *Biochemistry* **38,** 2697-2706.

Junemann, S., Heathcote, P. and Rich, P. R. (2000) The reactions of hydrogen peroxide with bovine cytochrome c oxidase. *Biochim. Biophys. Acta* **1456,** 56-66.

Kadenbach, B., Jarausch, J., Hartmann, R. and Merle, P. (1983) Separation of mammalian cytochrome c oxidase into 13 polypeptides by a sodium dodecyl sulfate-gel electrophoretic procedure. *Anal. Biochem.* **129,** 517-521.

Krab, K. and Wikstrom, G. (1978) Proton-translocating cytochrome *c* oxidase in artificial phospholipid vesicles. *Biochim. Biophys. Acta* **504,** 200-214.

Kubista, M., Sjoback, R., Eriksson, S. and Albinsson, B. (1994) Experimental correction for the inner-filter effect in fluorescence spectra. *Analyst* **119,** 417-419.

Kusnetzow, A. K., Altenbach, C. and Hubbell, W. L. (2006) Conformational states and dynamics of rhodopsin in micelles and bilayers. *Biochemistry* **45,** 5538-50.

Lakowicz, J. R. (2006) *Principles of Fluorescence Spectroscopy,* Third ed., Springer, New York.

Lambeth, D. O., Campbell, K. L., Zand, R. and Palmer, G. (1973) The appearance of transient species of cytochrome c upon rapid oxidation or reduction at alkaline pH. *J Biol Chem* **248,** 8131-8136.

Lee, H. J., Ojemyr, L., Vakkasoglu, A., Brzezinski, P. and Gennis, R. B. (2009) Properties of Arg481 mutants of the aa3-type cytochrome c oxidase from Rhodobacter sphaeroides suggest that neither R481 nor the nearby D-propionate of heme a3 is likely to be the proton loading site of the proton pump. *Biochemistry* **48,** 7123-7131.

Lee, S. J., Yamashita, E., Abe, T., Fukumoto, Y., Tsukihara, T., Shinzawa-Itoh, K., Ueda, H. and Yoshikawa, S. (2001) Intermolecular interactions in dimer of bovine heart cytochrome *c* oxidase. *Acta Crysallogr.* **D57,** 941-947.

Lepp, H., Salomonsson, L., Zhu, J. P., Gennis, R. B. and Brzezinski, P. (2008a) Impaired proton pumping in cytochrome c oxidase upon structural alteration of the D pathway. *Biochim. Biophys. Acta* **1777,** 897-903.

Lepp, H., Svahn, E., Faxen, K. and Brzezinski, P. (2008b) Charge transfer in the K proton pathway linked to electron transfer to the catalytic site in cytochrome c oxidase. *Biochemistry* **47,** 4929-4935.

Lincoln, J. A., Donat, N., Palmer, G. and Prochaska, L. J. (2003) Site-specific antibodies against hydrophilic domains of subunit III of bovine heart cytochrome c oxidase affect enzyme function. *Arch Biochem Biophys* **416,** 81-91.

Mackenzie, C., Choudhary, M., Larimer, F. W., Predki, P. F., Stilwagen, S., Armitage, J. P., Barber, R. D., Donohue, T. J., Hosler, J. P., Newman, J. E., Shapleigh, J. P., Sockett, R. E., Zeilstra-Ryalls, J. and Kaplan, S. (2001) The home stretch, a first analysis of the nearly completed genome of Rhodobacter sphaeroides 2.4.1. *Photosynth Res* **70,** 19-41.

Madden, T. D. and Cullis, P. R. (1985) Preparation of reconstituted cytochrome oxidase vesicles with defined trans-membrane protein orientations employing a cytochrome c affinity column. *Biochim Biophys Acta* **808,** 219-224.

Maklashina, E. and Cecchini, G. (2010) The quinone-binding and catalytic site of complex II. *Biochim. Biophys. Acta,* in press, doi:10.1016/j.bbabio.2010.02.015.

Mannella, C. A. (2006) The relevance of mitochondrial membrane topology to mitochondrial function. *Biochim. Biophys. Acta* **1762,** 140-147.

Mather, M. W. and Rottenberg, H. (1998) Intrinsic uncoupling of cytochrome *c* oxidase may cause the maternally inherited mitochondrial diseases MELAS and LHON. *FEBS Lett* **433,** 93-97.

Mills, D. A. and Hosler, J. P. (2005) Slow proton transfer through the pathways for pumped protons in cytochrome *c* oxidase induces suicide inactivation of the enzyme. *Biochemistry* **44,** 4656-66.

Mills, D. A., Tan, Z., Ferguson-Miller, S. and Hosler, J. (2003) A role for subunit III in proton uptake into the D pathway and a possible proton exit pathway in Rhodobacter sphaeroides cytochrome c oxidase. *Biochemistry* **42,** 7410-7.

Mitchell, D. M. and Gennis, R. B. (1995) Rapid purification of wildtype and mutant cytochrome c oxidase from Rhodobacter sphaeroides by Ni(2+)-NTA affinity chromatography. *FEBS Lett* **368,** 148-50.

Mitchell, P. (1961) Coupling of phosphorylation to electron and hydrogen transfer by a chemi-osmotic type of mechanism. *Nature* **191,** 144-148.

Mitchell, R. and Rich, P. R. (1994) Proton uptake by cytochrome c oxidase on reduction and on ligand binding. *Biochim. Biophys. Acta* **1186,** 19-26.

Mouncey, N. J., Gak, E., Choudhary, M., Oh, J. and Kaplan, S. (2000) Respiratory pathways of Rhodobacter sphaeroides 2.4.1(T): identification and characterization of genes encoding quinol oxidases. *FEMS Microbiol. Lett.* **192,** 205-210.

Muller, M. and Azzi, A. (1985) Morphology of proteoliposomes containing fluorescein-phosphatidylethanolamine reconstituted with native and subunit III-depleted cytochrome *c* oxidase. *J. Bioenerg. Biomembr.* **17,** 385-393.

Musatov, A., Ortega-Lopez, J., Demeler, B., Osborne, J. P., Gennis, R. B. and Robinson, N. C. (1999) Detergent-solubilized Escherichia coli cytochrome bo3 ubiquinol oxidase: a monomeric, not a dimeric complex. *FEBS Lett* **457,** 153-6.

Musatov, A. and Robinson, N. C. (2002) Cholate-induced dimerization of detergent- or phospholipid-solubilized bovine cytochrome *c* oxidase. *Biochemistry* **41,** 4371-4376.

Nagle, J. F. and Tristram-Nagle, S. (1983) Hydrogen bonded chain mechanisms for proton conduction and proton pumping. *J. Membr. Biol.* **74,** 1-14.

Nakanishi-Matsui, M., Sekiya, M., Nakamoto, R. K. and Futai, M. (2010) The mechanism of rotating proton pumping ATPases. *Biochim. Biophys. Acta*, in press, doi:10.1016/j.bbabio.2010.02.014.

Neupert, W. and Herrmann, J. M. (2007) Translocation of proteins into mitochondria. *Annu. Rev. Biochem.* **76,** 723-749.

Nguyen, X. T., Pabarue, H. A., Geyer, R. R., Shroyer, L. A., Estey, L. A., Parilo, M. S., Wilson, K. S. and Prochaska, L. J. (2002) Biochemical and biophysical properties of purified phospholipid vesicles containing bovine heart cytochrome *c* oxidase. *Protein Express. Purif.* **26,** 122-30.

Ogunjimi, E. O., Pokalsky, C. N., Shroyer, L. A. and Prochaska, L. J. (2000) Evidence for a Conformational Change in Subunit III of Bovine Heart Mitochondrial Cytochrome c Oxidase1. *J Bioenerg Biomembr* **32,** 617-26.

Ordys, B. B., Launay, S., Deighton, R. F., McCulloch, J. and Whittle, I. R. (2010) The Role of Mitochondria in Glioma Pathophysiology. *Mol. Neurobiol.,* in press, doi:10.1007/s12035-010-8133-5.

Organisciak, D. and Noell, W. (1976) Hereditary retinal dystrophy in the rat: lipid composition of debris. *Exp. Eye Res.* **22,** 101-113.

Owusu-Ansah, E., Yavari, A., Mandal, S. and Banerjee, U. (2008) Distinct mitochondrial retrograde signals control the G1-S cell cycle checkpoint. *Nat. Genet.* **40,** 356-361.

Perrier-Cornet, J. M., Baddouj, K. and Gervais, P. (2005) Pressure-induced shape change of phospholipid vesicles: implication of compression and phase transition. *J. Membrane Biol.* **204,** 101-107.

Pisliakov, A. V., Sharma, P. K., Chu, Z. T., Haranczyk, M. and Warshel, A. (2008) Electrostatic basis for the unidirectionality of the primary proton transfer in cytochrome c oxidase. *Proc. Natl. Acad. Sci. U. S. A.* **105,** 7726-7731.

Prochaska, L. J., Bisson, R., Capaldi, R. A., Steffens, G. C. and Buse, G. (1981) Inhibition of cytochrome c oxidase function by dicyclohexylcarbodiimide. *Biochim. Biophys. Acta* **637,** 360-373.

Prochaska, L. J. and Reynolds, K. A. (1986) Characterization of electron-transfer and proton-translocation activities in bovine heart mitochondrial cytochrome c oxidase deficient in subunit III. *Biochemistry* **25,** 781-787.

Puchalski, M. M., Morra, M. J. and von Wandruszka, R. (1991) Assessment of inner filter effect corrections in fluorimetry. *Fres. J. Anal. Chem.* **340,** 341.

Puettner, I., Carafoli, E. and Malatesta, F. (1985) Spectroscopic and functional properties of subunit III-depleted cytochrome oxidase. *J. Biol. Chem.* **260,** 3719-3723.

Qin, L., Hiser, C., Mulichak, A., Garavito, R. M. and Ferguson-Miller, S. (2006) Identification of conserved lipid/detergent-binding sites in a high-resolution structure of the membrane protein cytochrome *c* oxidase. *Proc. Natl. Acad. Sci. U.S.A.* **103,** 16117-16122.

Radermacher, M., Ruiz, T., Clason, T., Benjamin, S., Brandt, U. and Zickermann, V. (2006) The three-dimensional structure of complex I from Yarrowia lipolytica: a highly dynamic enzyme. *J. Struct. Biol.* **154,** 269-279.

Rich, P. R., Rigby, S. E. and Heathcote, P. (2002) Radicals associated with the catalytic intermediates of bovine cytochrome c oxidase. *Biochim. Biophys. Acta* **1554,** 137-146.

Sadoski, R. C., Zaslavsky, D., Gennis, R. B., Durham, B. and Millett, F. (2001) Exposure of bovine cytochrome *c* oxidase to high triton X-100 or to alkaline conditions causes a dramatic change in the rate of reduction of compound F. *J. Biol. Chem.* **276,** 33616-20.

Salomonsson, L., Faxen, K., Adelroth, P. and Brzezinski, P. (2005) The timing of proton migration in membrane-reconstituted cytochrome c oxidase. *Proc. Natl. Acad. Sci. U. S. A.* **102,** 17624-17629.

Saraste, M. (1999) Oxidative phosphorylation at the fin de siecle. *Science* **283,** 1488-1493.

Saraste, M. (1990) Structural features of cytochrome oxidases. *Quarterly Reviews of Biophysics* **23,** 331-339.

Sazanov, L. A. (2007) Respiratory complex I: mechanistic and structural insights provided by the crystal structure of the hydrophilic domain. *Biochemistry* **46,** 2275-2288.

Schagger, H. and von Jagow, G. (1991) Blue native electrophoresis for isolation of membrane protein complexes in enzymatically active form. *Anal. Biochem.* **199,** 223-231.

Sharpe, M. A. and Ferguson-Miller, S. (2008) A chemically explicit model for the mechanism of proton pumping in heme-copper oxidases. *J. Bioenerg. Biomembr.* **40,** 541-549.

Shinzawa-Itoh, K., Aoyama, H., Muramoto, K., Terada, H., Kurauchi, T., Tadehara, Y., Yamasaki, A., Sugimura, T., Kurono, S., Tsujimoto, K., Mizushima, T., Yamashita, E., Tsukihara, T. and Yoshikawa, S. (2007) Structures and physiological roles of 13 integral lipids of bovine heart cytochrome *c* oxidase. *EMBO J.* **26,** 1713-1725.

Sistrom, W. R. (1962) The kinetics of the synthesis of photopigments in Rhodopseudomonas spheroides. *J. Gen. Microbiol.* **28,** 607-616.

Smith, D., Gray, J., Mitchell, L., Antholine, W. E. and Hosler, J. P. (2005) Assembly of cytochrome-c oxidase in the absence of assembly protein Surf1p leads to loss of the active site heme. *J Biol Chem* **280,** 17652-6.

Stanicova, J., Musatov, A. and Robinson, N. C. (2004) Stability of bovine cytochrome *c* oxidase as studied after exposure to high hydrostatic pressure. *Acta Medica (Hradac Kralove)* **47,** 335-338.

Stanicova, J., Sedlak, E., Musatov, A. and Robinson, N. C. (2007) Differential stability of dimeric and monomeric cytochrome *c* oxidase exposed to elevated hydrostatic pressure. *Biochemistry* **46,** 7146-7152.

Steinrucke, P., Steffens, G. C., Panskus, G., Buse, G. and Ludwig, B. (1987) Subunit II of cytochrome c oxidase from Paracoccus denitrificans. DNA sequence, gene expression and the protein. *Eur. J. Biochem.* **167,** 431-439.

Stiburek, L. and Zeman, J. (2010) Assembly factors and ATP-dependent proteases in cytochrome c oxidase biogenesis. *Biochim. Biophys. Acta,* in press, doi:10.1016/j.bbabio.2010.04.006.

Suarez, M. D., Revzin, A., Narlock, R., Kempner, E. S., Thompson, D. A. and Ferguson-Miller, S. (1984) The functional and physical form of mammalian cytochrome c oxidase determined by gel filtration, radiation inactivation, and sedimentation equilibrium analysis. *J Biol Chem* **259,** 13791-9.

Sun, F., Huo, X., Zhai, Y., Wang, A., Xu, J., Su, D., Bartlam, M. and Rao, Z. (2005) Crystal structure of mitochondrial respiratory membrane protein complex II. *Cell* **121,** 1043-1057.

Svensson-Ek, M., Abramson, J., Larsson, G., Tornroth, S., Brzezinski, P. and Iwata, S. (2002) The X-ray crystal structures of wild-type and EQ(I-286) mutant cytochrome *c* oxidases from *Rhodobacter sphaeroides*. *J. Mol. Biol.* **321,** 329-39.

Tatsuta, T. and Langer, T. (2009) AAA proteases in mitochondria: diverse functions of membrane-bound proteolytic machines. *Res. Microbiol.* **160,** 711-717.

Thompson, D. A. and Ferguson-Miller, S. (1983) Lipid and subunit III depleted cytochrome c oxidase purified by horse cytochrome c affinity chromatography in lauryl maltoside. *Biochemistry* **22,** 3178-87.

Thompson, D. A., Gregory, L. and Ferguson-Miller, S. (1985) Cytochrome c oxidase depleted of subunit III: proton-pumping, respiratory control, and pH dependence of the midpoint potential of cytochrome a. *J Inorg Biochem* **23,** 357-64.

Tihova, M., Tattrie, B. and Nicholls, P. (1993) Electron microscopy of cytochrome c oxidase-containing proteoliposomes: imaging analysis of protein orientation and monomer-dimer behaviour. *Biochem. J.* **292,** 933-946.

Tiranti, V., Corona, P., Greco, M., Taanman, J. W., Carrara, F., Lamantea, E., Nijtmans, L., Uziel, G. and Zeviani, M. (2000) A novel frameshift mutation of the mtDNA COIII gene leads to impaired assembly of cytochrome c oxidase in a patient affected by Leigh-like syndrome. *Hum. Mol. Genet.* **9,** 2733-2742.

Tsujimoto, Y. and Shimizu, S. (2007) Role of the mitochondrial membrane permeability transition in cell death. *Apoptosis* **12,** 835-840.

Tsukihara, T., Aoyama, H., Yamashita, T. T., Yamaguchi, H., Shinzawa-Itoh, K., Nakashima, R., Yaono, R. and Yoshikawa, S. (1996) The whole structure of the 13-subunit oxidized cytochrome c oxidase at 2.8A. *Science* **272,** 1136-1144.

Tsukihara, T., Shimokata, K., Katayama, Y., Shimada, H., Muramoto, K., Aoyama, H., Mochizuki, M., Shinzawa-Itoh, K., Yamashita, E., Yao, M., Ishimura, Y. and Yoshikawa, S. (2003) The low-spin heme of cytochrome c oxidase as the driving element of the proton-pumping process. *Proc Natl Acad Sci U S A* **100,** 15304-9.

Tuppen, H. A., Blakely, E. L., Turnbull, D. M. and Taylor, R. W. (2010) Mitochondrial DNA mutations and human disease. *Biochim. Biophys. Acta* **1797,** 113-128.

van Gelder, B. (1966) On cytochrome *c* oxidase. I. The extinction coefficients of cytochrome *a* and cytochrome a_3. *Biochim. Biophys. Acta* **118,** 36-46.

Vanneste, W. H. (1966) The stoichiometry and absorption spectra of components *a* and a_3 in cytochrome c oxidase. *Biochemistry* **5,** 838-848.

Varanasi, L., Mills, D., Murphree, A., Gray, J., Purser, C., Baker, R. and Hosler, J. (2006) Altering conserved lipid binding sites in cytochrome *c* oxidase of *Rhodobacter sphaeroides* perturbs the interaction between subunits I and III and promotes suicide inactivation. *Biochemistry* **45,** 14896-14907.

Verkhovsky, M. I., Belevich, I., Bloch, D. A. and Wikstrom, M. (2006) Elementary steps of proton translocation in the catalytic cycle of cytochrome oxidase. *Biochim Biophys Acta* **1757,** 401-7.

Vogel, F., Bornhovd, C., Neupert, W. and Reichert, A. S. (2006) Dynamic subcompartmentalization of the mitochondrial inner membrane. *J. Cell Biol.* **175,** 237-247.

von Ballmoos, C., Wiedenmann, A. and Dimroth, P. (2009) Essentials for ATP synthesis by F1F0 ATP synthases. *Annu. Rev. Biochem.* **78,** 649-672.

Wallace, D. C. (2007) Why do we still have a maternally inherited mitochondrial DNA? Insights from evolutionary medicine. *Annu. Rev. Biochem.* **76,** 781-821.

Wallace, D. C. (2005) A mitochondrial paradigm of metabolic and degenerative diseases, aging, and cancer: a dawn for evolutionary medicine. *Annu. Rev. Genet.* **39,** 359-407.

Wallace, D. C. and Fan, W. (2010) Energetics, epigenetics, mitochondrial genetics. *Mitochondrion* **10,** 12-31.

Walsh, C., Barrow, S., Voronina, S., Chvanov, M., Petersen, O. H. and Tepikin, A. (2009) Modulation of calcium signalling by mitochondria. *Biochim. Biophys. Acta* **1787,** 1374-1382.

Wikstrom, M. and Verkhovsky, M. I. (2007) Mechanism and energetics of proton translocation by the respiratory heme-copper oxidases. *Biochim. Biophys. Acta* **1767,** 1200-1214.

Wikstrom, M. K. (1977) Proton pump coupled to cytochrome c oxidase in mitochondria. *Nature* **266,** 271-3.

Wilson, K. S. and Prochaska, L. J. (1990) Phospholipid vesicles containing bovine heart mitochondrial cytochrome c oxidase and subunit-III deficient enzyme: Analysis of respiratory control and proton translocation activities. *Arch Biochem Biophys* **282,** 413-420.

Wurm, C. A. and Jakobs, S. (2006) Differential protein distributions define two sub-compartments of the mitochondrial inner membrane in yeast. *FEBS Lett.* **580,** 5628-5634.

Xu, J., Sharpe, M. A., Qin, L., Ferguson-Miller, S. and Voth, G. A. (2007) Storage of an excess proton in the hydrogen-bonded network of the d-pathway of cytochrome C oxidase: identification of a protonated water cluster. *J. Am. Chem. Soc.* **129,** 2910-2913.

Yappert, M. C. and Ingle, J. D. (1989) Correction of polychromatic luminescence signals for inner-filter effects. *Applied Spect.* **43,** 759-767.

Yonetani, T. (1961) Studies on cytochrome oxidase. *J Biol Chem* **236,** 1680-1688.

Yoshikawa, S., Shinzawa-Itoh, K. and Tsukihara, T. (1998) Crystal Structure of Bovine Heart Cytochrome c Oxidase at 2.8 A Resolution. *J Bioenerg Biomembr* **30,** 7-14.

Zhen, Y., Qian, J., Follmann, K., Hayward, T., Nilsson, T., Dahn, M., Hilmi, Y., Hamer, A. G., Hosler, J. P. and Ferguson-Miller, S. (1998) Overexpression and purification of cytochrome *c* oxidase from *Rhodobacter sphaeroides*. *Protein Express. Purif.* **13,** 326-36.

Zick, M., Rabl, R. and Reichert, A. S. (2009) Cristae formation-linking ultrastructure and function of mitochondria. *Biochim. Biophys. Acta* **1793,** 5-19.

Zickermann, V., Kerscher, S., Zwicker, K., Tocilescu, M. A., Radermacher, M. and Brandt, U. (2009) Architecture of complex I and its implications for electron transfer and proton pumping. *Biochim. Biophys. Acta* **1787,** 574-583.